Processing of Vietnamese lithium ores to produce LiCl

Thesis submitted in partial fulfillment of the requirement of
the degree Doctor rer. nat. of the
Faculty of Environment and Natural Resources,
Albert-Ludwigs-Universität
Freiburg im Breisgau, Germany

By

Dinh, Thi Thu Hien

Freiburg im Breisgau, Germany
2015

Name of Dean: Prof. Dr. Tim Freytag

Name of Supervisor: Prof. Dr. Reto Gieré

Name of 2nd Reviewer: Prof. Dr. Tam Tran

Date of thesis' defence: 16.11.2015

Contents

Acknowledgements

I am greatly indebted to my supervisors Prof. Dr. Reto Gieré and Prof. Dr. Tam Tran for their guidance throughout the research and the writing of this dissertation. They were also able to help me overcome difficulties during my scientific experiments in my Ph.D.'s work and gave me opportunity to attend an international conference. In addition, I would like to thank PD. Dr. Eckardt Stein who has contributed significantly to make this dissertation possible.

For my Ph.D. work, I appreciate the financial support of Prof. Dr. Reto Gieré, which made the scientific aspects of my research possible, and the Ministry of Education and Training of Vietnam (MOET) and German Academic Exchange Service (DAAD) for the 4-year scholarship.

Furthermore, I would like to thank Mrs Sigrid Hirth-Walther, Mrs. Isolde Schmidt, Mr. Paul Robert Keppner, and Dr. Hiltrud Müller-Sigmund for their assistance during the laboratory and analytical work, and I also would like to thank to Mrs. Christine Höher, Mrs. Slavica Drndelic-Eich for providing a friendly atmosphere during the time of my thesis work.

I also would like to thank my colleagues in Vietnam, especially MSc. Duong Ngoc Tinh and Mr. Nguyen Huong for sampling and providing geological references. Dr. Nguyen Van Hanh, Dr. Dao Duy Anh and MSc. Nguyen Van Trong for lepidolite concentration via froth flotation at the Vietnamese Academy of Science and Technology (VAST). I am thankful to General Department of Geology and Minerals of Vietnam for facilitating my stay abroad.

Finally, I am greatly thankful to my parents, my husband for taking care my daughter, their support and encouragement during the whole of my studies in Germany. This dissertation is dedicated with love to my big family.

Abbreviations and symbols

USGS	The United States Geological Survey	Ltd	Limited
°C	Degree Celsius	M	Molar
AAS	Atomic absorption spectroscopy	Ms	Muscovite
aq	Aqueous	Mt	Million tones
BSE	Back-Scattered Electron	NW-SE	NorthWest-SouthEast
CIF	Crystallographic Information File	PHEVs	Plug-in hybrid electric vehicles
Conc.	Concentrated	ppm	Parts per million
DTA	Differential Thermal Analysis	s	Solid
EPMA	Electron probe microanalysis	SIMS	Secondary ion mass spectrometry
EVs	Electric vehicles	SW	SouthWest
g/L	Gram per little	TAS	Total alkali *vs*. silica
h	Hour	Temp.	Temperature
HEVs	Hybrid electric vehicles	TG	Thermal gravimetry
IC	Ion Chromatography	TGA	Thermogravimetric Analysis
ICP-MS	Inductively coupled plasma-mass spectroscopy	ToF-SIMS	Top-flight secondary ion mass spectrometry
kg	Kilogram	wt.%	Weight percent
LMIG	Bi-liquid metal ion source	XRD	X-ray diffraction
LMO	Lithium manganese oxide	XRF	X-ray fluorescence
Lpd	Lepidolite		

List of Tables

List of Figures

Abstract

A potential lithium deposit has been discovered in the La Vi mining district, located in Quang Ngai Province, Central Vietnam. The Li-rich rocks (average contents: 1.3±0.9 wt.% Li_2O) are highly fractionated, peraluminous granites, which are further characterized by high contents of Al_2O_3, Na_2O, K_2O, F, and P_2O_5, but very low concentrations of all other main components (MgO, CaO, Fe_2O_3tot, TiO_2). The granites exhibit a light pink color and contain mainly albite, quartz, muscovite, lithian muscovite, and lepidolite, with minor amounts of amblygonite–montebrasite, herderite, fluorapatite, topaz, and cassiterite, and accessory beryl and goyazite.

Lepidolite from La Vi deposit was extracted to produce lithium chloride by using iron II sulphide (FeS)-CaO roasting and water leaching. The HSC program was applied for the simulation of the behavior of lepidolite and the additives during roasting, confirming the important role of SO_2/SO_3 gas for extracting lithium from lepidolite. At optimum conditions roasting at 750 ^oC using FeS/Li and Ca/F molar ratios of 5:1 and 1:1, respectively, followed by leaching at 50 ^oC using water/calcine mass ratios of >5:1 could yield a maximum of ~85% Li recovery (at <1 g/L Li concentration). Addition of CaO led to a decrease in the liberation of HF gas and insoluble LiF formation.

NaOH and $BaCl_2$ were used for removing the metal and sulphate impurities from the leach liquor by precipitation at ambient temperature. The efficiency of lithium extraction reached ~100 % with washing of the precipitates after filtering. Alkali salts were separated from the LiCl solution via solar evaporation and isopropanol leaching. 96.3 wt.% LiCl could be produced using an isopropanol/salt mass ratio of 5:1 at ambient temperature in 3 h.

Kurzfassung

Eine potentielle Lithium-Lagerstätte wurde im La Vi Distrikt der Quang Ngai Provinz in Zentral Vietnam entdeckt. Bei den Li-reichen Gesteinen (durchschnittliche Gehalte: 1.3 ± 0.9 Gew.% Li_2O) handelt es sich um hoch fraktionierte peralumine Granite, die sich durch hohe Gehalte an Al_2O_3, Na_2O, K_2O, F und P_2O_5 und sehr niedrige Konzentrationen anderer Hauptelemente (MgO, CaO, Fe_2O_3tot, TiO_2) auszeichnen. Die Granite sind schwach rosa gefärbt und enthalten überwiegend Albit, Quarz, Muskovit, Lithium-Muskovit und Lepidolith, kleinere Mengen an Amblygonit-Montebrasit, Herderit, Fluorapatit, Topaz und Kassiterit sowie akzessorische Anteile von Beryll und Goyazit.

Zur Lithiumchlorit-Herstellung wurde der aus der La Vi Mine stammende Lepidolith mit Eisen II Sulfid (FeS)-Ca geröstet und mit Wasser gelaugt. Mittels HSC Programm wurde das Verhalten von Lepidolith und der Zusatzstoffe während des Röstprozesses simuliert und es zeigte sich, dass das SO_2/SO_3 Verhältnis bei der Extrahierung von Lithium aus Lepidolith eine entscheidende Rolle spielt. Eine Röstung bei 750 °C und molaren FeS/Li und Ca/F Verhältnissen von 5 : 1 bzw. 1 : 1 und anschließende Laugung bei 50 °C und einem Wasser/Kalk Verhältnis >5 : 1 lieferte eine maximale Ausbeute von *c*. 85% Li (für Konzentrationen <1 g/L Li). Dagegen führte eine Zugabe von CaO zu einer Abnahme der HF Gasfreisetzung und zu Ausfällung von unlöslichem LIF.

Durch Zusatz von NaOH und $BaCl_2$ wurden Verunreinigungen aus der gelaugten Flüssigkeit bei Raumtemperatur ausgefällt. Nach Filtern und Waschen der Ausfällungsprodukte lag die Effizient der Lithium-Extraktion bei *c*. 100 %. Durch solare Evaporation und anschließender Laugung mit Isopropanol wurden Alkalisalze von der LiCl-Lösung separiert. Bei einen Isopropanol/Salz Massenverhältnis von 5 : 1 konnten auf diese Weise bei Raumtemperatur und in einem Zeitraum von 3 Stunden 96.3 Gew.% LiCl produziert warden.

Chapter 1. Introduction

1.1. Background

Lithium, the lightest metal, has been utilised in the manufacture of glass, ceramics, and lubricating greases since its discovery in 1817. Lithium presently plays an important role in the high-tech industry due to its application in many fields including pharmaceuticals, rechargeable batteries and electronics. The global production was estimated to be 35,000 tonnes lithium in 2013 whilst its worldwide consumption was forecast to be approximately 30,000 tones, representing an increase of 6% compared to 2012 (USGS, 2014). An annual increase in lithium demand of 9.7% was projected until 2017 according to Roskill Information Services Ltd. (Roskill, 2013).

Many lithium (Li) deposits in the world are hosted by granitic pegmatites, and there are only a few minerals that may contain high Li concentrations, namely micas, clays, and some relatively rare phases (Garrett, 2004; Linnen *et al.*, 2012). The most economically important Li minerals are: *spodumene*, $LiAlSi_2O_6$, which has been mined, *e.g.*, at Greenbushes (Australia), Kings Mountain (North Carolina), Etta mine (Black Hills, South Dakota), Harding mine (Dixson, New Mexico), Strickland Quarry (Portland, Oregon), Pala (California), and Bernic Lake (Manitoba, Canada) (Heinrich *et al.*, 1978); *zinnwaldite*, $KLiFe^{2+}Al(AlSi_3O_{10})(F,OH)_2$, which occurs, for example, in the Omchikandja mine, Yakutija, Russia (Paukov *et al.*, 2010) and Krušnéhory, Cinovec area, Czech Republic (Kondás J. & Jandová J., 2006); *petalite*, $LiAlSi_4O_{10}$, with major deposits at Bikita (Zimbabwe), Kenora (Ontario, Canada), Karibib (Namibia), Aracuai (Brazil), Londonderry (Australia), Zavitinskoye (East Transbaikalia, Russia), and Uto (Sweden); *lepidolite*, $K(Li,Al)_3(Si,Al)_4O_{10}(F,OH)_2$, which has been mined at Bikita (Zimbabwe), Bernic Lake (Manitoba, Canada), Karibib (Namibia), Minas Gerais (Brazil), and Gonçalo (Portugal); and *amblygonite*, $LiAlPO_4F$, extracted from various

deposits in Canada, Brazil, Surinam, Zimbabwe, Rwanda, Mozambique, Namibia, South Africa, California (Garrett, 2004).

Manufacturers have processed salar deposits (evaporated brines) and spodumene ores as dominant feedstocks for the production of lithium and lithium chemicals around the world. Containing 0.06-0.15% lithium, salar deposits are widely used to produce high-purity lithium compounds because of low operation costs and the simplicity in processing. Meanwhile, spodumene ores have been treated to preferentially yield technical-grade concentrates containing <6% Li_2O directly used in glass and ceramic manufacturing although chemical-grade concentrates used for high-purity lithium production are also generated. The largest global salar deposits are found in the "Lithium Triangle", a region located in the Andes Mountains, South America, whereas the largest reserve of spodumene was found at Greenbushes, Australia (Kesler *et al*., 2012).

Acid-roasting and lime-roasting of spodumene have been used by many manufacturers to produce lithium chemicals of technical, battery grade (99.5%) or high-purity (>99.9%) lithium carbonate (Roskill, 2013; Galaxy Resources Ltd, 2012). Such a well-known acid-roasting method involves firstly decrepitation (at 1070-1090 ^{o}C) to convert α-spodumene to a more reactive β structure, followed by sulphation using sulphuric acid at 250 ^{o}C and subsequent leaching (at 90 ^{o}C) of the calcine obtained to extract lithium into solution (Galaxy Resources Ltd, 2011; Nemaska Lithium Inc, 2014). This process has been applied by Galaxy Resources Ltd to spodumene concentrates mined at the Mt. Catlin and Greenbushes deposits, Australia. The same process is currently proposed by Nemaska Lithium Inc. to treat its spodumene resource at Whabouchi, Canada. The lime-roasting process, on the other hand, relies on the roasting of spodumene and lime at 1030-1040 ^{o}C before leaching the yielded clinker using water to recover lithium. The scheme was commercialized by Foote Mineral Company (now Chemetall) to produce lithium hydroxide from the 1950s to 1984 (Roskill, 2009). Other routes used to extract lithium from spodumene via pressure leaching with soda ash (Chen *et al*., 2011) or chlorination roasting (Barbosa *et al*., 2014) were also proposed.

Studies on lithium recovery from various lithium-bearing ores containing minerals such as petalite, zinnwaldite and lepidolite have also been developed. In recent years, zinnwaldite wastes discharged from processing of tin-tungsten ores in Cinovec, the

Czech Republic (Jandová *et al*., 2010) and china clay in Cornwall, the United Kingdom (Siame and Pascoe, 2011) were tested to extract lithium. Limestone, gypsum and quenched lime were used to liberate lithium from zinnwaldite concentrates via roasting, and Li was then leached by water (Jandová *et al*., 2009 & 2010; Vu *et al*., 2013). The concentrates (1.21-1.4 wt% Li) were first recovered from zinnwaldite wastes (0.21 wt% Li) using dry magnetic and grain-size separations. Sintering of mixtures of the concentrates and the additives at different temperatures ranging from 825 ^{o}C to 950 ^{o}C, followed by water leaching of the yielded calcines at 90-95 ^{o}C resulted in >90% Li extractions. Siame and Pascoe (2011) first mixed a zinnwaldite concentrate with either gypsum or sodium sulphate as a feed for roasting at 1050 ^{o}C and 850 ^{o}C, respectively. The calcines obtained were then leached with water at 85^{o}C, resulting in lithium recoveries of 85% and 97%, of which sodium sulphate roasting was noted to give a higher yield of lithium.

Lepidolite, one of the major mineral resources of lithium, has been recently studied to produce high-grade lithium compounds. However, no commercial processing plant has commenced up to now. Sodium and potassium sulphate salts were mixed with lepidolite for roasting to extract lithium in studies by Yan *et al*. (2012a&b). Sulphation roasting of lepidolite using Na_2SO_4 was subsequently conducted by Luong *et al*. (2013) in which the role of $LiKSO_4$ and LiF in controlling the release of lithium during leaching was emphasized. Recently, a scheme using $FeSO_4.7H_2O$ to extract lithium from a Korean lepidolite ore was also examined (Luong *et al*., 2014). It was believed that SO_2/SO_3 gases generated from the decomposition of such ferrous sulphate play a key role in the extraction of Li from lepidolite via a gas-solid interaction. The presence of CaO or $CaCl_2$ as a secondary additive to reduce the amounts of HF gas liberation by forming CaF_2 was also reported in these studies.

1.2. Objectives

The main goals of this research:

- To evaluate the geological and petrographic features of potentially economic Li deposits in the Dong Ram area of the La Vi mining district, located in the Quang Ngai province in Central Vietnam based on bulk compositional data of the rocks and

chemical compositions of the various mineral constituents, which include some relatively rare beryllium and strontium phosphates.

- To investigate cheaper sources of SO_2/SO_3, such as iron sulphide (FeS), for roasting in recovering lithium after its concentration using froth flotation from a lepidolite ore collected from the La Vi deposit, Vietnam. The role of CaO in capturing fluorine and enhancing the extraction of lithium during lepidolite roasting was also studied. Thermodynamic modelling based on the HSC program (Outotec, 2011) was conducted to predict different factors controlling the extraction of lithium during roasting, e.g. temperature and FeS/Li molar ratio.
- To optimize the conditions of water leaching and purification processes to produce LiCl from La Vi lithium ores.

1.3. Dissertation structure

Chapter 1 introduces to lithium, mineral contain lithium in the deposit, the supply and demand of lithium and lithium compounds in the world, as well as how important lithium is in the industries and life. It also summarizes the methods to extract lithium from ores and brine.

Chapter 2. Literature Review, provides the various use of lithium in industries such as ceramics, batteries, lubricating greases, and others. In addition, a summary review of common recovery lithium technologies from brines and minerals is presented in this chapter.

Chapter 3. Material and Analytical Procedures, explains the sample preparation methods for petrographic features, mineral component studies, and lithium processing to produce LiCl. All the physical and chemical analysis procedures used for this study are listed, such as X-ray diffraction, X-ray fluorescence, thermal gravimetric techniques, and atomic absorption spectroscopy.

Chapter 4. Geological setting. In this chapter the location of La Vi mining district in Vietnam is described with distinctive minerals. The geologic history of the mine is expressed in the description of the Kan Nack complex, the Sa Huynh complex and the

Dai Nga formation, as well as the development of mineral features in difference temperature stages. Moreover, the faults are also discussed in this chapter.

Chapter 5. Bulk-rock and mineralogical composition of the La Vi rocks. The physical and chemical analysis of rock samples are used to determine the mineralogical composition of La Vi ores. Publications that describe similar minerals are compared with samples from La Vi.

Chapter 6. Experimental Procedures for Lithium Extraction. The flowchart of lithium recovery from the La Vi ore presents in a general scheme the production of LiCl through roasting, leaching, purification and chlorination. The experimental conditions for each process are chosen based on physical and chemical properties of the sample and earlier publications in journal articles.

Chapter 7. Results and Discussion of the Lithium Extraction Study. The optimum experimental conditions of roasting, leaching, purification and chlorination applied to the lithium La Vi ore to produce LiCl are elaborated. The result will be explained, discussed in tables and graphs and compared with other methods.

Chapter 8. Conclusions and Recommendations. This chapter will answer the aim of doctoral thesis that is presented in the introduction. The advantages, disadvantages of the method used and recommendations for future work around this topic.

1.4. List of publications

Journal article

Hien-Dinh, T. T., Luong, V. T., Gieré, R., and Tran, T. (2015). Extraction of lithium from lepidolite via iron sulphide roasting and water leaching. *Hydrometallurgy* 153, 154-159.

Conference papers

Hien-Dinh, T. T., Dao, D. A. (2014). Apply XRD and Topas for mineral component study of lepidolite from lithium ore. The 4th Mineral processing conference, November 11th, Hanoi, Vietnam.

Hien-Dinh, T. T., Gieré, R., Luong, V. T., and Tran, T. (2015). Sulfation roasting and water leaching of lepidolite. The 24th International mining congress and exhibition of Turkey, April 14-17th, Antalya, Turkey, 1357-1363.

Chapter 2. Literature Review

2.1. Use of lithium

Worldwide lithium end-use markets increase every year, in major industries, such as ceramics and glass, batteries, pharmaceuticals, rubber and thermoplastics, continuous casting, air treatment, aluminum, metallurgical, greases and others (Table 2.1 and Fig. 2.1). The most important lithium compound is lithium carbonate used as a feedstock for processing, whereas other lithium products are lithium chloride, lithium hydroxide, lithium sulfate, etc.

Table 2.1. Worldwide consumption (in %) and end-use of lithium.

Industrial applications	(Roskill, 2010)	(Roskill, 2012)	(USGS, 2013)	(USGS, 2014)
Ceramics and glass	31	30	30	35
Batteries	23	22	22	29
Greases	9	11	11	9
Aluminum	6	2	1	1
Air treatment	6	4	4	5
Others	25	31	32	21

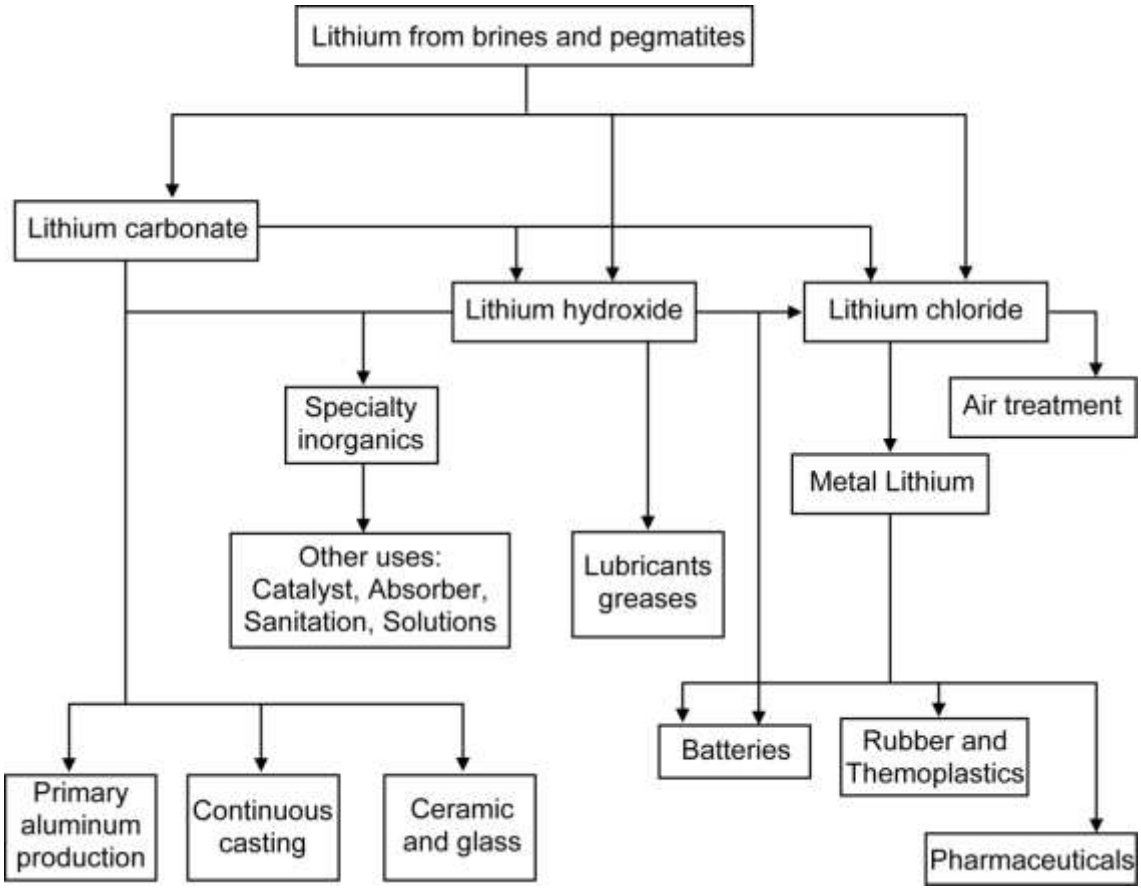

Figure 2.1. Application of lithium compounds for end-used of lithium (after Peiró *et al*., 2013).

2.1.1. Ceramics and glass

Lithium oxide is made from lithium carbonate used for the manufacture of glass, enamel and ceramics. Lithium mineral concentrates are applied directly in making ceramics and glass to lower their melting points and thermal expansion coefficient to save energy.

2.1.2. Batteries

Lithium compounds are major components of rechargeable batteries that are used in cell phones, power tools, MP3 players, laptops, notebooks, tablets and electric vehicles.

Additionally, calculators, cameras, watches also use non-rechargeable lithium batteries (USGS, 2014). Roskill (2012) and USGS (2012) reported an increase in Li-ion battery use in HEVs, PHEVs, EVs produced by major car producers such as GM, Nissan, Mitsubishi & Hyundai, BMW, Ford, Toyota, Volkswagen, Honda, Hyundai, etc. with continuous annual growth of 5 % by 2020.

2.1.3. Lubricating greases

Lubricating greases produced from lithium hydroxide monohydrate, are used in automotive, aircraft, and marine industries. The reasons are for maintaining the vast temperature band in the property of lubricating greases and endurance to water, oxidation and hardening.

2.1.4. Air treatment

Air conditioners, gas and air treatment use LiCl and LiBr as desiccants for air conditioning and process cooling (Rockwood Lithium, 2015). 54 wt.% LiBr brines in solution are applied in industrial absorption chilling systems. In addition, LiCl is used in humidity control system of photographic processing, laboratories, food processing, and pharmaceutical manufacturing (Pan Global Resources, 2015).

2.1.5. Others

High quality lithium compounds are used in chemical facilities, polymerization and pharmaceuticals industries as a catalyst. The catalyst from lithium also is applied for producing synthetic rubber with resistance in abrasion and thermoplastic rubber without vulcanization properties (Wallace, 2012).

2.2. Lithium processing technologies

According to Vikström *et al*. (2013) lithium was produced in small quantities until the 1950s. The next period from 1950s to the mid-1980s, the USA was the principal lithium manufacturer. Lithium production was strong in 1997 due to the cheaper Li_2CO_3 produced from brine (Ebensperger *et al*., 2005).

The lithium demand exhibits considerable growth in the last ten years, due to the expanding industrial production of lithium. The main sources of lithium are brines (as salar and seawater) and minerals (as pegmatites from igneous rocks and clays). Nearly 60 % of lithium production is from brines located in Chile, China, USA, and Argentina. Over 85 % spodumene from pegmatite resources is used for lithium production (Peiró *et al*., 2013).

Lithium in brines can be recovered by ion exchange, precipitation, solvent extraction and adsorption. Meanwhile, lithium from minerals can be recovered by roasting, leaching, purification and recovery to produce lithium compounds such as LiCl, Li_2CO_3 and LiOH.

2.2.1. Recovery lithium from brines

Uyuni in Bolivia is the largest salar in the world with 10000 km^2 but most production of lithium is from salar de Atacama in Chile with 3000 km^2 of surface area (Kesler *et al*., 2012), as present in Table 2.2.

The technologies for lithium recovery from the brine deposits are mostly via solar evaporation, precipitation using different precipitants or via adsorption as shown in Table 2.3. In some cases it is required to first remove Ca and Mg (from Uyuni salar brine) by precipitation using lime or sodium oxalate (An *et al*., 2012). Chitrakar *et al*. (2013 & 2014) describe the adsorption methods with $Li_{0.15}H_{0.76}Mg_{0.40}Mn^{III}_{0.08}Mn^{IV}_{1.59}O_4$ derived from magnesium-doped lithium manganese oxide (LMO), H_2TiO_3, as adsorbent to remove Li and eluent is HCl for desorption.

The process of solar evaporation using a shallow pond system of large surface area to raise the concentration of lithium salts, while calcium and sodium compounds have been used to remove Na, K, Ca, Mg, B, etc. from solution ($Ca(OH)_2$, Na_2SO_4, NaOH, and Na_2CO_3) (Galli *et al*., 2014). $CaCl_2$ is used to transfer Li_2SO_4 in solution to LiCl by $CaSO_4$ precipitation, which was described by Kawata *et al*. (2013); Brown & Boryta (1993); Brown & Beckerman (1990); and Brown *et al*. (1981c).

Table 2.2. Resources and compositions of brine deposits around the world (data extracted from Vikström *et al*., 2013).

Country	Deposit	Li, wt.%	Predicted resources (Mt)
Argentina	Cauchari	0.062	0.9
	Diablillos	unstated	0.9
	Olaroz	0.09	0.2-0.3
	Rincon	0.04	0.5-2.8
	Salar del Hombre Muerto	0.062	0.8-0.9
	Sal de Vida	unstated	0.3
Bolivia	Salar de Uyuni	0.096	5.5-10.2
Canada	Beaverhill Lake	unstated	0.52-0.59
	Fox Creek	0.01	0.5
Chile	Maricunga	0.092	0.2-0.4
	Salar de Atacama	0.14	3-35.7
China	Dangxioncuo/DXC	0.045	0.1-0.2
	Lake Zabuye	0.097	1.3-1.5
	Qaidam/Qinghai/Taijinaier	0.03	1-3.3
India	Sua Pan	0.002	unstated
Israel	Dead Sea	0.002	2
USA	Bonneville Salt Flats	0.004	unstated
	Brawley	unstated	1
	Great Salt Lake	0.006	0.5
	Salton Sea	0.022	1-2
	Searles Lake	0.0083	0.03
	Clayton Valley/ Silver Peak	0.03	0.3
	Smackover	0.038	0.75-1

In addition, other processes of lithium extraction from brine are using compounds derived from lithium manganese oxide or titanium antimonite and tin antimonate as main adsorbents and HCl or HNO_3 as stripping agents. Tin and titanium antimonate

cation exchanger (SnSbA and TiSbA; where A = cation exchanger) are the most effectively and highly selective adsorbent for lithium ions recovery, compared to other alkali ions from seawater and hydrothermal water (Abe & Chitrakar, 1987), (Abe & Hayashi, 1984). Both SnSbA and TiSbA could be reused afterwards, recovered from HNO_3 eluent.

Table 2.3. Precipitation methods for purification of some brine deposits to produce lithium compounds.

Reference	Method	Precipitate of	Final product	Deposit
Galli *et al*., 2014	$Ca(OH)_2$, Na_2SO_4, NaOH Evaporation Na_2CO_3	Mg, Ca, B unstated Ca	Li_2CO_3, LiCl	Rincon-Argentina
An *et al*., 2012	Lime $Na_2C_2O_4$	Mg, Ca, adsorbed B Ca, Mg	Li_2CO_3	Salar de Uyuni-Bolivia
Brown & Boryta, 1993	$CaCl_2$ Solar evaporation unstated	$CaSO_4 \cdot 2H_2O$ unstated Mg, Ca	Li_2CO_3	Salar de Atacama-Chile
Brown & Beckerman, 1990	$CaCl_2$ Solar evaporation	Gypsum salts of alkali, Mg, etc.	LiCl	
Brown *et al*., 1981c	Solar evaporation + CaO $CaO + CaCl_2$ Solar evaporation ± pH adjustment	salts of alkali, Mg Mg, Ca ($CaO_4 \cdot 2H_2O$, $CaB_2O_4 \cdot 6H_2O$) salts of alkali, Mg, Ca sulphate, etc.	LiCl	Clayton Valley-USA
Boryta, 2000	Solar evaporation + lime	$LiCl \cdot MgCl_2 7H_2O$, $Mg(OH)_2$, $CaCO_3$	Li_2CO_3	

2.2.2. Recovery of lithium from minerals

More than 145 different lithium minerals from pegmatites are found, but lithium is extracted only from spodumene, lepidolite, petalite, amblygonite, and eucryptite (Peiró *et al*., 2013), as show in Table 2.4. According to Garrett (2004), Australia is globally the largest producer of lithium from spodumene. Lepidolite was used previously but its use nowadays is reduced because of its generally high fluorine content. Petalite is applied for glass production because it has a high iron content (Vikström *et al*., 2013). Lithium in granitic pegmatites usually exists with other rare metals such as tin, beryllium, and tantalum-niobium (Kesler *et al*., 2012).

Lithium minerals have been concentrated by mechanical separation such as gravity separation, magnetic separation, and flotation. The concentrates recovered are roasted with additives to create new lithium compounds, which are easily dissolved into water. In order to remove impurities such as Ca, Mg, Fe, SO_4 and Al from the leach liquors, precipitation is carried out. Li_2CO_3, LiCl, and LiOH are extracted from lithium solution by carbonation, chlorination, crystallization, or electrodialysis subsequent to evaporation or ion exchange.

Table 2.4. Lithium mineral resources for lithium production.
Source: http://webmineral.com/.

Lithium sources	Minerals	Formula	Li content (wt.%)
Pegmatites	Spodumene	$LiAlSi_2O_6$	3.73
	Lepidolite	$K(Li,Al)_3(Si,Al)_4O_{10}(F,OH)_2$	3.58
	Zinnwaldite	$KLiFe^{2+}Al(AlSi_3O_{10})(F,OH)_2$	1.59
	Petalite	$LiAlSi_4O_{10}$	2.09
	Amblygonite	$LiAlPO_4F$	3.44
	Eucryptite	$LiAlSiO_4$	5.51
Clays and others	Hectorite	$Na_{0.3}(Mg,Li)_3Si_4O_{10}(OH)_2$	0.54
	Montmorillonite	$(Na,Ca)_{0.3}(Al,Mg)_2Si_4O_{10}(OH)_2•n(H_2O)$	not specified

2.2.2.1. Lithium recovery from spodumene

Spodumene is the most common pegmatite mineral used for Li production. Table 2.5 lists several lithium mines, which recover and process the main mineral as spodumene around the world. A summary of lithium processes based on spodumene to produce lithium compounds is shown in Table 2.6.

According to Kesler *et al*. (2012), Greenbushes is the largest mine in Western Australia, from which tantalum and high lithium grade are recovered. The processes applied to extract lithium in Greenbushes are gravity, heavy medium, froth flotation and magnetic separation (Talison Lithium Limited, 2012). In Zimbabwe, metal production of the Bikita pegmatite includes tantalum, tin, beryllium, cesium and lithium; and the Kamativi pegmatite contains tin and lithium. Kings Mountain Belt is the biggest pegmatite deposit of lithium in North America and contains tin and lithium (Kesler *et al*., 2012). Other pegmatites rich beryllium and lithium in both spodumene and beryl-spodumene are located at La Motte (Canada) (Mulja *et al*., 1995).

Additives containing Cl^-, SO_4^{2-}, CO_3^{2-} are used for roasting to form new lithium salts. Depending on the chosen additives, roasting temperatures range from 100 °C to 1200 °C. Similarly, the leaching temperature is a major parameter, varying with different leachants and Li compounds produced. Archambault *et al*. (1963) used sodium hydroxides, sodium silicates, sodium borates and sodium sulphides for roasting in the range of 70-130 °C and ammonium carbonate for leaching to produce lithium carbonate. Other mixtures (limestone and gypsum) are also used for sulphating spodumene at ~1100 °C, the calcine was then leached in a solution of $CaCl_2$ as reported by Hayes *et al*. (1950). Dwyer (1957) used a similar method but different additives ($(NH_4)_2SO_4/NH_4HSO_4$), and the calcine was leached in a NH_4OH solution.

Leaching with water, Ellestad & Leute (1950) and Robinson (1961) digested spodumene with concentrated H_2SO_4 at 200-300 °C and 250-400 °C, respectively under pressure. Peterson (1960) used a mixture of sodium formate and sodium carbonate for carbonation of β-spodumene at ~290 °C after roasting α-spodumene at ~1000 °C. A natural mineral, tachyhydrite, was used for roasting at ~1150 °C by Medina & El-Naggar (1984).

Table 2.5. Spodumene ores in mines around the world (data extracted from Vikström *et al*., 2013)

Country	Mine	Li (wt.%)	Predicted resources (Mt)
Afghanistan	Helmand Basin	unstated	unstated
	Katawaz Basin	unstated	unstated
	Parun	1.5	unstated
	Taghawkor	1.7-2.8	unstated
Australia	Greenbushes	1.9	0.3-0.7
	Mt Marion	0.65	0.02
	Mt Cattlin	0.5	0.07
Austria	Koralpe	0.78	0.1
Brazil	Mibra/Minas Gerais	unstated	0.1-0.9
Canada	Barraute/Quebec	0.23-0.53	0.1-0.37
	Bernic Lake/ Tanco	0.64-1.28	0.1-0.14
	Big Bird/ Curlew	1.24-1.72	unstated
	English River Greenstone	unstated	unstated
	La Corne	0.52	0.1-0.4
	La Motte	0.5	0.023-1.023
	McAvoy	3.3-4.5	unstated
	Moblan	1.7	0.04
	Moose 2	unstated	0.016
	Niemi Lake	unstated	0.001
	Wekusko Lake	0.79	0.028
	Yellowknife	0.66	0.1-0.13
China	Gajika	unstated	0.56-0.6
	Jaijika	0.6	0.2-0.5
	Maerkang	unstated	0.2-0.5
Congo	Kitotolo	0.6	0.8
	Manono	0.6	1-3

Table 2.5. *Continued.*

Country	Mine	Li (wt.%)	Predicted resources (Mt)
Finland	Laenttae	0.43	0.01-0.68
Russia	Alahinskoe	unstated	unstated
	Belerechenskoe	unstated	0.05
	Goltsovoe	0.37	0.14-0.29
	Suglugskoe	unstated	unstated
	Urikskoe	unstated	0.1-0.3
	Tastyg	1.86	0.05
	Voronietundrovskoe	unstated	0.05-0.82
	Zavitinskoe	unstated	0.05-0.14
Sweden	Jaerkvissle	0.45	0.003
	Varutraesk	unstated	0.001
USA	Kings Mountain Belt	0.68	0.2-5.9
	North Carolina	unstated	2.6-5.5
Zimbabwe	Bikita	0.58-1.4	0.06-0.17
	Kamativi	0.28	0.28
	Masvingo	unstated	0.057

Chlorination of spodumene at a high temperature (> 1000 °C) was described by Cunningham (1953) using a mixture of limestone, $CaCl_2$ and sand while Barbosa *et al*. (2013) used directly pure Cl_2 gas. In both methods lithium was extracted as gas. Medina & El-Naggar (1984) and Peterson & Gloss (1959) used natural minerals (muriate of potash and sylvinite) for roasting, and then leached the calcines in HCl.

Different methods without roasting, using a strong acid (7% HF) or caustic for leaching directly spodumene under pressure at high temperature (> 90 °C) to produce Li_2CO_3 were reported by Rosales *et al*. (2014) and Chubb (1963). β-spodumene was leached in lime milk at 100-205 °C under pressure, thereafter spodumene was heated at 1100-1150 °C (Nicholson, 1946).

Table 2.6. The results of published studies on processing of spodumene.

Reference	Roasting		Leaching		Li recovery %	Final product
	Additive	Temp. °C	Solvent	Temp. °C		
Archambault *et al*., 1963	H_2O + NaOH/ Na_2SiO_3/ $2Na_2O.B_2O_3$/ Na_2S	70-130	$(NH_4)_2CO_3$ solution	0-40	93	Li_2CO_3
Ellestad & Leute, 1950	Conc. H_2SO_4	200-300	H_2O	unstated	86	not included
Dwyer, 1957	$(NH_4)_2SO_4$/ NH_4HSO_4	150-370	NH_4OH	unstated	unstated	not included
Peterson, 1960	NaCOOH + Na_2CO_3	~290	H_2O	unstated	98-100	not included
Cunningham, 1953	Limestone + $CaCl_2$ + sand	1100-1200	Li was extracted as gas		90-95	LiCl
Nicholson, 1946	not included		Lime milk	100-205	>90	Li_2CO_3
Chubb, 1963	not included		H_2O + NaOH/ Na_2CO_3 + CaO/ $Ca(OH)_2$	100-200	unstated	Li_2CO_3
Hayes *et al*., 1950	Limestone + gypsum	~1100	$CaCl_2$ solution	unstated	85-90	LiCl
Peterson & Gloss, 1959	Muriate of potash (KCl) + sylvinite (KCl·NaCl)	1000	HCl solution	85	100	Li_2CO_3
Robinson, 1961	Conc. H_2SO_4	250-400	H_2O	95	96	not included
Rosales *et al*., 2014	not included		7% HF solution	75	92	Li_2CO_3

Temp.: Temperature; Conc.: Concentrated

Table 2.6. *Continued*.

Reference	Roasting		Leaching		Li recovery %	Final product
	Additive	Temp. °C	Solvent	Temp. °C		
Chen *et al*., 2011	not included		H_2O + Na_2CO_3	225	~96	Li_2CO_3
Medina & El-Naggar, 1984	Tachyhydrite ($CaMg_2Cl_6.12H_2O$)	~1150	H_2O	~100	87	not included
Barbosa *et al*., 2013	Pure Cl_2 gas	1000-1100	Li was extracted as gas		unstated	LiCl

Temp.: Temperature; Conc.: Concentrated

2.2.2.2. Recovery of lithium from lepidolite

The Yichun region in China has topaz-lepidolite granites containing with rich in Ta, Nb and Sn (Yin *et al*., 1995). Similarly, lepidolite-bearing granite at Orlovskoe and Etykinskoe has mainly lithium, tin and tantalum (Kesler *et al*., 2012) (Table 2.7).

Table 2.7. Lepidolite ores in mines around the world (data extracted from Vikström *et al*., 2013).

Country	Mine	Li (wt.%)	Predicted resources (Mt)
China	Daoxian	0.55	0.18-0.2
	Yichun	2.0	0.3-0.5
Russia	Etykinskoe	0.23-0.79	0.046
	Orlovskoe	unstated	0.05
Spain	Mila Feli	0.5	0.005

Chlorination and sulphation were applied for roasting lepidolite at around 800-1000 °C (Table 2.8) before the calcines were leached in water. Luong *et al*. (2014 & 2013) proved that SO_2/SO_3 from Na_2SO_4 or $FeSO_4$. $7H_2O$ is a key factor for extracting lithium from lepidolite to create Li_2SO_4 and $LiKSO_4$, which are easily dissolved in water. Fluorine in lepidolite was reduced by a secondary additive (CaO) to avoid LiF formation. SO_3 also was previously applied for roasting lepidolite at 800-900 °C and water leaching by Frevel & Kressley (1962). A combination of sodium sulphate with other additives was used by Yan *et al*. (2012a & b) during roasting, and the calcines produced were leached in water at ambient temperature.

Another additive for sulphation of lepidolite is H_2SO_4, which was investigated by Botton *et al*. (1965) and Schieffelin &Stenger (1961). Lepidolite was roasted with concentrated H_2SO_4 at 165 °C (Botton *et al*., 1965) or 120-340 °C (Schieffelin &Stenger, 1961), followed by leaching in water to produce lithium carbonate.

Chlorination of lepidolite during the roasting procedure was carried out by Kepfer & Pfanstiel (1953), Löf & Lewis (1942) and Yan *et al*. (2012d). Lepidolite was first roasted with $CaCl_2$ at 843 °C (Kepfer & Pfanstiel, 1953) or mixtures of NaCl and $CaCl_2$ at 880 °C (Yan *et al*., 2012d), followed by water leaching for liberating lithium into the leach liquor. Löf & Lewis (1942) used HCl gas during the lepidolite roasting at 910 °C; the mixtures of LiCl and other impurities were then captured, and then LiCl was purified by distillation, fractional crystallization, and solvent extraction.

Mazza *et al*. (1960) proposed to roast lepidolite with limestone at 900 °C. After leaching in water and removal of impurities, lithium carbonate was recovered via carbonation of a mixture of lithium hydroxide monohydrate and lithium fluoride. In 1961, Goodenough & Stenger (1961) heated lepidolite at around 1000 °C, then used strongly acidic cation exchange resins to leach the calcine at 100 °C. Lime milk was used for pressure leaching of the calcine at 150 °C to produce pure lithium carbonate after pretreatment of lepidolite via defluoridation by roasting lepidolite with water steam at 860 °C.

Table 2.8. Results of published studies on processing of lepidolite.

Reference	Roasting		Leaching		Li recovery %	Final product
	Additive	Temp. °C	Solvent	Temp. °C		
Botton *et al*., 1965	72 % H_2SO_4 solution	165	H_2O	unstated	~92	Li_2CO_3
Mazza *et al*., 1960	Limestone	900	H_2O	unstated	~80	Li_2CO_3
Frevel & Kressley, 1962	SO_3	800-900	H_2O	unstated	~90	not included
Kepfer & Pfanstiel, 1935	$CaCl_2$	~843	H_2O	unstated	88	not included
Goodenough & Stenger, 1961	Air	1000	Resin + H_2O	100	88	not included
Schieffelin & Cappon, 1908	Conc. H_2SO_4	120-340	H_2O	unstated	~94	Li_2CO_3
Löf & Lewis, 1942	HCl gas	910	Li was extracted as gas		95	LiCl
Yan *et al*., 2012a	Na_2SO_4 + $CaCl_2$	880	H_2O	ambient	~95	Li_2CO_3
Yan *et al*., 2012b	Na_2SO_4 + K_2SO_4 + CaO	850	H_2O	ambient	~92	not included
Yan *et al*., 2012c	H_2O steam	860	Lime milk	150	~99	Li_2CO_3
Yan *et al*., 2012d	NaCl + $CaCl_2$	880	H_2O	60	~93	not included
Luong *et al*., 2013	Na_2SO_4	1000	H_2O	85	~90	not included
Luong *et al*., 2014	$FeSO_4 \cdot 7H_2O$ + CaO	850	H_2O	ambient	~93	not included

Temp.: Temperature; Conc.: Concentrated

2.2.2.3. Recovery of lithium from zinnwaldite, petalite, and amblygonite

There are several mines found containing the lithium minerals zinnwaldite, petalite, and amblygonite around the world (Table 2.9). In the Karibib district of Namibia, petalite also contains beryllium, tantalum and cesium (Kesler *et al*., 2012). Zinnwaldite was found in gravity wastes of a Sn-W mine in the Czech Republic (Jandová *et al*., 2009), as well as in South West England (Siame & Pascoe, 2011). Amblygonite is a lithium phosphate mineral, which is usually found with spodumene, lepidolite and other lithium minerals.

Jandová *et al*. (2009 & 2010) produced Li_2CO_3 from the zinnwaldite wastes of Sn-W ores by roasting with $CaSO_4$ and $Ca(OH)_2$ at 950 °C or $CaCO_3$ at 825 °C, followed by water leaching at 90 °C or 90-95 °C, respectively. Siame & Pascoe (2011) used natural gypsum for roasting a zinnwaldite feed at 1050 °C and also conducted experiments with Na_2SO_4 as an additive at 850 °C. All calcines were leached in water at 85 °C in order to liberate lithium into solution (Table 2.10).

A Zimbabwean petalite concentrate was transformed into Li_2CO_3 by first converting spodumene to β-spodumene at 1100 °C, followed by roasting with concentrated H_2SO_4 at 300 °C, and finally by leaching the resulting calcine in water at 50 °C (Sitando & Crouse 2012) (Table 2.11).

Sulphation processes were investigated for roasting amblygonite by Slegen & Roder (1936), Frevel & Kressley (1962), and Kalenowski & Runke (1952) (Table 2.12). Slegen & Roder (1936) used a solution of 73% H_2SO_4 to preheat amblygonite first at 100-200 °C, followed by roasting at 850 °C. Water was chosen for the leaching process. Later, Kalenowski & Runke (1952) roasted the mineral with a mixture of gypsum and lime at 950 °C, followed by leaching in water. Another method for sulphation of amblygonite was patented by Frevel & Kressley (1962), in which amblygonite was reacted with SO_3 gas during the roasting process.

Coleman & Jaffa (1935) investigated direct leaching of amblygonite through 3 stages. Amblygonite was first mixed with NaOH for digesting at 93 °C for 3 h, the slurry included dissolved aluminium phosphate and an insoluble lithium residue. The residue

was treated by either NaH_2PO_4 or H_3PO_4 to remove P_2O_5 in the second stage, and then digested with a solution of 35 % H_2SO_4 to produce a Li_2SO_4 solution in the last stage.

Table 2.9. Petalite, amblygonite ores in mines around the world (data extracted from Vikström *et al*., 2013).

Country	Mine	Minerals	Li (wt.%)	Predicted resources (Mt)
Brazil	Aracuai/Cachoeira	Petalite	unstated	0.01-0.023
Canada	Separation Rapids		0.62	0.05-0.072
China	Hupei		unstated	0.042
	Lijiagou		unstated	0.06
	Jinchuan		unstated	unstated
	Ningdu		unstated	unstated
Portugal	Barroso		0.37-0.72	0.01
Namibia	Karibib		0.93-1.4	0.012-0.015
Mali	Bougouni	Amblygonite	1.4	0.03

Table 2.10. Results of published studies on processing of zinnwaldite.

Reference	Roasting		Leaching		Li recovery %	Final product
	Additive	Temperature °C	Solvent	Temperature °C		
Jandová *et al*., 2009	$CaSO_4$ and $Ca(OH)_2$	950	H_2O	90	~96	Li_2CO_3
Jandová *et al*., 2010	$CaCO_3$	825	H_2O	90-95	~90	Li_2CO_3
Siame & Pascoe, 2011	Na_2SO_4	850	H_2O	85	97	Li_2CO_3
	Gypsum	1050	H_2O	85	~84	not included

Table 2.11. Results of published studies on processing of petalite.

Reference	Roasting		Leaching		Li recovery %	Final product
	Additive	Temp. °C	Solvent	Temp. °C		
Sitando & Crouse, 2012	Heating Concentrated. H_2SO_4	1100 300	H_2O	50	~97	Li_2CO_3

Table 2.12. Results of published studies on processing of amblygonite.

Reference	Roasting		Leaching		Li recovery %	Final product
	Additive	Temp. °C	Solvent	Temp. °C		
Coleman & Jaffa, 1935	not included		Stage 1: NaOH Stage 2: NaH_2PO_4/H_3PO_4 Stage 3: 35 % H_2SO_4	93 unstated unstated	83	Li_2CO_3
Slegen & Roder, 1936	73% H_2SO_4 solution Stage 1: 100-200 Stage 2: <850		H_2O	unstated	95	not included
Frevel & Kressley, 1962	SO_3	900	H_2O	unstated	~68	not included
Kalenowski & Runke, 1952	Gypsum + lime	950	H_2O	unstated	~97	not included

Temp.: Temperature

2.2.2.4. Recovery of lithium from clays and other ores

Table 2.13 describes methods to recover lithium from clay minerals. Sulphation is also the main method for extracting lithium from clay minerals. In addition, carbonation was also applied for these ores.

Zbranek (2013) extracted lithium from hectoritic montmorillonite by roasting with dolomite and $CaSO_4$ at 1000 °C, followed by leaching in water at 95 °C. Li_2CO_3 was recovered from the leach liquor by carbonation. Using gypsum + limestone at 1000 °C or SO_2 gas at 700 °C and water leaching to produce Li_2CO_3 were investigated to extract lithium from low-grade Nevada clays (Crocker *et al*., 1988). Similarly, Büyükburç & Köksal (2005) reported the gypsum + limestone method for extracting lithium from boron-rich clays. El-Fayoum bentonite was leached directly by H_2SO_4 7M at 250 °C to produce Li_2CO_3.

Crocker *et al*. (1988) also studied using anhydrous HCl or $CaCO_3$ and HCl for roasting at 700 °C or 750 °C, respectively, followed by water leaching at 80 °C.

Table 2.13. Results of published studies on processing of clays.

Reference	Roasting		Leaching		Li recovery %	Final product
	Additive	Temp. °C	Solvent	Temp. °C		
Zbranek, 2013	Dolomite + $CaSO_4$	1000	H_2O	95	92	Li_2CO_3, LiOH
	SO_2	700	H_2O	unstated	~86	not included
Crocker *et al*., 1988	Anhydrous HCl	700	H_2O	80	~70	not included
	$CaCO_3$ + HCl	750	H_2O	80	~80	Li_2CO_3
	Gypsum + limestone	1000	H_2O	unstated	~90	Li_2CO_3
Büyükburç & Köksal, 2005	Gypsum + limestone	915	H_2O	ambient	~88	Li_2CO_3
Amer, 2008	not included		7M H_2SO_4	250	~90	Li_2CO_3

Chapter 3. Material and Analytical Procedures

3.1. Material

The studied rock samples (n = 6) were collected from granitic rocks in the Dong Ram area (Fig. 4.2). In order to prepare the samples for bulk-rock analysis, hand specimens were ground in an automatic agate mill and polished thin sections (30 µm thick) with 20 nm carbon coating were used to study the mineral content of the rock samples.

3.2. X-ray diffraction (XRD)

All rock powders were further analyzed by powder X-ray diffraction (XRD), using a Bruker AXS D8 Advance instrument and Cu-Kα radiation. The samples were scanned between 2 and 60 ° 2θ, using a step size of 0.005 ° and an acquisition time of 2s/step. Structure refinement was performed using the Bruker AXS topas 3 software. The Rietveld method with least-squares approach was used to match data of a theoretical species until it fits an experimental pattern based on the database, given in the Crystallographic Information File (CIF) of minerals.

3.3. X-ray fluorescence (XRF)

The contents of bulk-rock major and trace elements were determined by X-ray fluorescence spectrometry (XRF), using a PHILIPS PW2404 spectrometer and standard analytical routines at the Institute of Earth and Environmental Science, University of Freiburg.

3.4. Thermal gravimetry (TG)

Differential Thermal Analysis (DTA) and Thermogravimetric Analysis (TGA) were conducted by using a Netzsch STA 449C instrument.

3.5. Atomic absorption spectroscopy (AAS)

Lithium and Be were analyzed by using flame atomic absorption spectroscopy (AAS), whereas Al and Ba were analyzed by graphite-furnace AAS. AAS was also used to verify the Na concentrations determined by XRF. Water contents were analyzed by LECO-infrared spectroscopy.

3.6. Electron probe microanalysis (EPMA)

Ten polished thin sections (30 µm) prepared from rock slabs were investigated using a petrographic polarizing microscope (Zeiss Axio Imager A1). After coating with 20 nm of carbon, the same polished sections were also used for the determination of the chemical composition of the individual minerals by electron probe microanalysis (EPMA). The instrument used was a Cameca SX100 electron microprobe, equipped with 5 crystal spectrometers and both energy-and wavelength-dispersive X-ray systems. Quantitative analyses were performed in wave-length-dispersive mode at an acceleration voltage 15 kV, and with a beam current 8 nA measured on a Faraday cup. The following components of silicate and phosphate minerals were analyzed by EPMA: SiO_2, TiO_2, Al_2O_3, Fe_2O_3, MnO, MgO, CaO, Na_2O, K_2O, SrO, Ce_2O_3, P_2O_5, F, Cl, and SO_3. Standards used were hematite (Fe-*K*α), rhodonite (Mn-*K*α), orthoclase (K-*K*α, Si-*K*α), wollastonite (Ca-*K*α, Si-*K*α for phosphate minerals), albite (Na-*K*α), corundum (Al-*K*α), scapolite (Cl-*K*α), rutile (Ti-*K*α), synthetic F-phlogopite (F-*K*α), MgO (Mg-*K*α), apatite (Ca-*K*α, P-*K*α), $SrSO_4$ (S-*K*α, Sr-*L*α), and $CePO_4$ (Ce-*L*α). Nearly 500 EPMA data were acquired from ten polished thin sections.

3.7. Secondary ion mass spectrometry (SIMS)

To study the distribution of the light element Li and of elements that occur at low concentrations and thus cannot to be easily detected by EPMA (e.g., B, Mg, Ba), time-of-flight (ToF) secondary ion mass spectrometry (SIMS) was used for one thin section, which was pre-characterized by optical microscopy and EPMA. In general, SIMS is a technique used for surface analysis (Vickerman & Briggs, 2001). Briefly, samples are bombarded with primary ions with typical energies of 1–30 keV, leading to a release of secondary particles from layers close to the surface in a so-called sputtering process. Besides electrons, these secondary particles are atoms and molecules, which are in part (approximately < 1 %) positively or negatively charged. These so-called atomic and molecular secondary ions (SI) are extracted with an electric field and then separated and detected in a mass analyzer. In this study, a ToF-SIMS IV instrument from ION-TOF equipped with a Bi-liquid metal ion source (LMIG) was used. The energy of the Bi^+ primary ions was 25 keV. A pre-sputtering with low-energy O ions (1 kV) was applied to the sample in order to remove the 20 nm carbon coating stemming from prior EPMA analysis as well as possible contaminations resulting from the preparation of the polished thin section.

To achieve a high sensitivity in combination with a high mass resolution ($m/\Delta m>4000$) and a moderate lateral resolution (~3-5 µm), the LMIG was operated in the "high-current mode", using Bi_3-clusters with a pulse length of <1 ns and a repetition rate of 10 kHz. Sample charging, resulting from the primary ion beam, was compensated by using low-energy electrons. More details of the ToF-SIMS analysis are given in (Vickerman & Briggs, 2001). To map the spatial distribution of the emitted elemental SI (beginning with H) and the characteristic molecules (e.g. SiO_x, AlO_x, PO_x) the primary beam was scanned over an area of 500 x 500 μm^2 using a pixel resolution of 256x256. If necessary, a higher lateral resolution (~200–400 nm) can be achieved using a different operational mode of the LMIG, if the lower detection sensitivity and mass resolution of this mode are acceptable. Because of the complex mechanism of the SI emission in contrast to other analysis methods (e.g. EPMA) no direct quantification of the measured SI intensities is possible. Therefore all images presented in this study display intensities rather than concentrations.

3.8. Inductively Coupled Plasma Mass Spectrometry (ICP-MS)

All samples were analyzed by inductively coupled plasma-mass spectroscopy (ICP-MS) in the laboratories of SGS Canada, Inc. (Method code: GE_ICM90A, ICP-MS preceded by Na_2O_2 fusion), in order to obtain additional element concentrations and to verify our own XRF data.

3.9. Ion Chromatography (IC)

Ion Chromatography (IC) was applied by using a Dionex DX 120 ion chromatograph to determine concentrations of cations and anions present in the leach liquors.

Chapter 4. Geological setting

The La Vi mining region is located in the Ba To district, situated in the southwestern part of Quang Ngai Province, Central Vietnam (Fig. 4.1). It spans an area between 14°44'15" and 14°47'45" latitude (Gauss net), and between 108°51'05" and 108°55'18" longitude (Thong *et al*., 2009). It is characterized by the occurrence of granitic rocks, which contain Li and tin (Sn) in the areas of Dong Ram and Nuoc Giap area (Fig. 4.2). These rocks contain economically viable Li_2O concentrations (0.21–1.44 wt. %) in the Dong Ram; whereas in the Nuoc Giap area the rocks contain economic concentration of tin (0.1-0.3 wt. %).

The Kan Nack complex (Fig. 4.2) is a suite of Archean and Paleoproterozoic metamorphic rocks, which covers an area of about 30 km^2 in the centre, south, and southeastern part of the La Vi region (Tinh, 2011). Six rock types can be distinguished in the Kan Nack complex: mafic granulites, gabbro-amphibolites, gneissic pyroxene, biotite gneiss interlayered with marble, quartzite, crystalline schist, and aluminum-rich crystalline schist. Lithium-rich minerals occur in pegmatoid granites, which cross-cut the metamorphic Kan Nack complex in the southeastern part of the La Vi mining district, near Dong Ram (Fig. 4.2) (Thong *et al*., 2009).

The Triassic Sa Huynh complex is a granitic pluton with a surface exposure of 38 km^2 in the northern part of the La Vi region (Fig. 4.2). It consists of two distinct units, formed during different intrusive phases: the phase-1 rocks comprise mostly biotite-granite, with subordinate amounts of coarse-grained two-mica-granite, they occur in the northern part of the La Vi mining district, and consist mainly of plagioclase, potassium feldspar, quartz, biotite, and muscovite, as well as accessory ilmenite, garnet, monazite, apatite, and zircon (Thong *et al*., 2009). The phase-2 rocks comprise a biotite-granite, a fine-grained two-mica-granite, and a leucogranite, all of which only occur as small stocks, with individual surface areas of 0.1-1 km^2, in the Nuoc Giap area (Fig. 4.2). The mineral components are the same as in the coarse-grained phase-1 granite, but the

abundances of quartz, muscovite, and garnet are higher (Tinh, 2011). In addition to these two main intrusive rocks, there are numerous leucocratic aplitic and pegmatitic granites, which belong to the Sa Huynh complex but occur as dikes that crosscut the Ka Nack complex (Fig. 4.2). These rocks display various, level of greisenization and are the main sources of tin and rare metals in the Dong Ram area and in the Nuoc Giap area.

The Dai Nga formation overlies both the metamorphic Kan Nack complex and the Sa Huynh granitoids, and consists of Miocene basalts (Cau *et al*., 2004). This formation, which occurs in the SW part of La Vi mining district in 3 km^2, is characterized by a lower plagio-basalts layer and as upper olivine basalts layer, which are separated by thin clay layers (Thong *et al*., 2009).

Overlying the Miocene Dai Nga formation are other olivine basalts, which have formed during the Pliocene Pleistocene, which occur in the center and in the north part of La Vi mining district (Thong *et al*., 2009).

The Quaternary is represented by mostly fluviatile alluvial rocks, and consists of sandstone, gritstones, and conglomerates (Tinh, 2011).

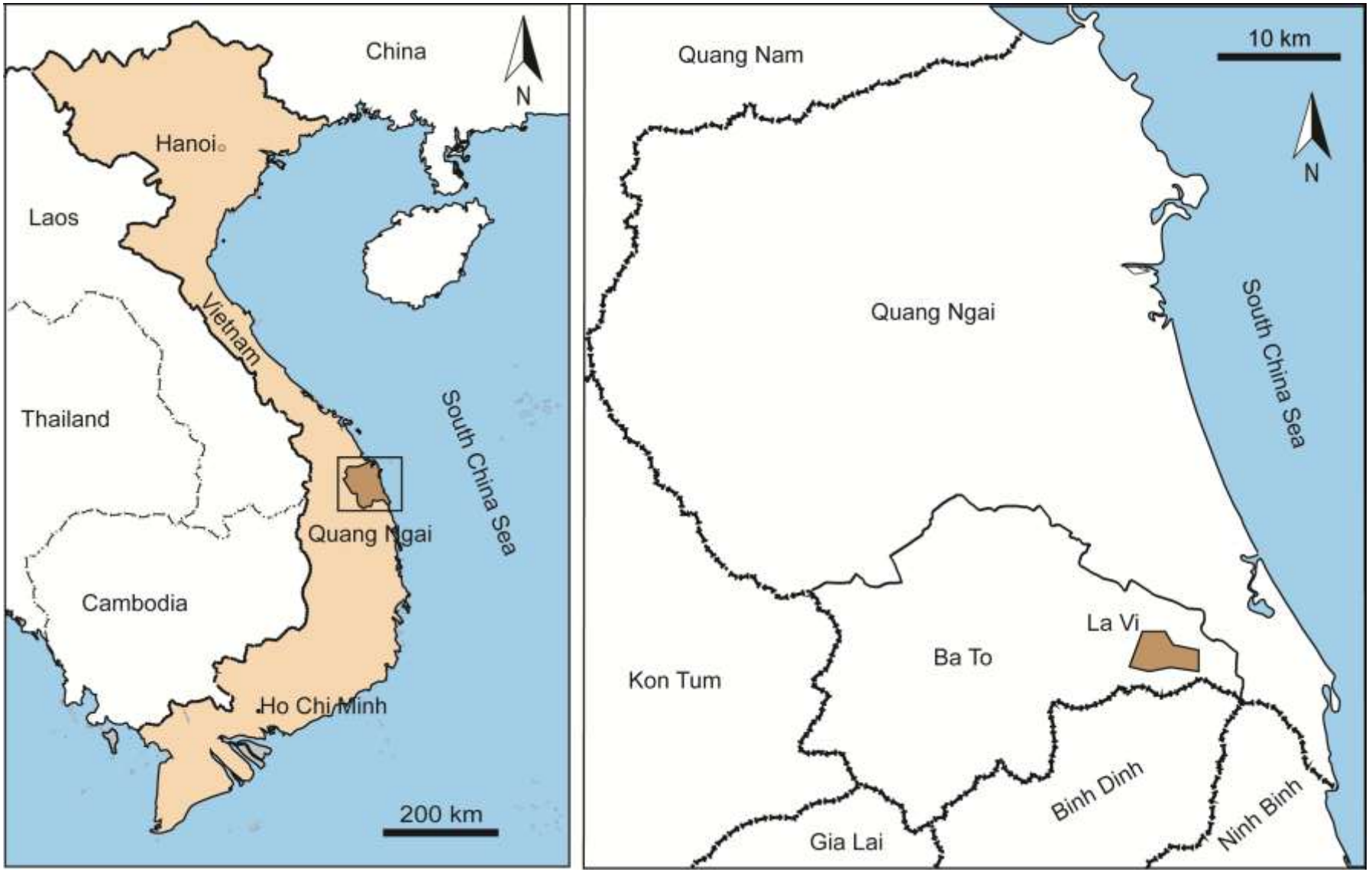

Figure 4.1. Map showing the location of the La Vi mining district in the Quang Ngai Province, Vietnam.

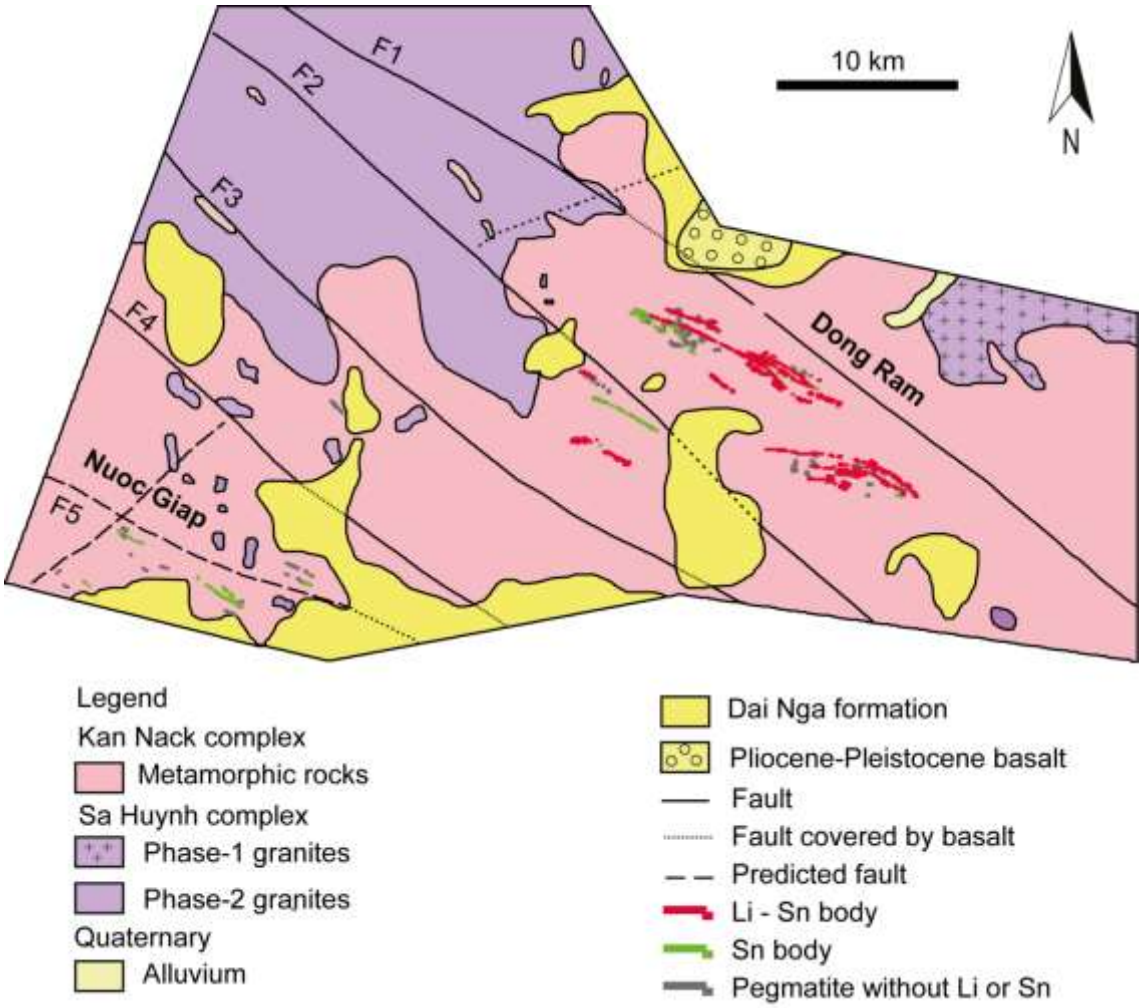

Figure 4.2. Simplified geological map of the La Vi mining district, showing the main geological units and the areas of Dong Ram and Nuoc Giap, where the Li-Sn and Sn ore bodies occur, respectively. Map complied from Thong *et al*. (2009).

The mineralization in the La Vi mining district took place in three stages:

(1) Pegmatitic stage: during this stage, rare-metal bodies were formed at temperatures between 617 ºC and 520 °C. These ore bodies are either pegmatoid or fine-grained granites and contain Li and Be veins, which consist essentially of potassium feldspar, plagioclase, quartz, biotite, and muscovite, as well as of the accessory minerals ilmenite, garnet, monazite, apatite, and zircon (Tinh, 2011).

(2) Postmagmatic stage: cassiterite-rich greisens were formed in the granitic rocks during this stage, between 490 ºC and 305 °C. The greisens occur predominantly south of Dong Ram and in the Nuoc Giap area (Fig. 4.2). The mineral assemblage of these

rocks comprises quartz, muscovite, residual plagioclase, and cassiterite (Cau *et al*., 2004).

(3) Hydrothermal stage: characteristic of this last stage are quartz-cassiterite veins, which were formed between 294 ºC and 210 °C (Cau *et al*., 2004).

The La Vi mining district is crosscut by a NW-SE-directed fault system (Fig. 4.2), known as the Ba Trang-Nui Chua system (Tinh, 2011), which cuts through both the plutonic and metamorphic rocks. This fault system plays an important role in controlling the orientation of the greisen-cassiterite and rare-metal veins, which are located in the southwestern part of the Dong Ram area (Fig. 4.2). The Ba Trang-Nui Chua system comprises five major faults (Thong *et al*., 2009), as shown in Figure 4.2:

(F1): the orientation is NW-SE, with a 50-60 ° dip to the north.

(F2): this fault, showing the same orientation as F1, crosscuts the granites of the Sa Huynh complex and was overlain by basalt cap of Dai Nga formation.

The pegmatoid bodies rich in Li and Sn, discovered in the Ka Nack complex, occur mostly between F1 and F2 and display a similar orientation as F1 and F2 (Fig. 4.2).

(F3): this fault is subparallel to F1 and F2, crosscuts the granites of the Sa Huynh complex, and was covered by the basalt of the Dai Nga formation.

Some pegmatoid bodies containing Li and Sn and coarse-grained pegmatoid bodies occur between F2 and F3 in the metamorphic rocks of the Ka Nack complex (Fig. 4.2).

(F4): parallel to F3, the F4 fault controls the SW part of the La Vi mining district and crosscuts the schistose rocks of the Ka Nack complex.

(F5): this fault is subparallel to F4, crosscuts the granitic rocks of the Sa Huynh complex, and was overlain by the basalt of Dai Nga formation.

In addition to the Ba Trang-Nui Chua system, there is the Ba To-Gia Vuc fault system, which interferes with the development of Ba Trang-Nui Chua system in the southwestern part of the La Vi mining district (Fig. 4.2).

Chapter 5. Bulk-Rock and Mineralogical Composition of the La Vi Ores

5.1. Bulk-Rock Composition

The bulk-rock XRF and AAS data reveal that the studied rock samples from the Dong Ram area are composed mainly of SiO_2, Al_2O_3, Na_2O, K_2O, and Li_2O (Table 5.1). The Li_2O content ranges from 0.54 to 2.15 wt.%, with an average value of 1.3±0.9 wt.% (*n* = 6). The rocks are further characterized by high Al_2O_3 (average: 17.4±0.8 wt.%) and Na_2O (average: 4±1 wt.%) contents. The latter are as high as those of K_2O. Based on the total alkali and SiO_2 contents, all samples fit in the granite field (Fig. 5.1) of the total alkali *vs*. silica (TAS) plot of Cox *et al.* (1979). Moreover, these granites are also relatively rich in F (average concentration: 1.3±0.8 wt. %), with concentrations ranging up to 2.19 wt.% (LAV04), and exhibit rather high P_2O_5 contents (average: 0.5±0.2 wt.%). On the other hand, the granite samples from Dong Ram are characterized by extremely low contents of TiO_2, and MgO (both ~0.01 wt.%) as well as total Fe_2O_3 (average: 0.11±0.03 wt.%). They further contain only small amounts of MnO and CaO (average contents: ≤0.2 wt.%).

In the (Na_2O+K_2O-CaO) *vs.* SiO_2 diagram of Frost *et al.* (2001), the granites from the La Vi mining district plot mostly along the boundary between alkalic and alkali-calcic granites (Fig. 5.2). Moreover, they have a peraluminous bulk composition (Fig. 5.3), as documented by the molar Al_2O_3 to ($CaO+Na_2O+K_2O$) ratio, which is considerably greater than 1.0 for all samples (Table 5.1) and has an average value of 1.6±0.2.

Notable among the trace elements are Rb and Cs, which occur in relatively high concentrations (up to 4360 ppm and 376 ppm, respectively; see Table 5.1). The analytical data obtained for the 8 major and the 21 trace elements, which were analyzed by both ICP-MS and XRF, were in excellent agreement, except for minor components of Y, Ba, La, Ce, and U). For all trace elements in Table 5.1 was chosen in the list of the ICP-MS data. On the other hand, the contents of base metals, such as Ni and Cu, are exceedingly low, typically below the ICP-MS detection limit. Tin contents vary

between 88 and 708 ppm. The average Nb content is 60±20 ppm, higher than that of Ta (50±20 ppm), whereby the average Nb/Ta ratio is 1.1±0.4.

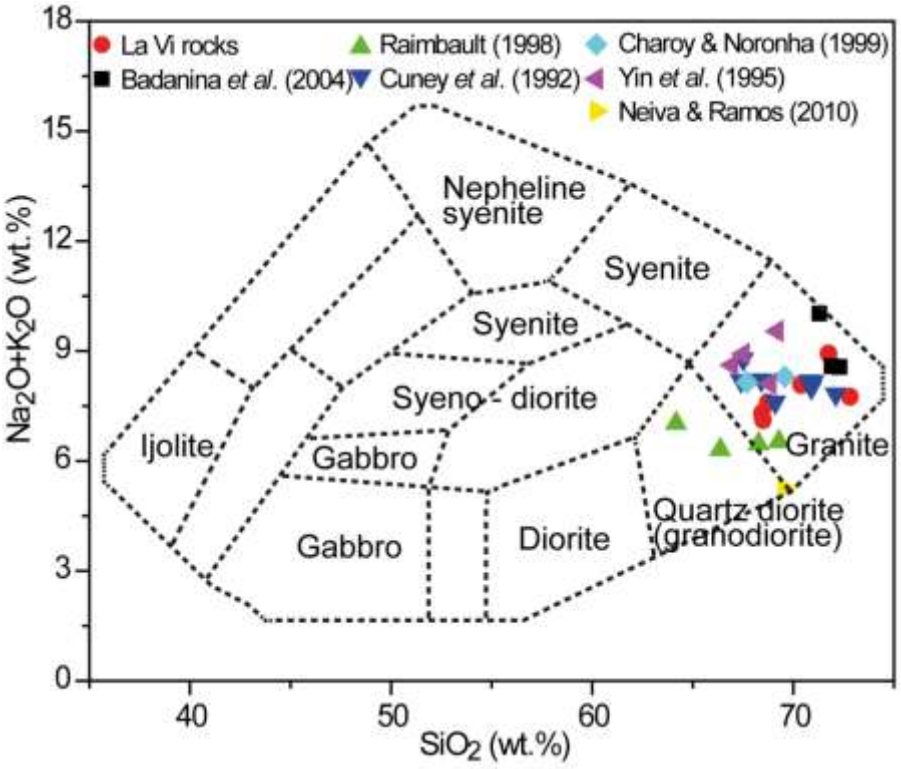

Figure 5.1. Total alkalis vs. silica (TAS) diagram showing the classification of plutonic rocks after Cox *et al*. (1979) and displaying the chemical data (in wt.%) for the Dong Ram rocks in comparison with literature data for other albite-topaz-lepidolite granites.

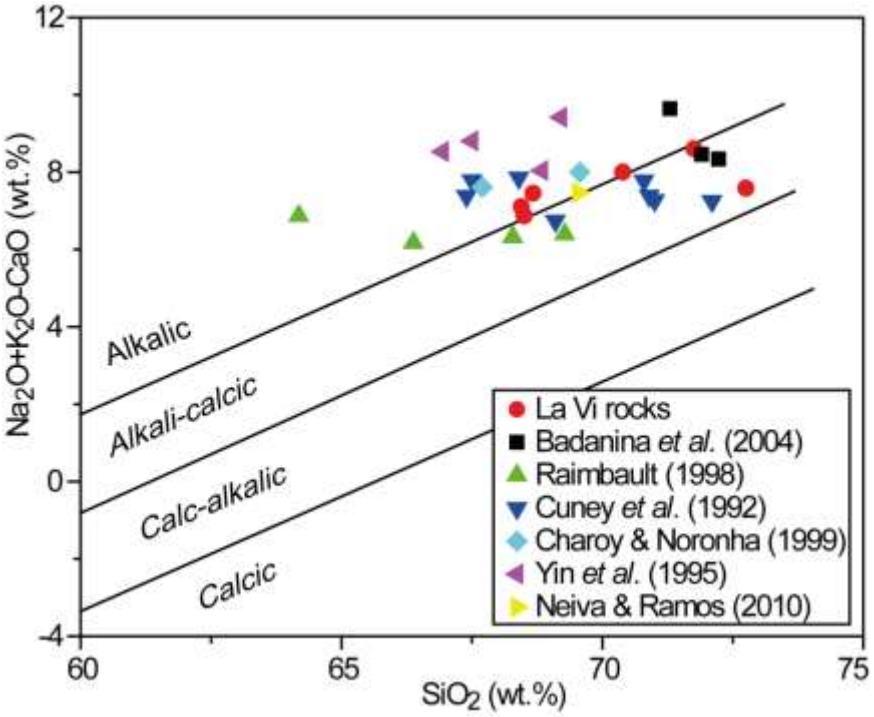

Figure 5.2. $Na_2O + K_2O – CaO$ *vs*. SiO_2 diagram displaying the chemical data (in wt.%) for the Dong Ram rocks in comparison with literature data for other albite-topaz-lepidolite granites. Diagram after Frost *et al*. (2001).

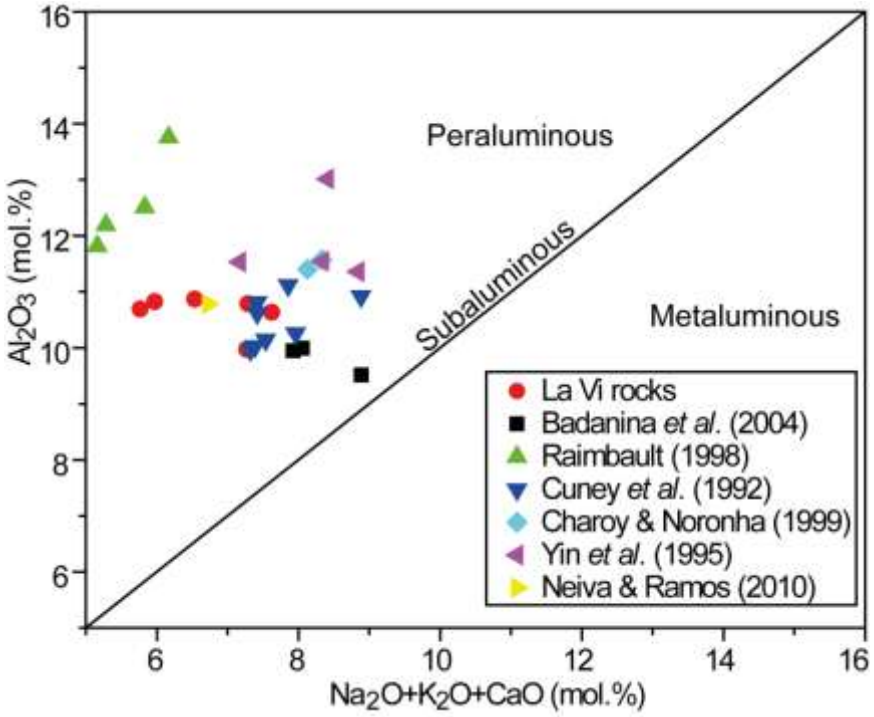

Figure 5.3. Classification diagram after Černý & Ercit (2005) showing the Dong Ram rocks in comparison with other albite-topaz-lepidolite granites (data from the literature).

Table 5.1. Bulk chemical composition of the granitic rocks from the Dong Ram area in the La Vi mining District, Vietnam.

wt.%	LAV01	LAV02	LAV03	LAV04	LAV06	LAV08
SiO_2	72.8	68.4	71.8	68.5	68.7	70.4
TiO_2	0.01	0.01	0.01	0.01	0.01	0.01
Al_2O_3	16.14	17.94	16.7	18.01	18.05	17.75
Fe_2O_3 tot	0.08	0.15	0.07	0.12	0.14	0.11
MnO	0.08	0.21	0.07	0.2	0.19	0.11
MgO	0.02	0.01	0.01	0.01	0.01	<0.01
CaO	0.17	0.10	0.42	0.15	0.14	0.07
Na_2O	5.46	3.23	2.75	3.10	4.24	5.56
K_2O	2.29	4.07	6.18	4.01	3.35	2.51
Li_2O	0.54	2.15	0.03	2.15	1.71	1.04
P_2O_5	0.36	0.65	0.55	0.63	0.65	0.19
F	0.55	2.05	0.08	2.19	1.60	1.35
H_2O	0.90	0.43	0.97	0.85	0.85	0.72
Total	99.4	99.4	99.6	99.9	99.6	99.8
ppm						
Be	406	0.316	1.27	0.169	0.919	0.111
S	30	151	14	127	61	38
V	8	12	5	10	11	5
Cr	31	36	23	33	33	14
Co	1	2	1	1	1	1
Ni	3	6	2	6	7	7
Cu	< 5	< 5	< 5	< 5	< 5	< 5
Zn	11	18	12	11	17	10
Ga	22	40	29	40	37	33
Ge	12	40	25	33	32	25
Rb	1252	4175	804	4183	3248	2151
Sr	28	25	74	26	34	31
Y	10	42	11	39	32	21
Zr	29	42	21	30	28	30
Nb	36	62	31	46	55	50
Mo	1	4	1	3	2	1
Sn	62	376	137	160	601	217
Cs	<200	270	<200	390	<200	<200
Ba	8	28	57	4	20	16
La	16	23	10	24	18	14
Ce	39	41	34	39	44	39
Hf	4	4	3	3	4	4
Ta	32	106	39	78	64	56
Tl	9	24	9	21	19	12
Pb	4	5	36	4	7	4
U	26	75	21	74	59	42
A/CNK	1.37	1.81	1.39	1.85	1.66	1.48

A = Al_2O_3, CNK = CaO + Na_2O + K_2O in molar quantities

5.2. Petrographic Features

The hand specimens of the granitic rocks from the Dong Ram area have a pinkish appearance, and are medium- to coarse-grained. When viewed with a petrographic microscope, the rocks stand out by consisting almost entirely of colorless minerals.

The mineral content was determined by using a combination of optical microscopy, XRD and subsequent Rietveld refinement, EPMA, and ToF-SIMS mapping of selected areas, which were previously investigated by electron microprobe (Appendix 1&2). The studied samples contain mainly albite (on average ~34 wt.%), quartz (~31 wt.%), and colorless micas (muscovite: ~34 wt.%; lepidolite: ~15 wt.%). The following minor minerals, listed in decreasing abundance, were identified: members of the amblygonite ($LiAlPO_4F$) – montebrasite ($LiAlPO_4OH$) series; herderite, $CaBePO_4(F,OH)$; fluorapatite; topaz, $Al_2SiO_4(F,OH)_2$; and cassiterite, SnO_2. In addition, the rocks also contain beryl, $Be_3Al_2Si_6O_{18}$, and goyazite, $SrAl_3(PO_4)_2(OH)_5 \cdot H_2O$, as accessory minerals. The mineral abundances vary in the different samples.

Albite and quartz are associated with the colorless micas. Albite is typically present as anhedral crystals, with a size of 0.5–1 mm and in many cases with lamellar twins (Fig. 5.4). Quartz is always anhedral and smaller than albite (150–500 µm across; Fig. 5.4, 5.5a, b, c, e).

The micas concentrate in large areas of the thin sections, where they form a fine-grained matrix, which surrounds albite and quartz and which is easily recognized in double-polarized light (Fig. 5.4a). They are colorless in plane-polarized light (Fig. 5.4d, f), may be anhedral or euhedral (Fig. 5.5e, f), and occur as small laths to large flakes. In double-polarized light, the micas are seen to form fringes around and between albite crystals (Fig. 5.4b), which they seem to overgrow (Fig. 5.4c). In some cases, the micas also enclose large quartz grains. In addition, the micas are in contact with topaz (Fig. 5.4e), cassiterite (Fig. 5.4f), and beryl (Fig. 5.5e). Frequently, the micas are also associated with phosphate minerals (Fig. 5.5b, d, f). There exist two chemically distinct types of colorless micas (see below), but it is almost impossible to distinguish between the two species optically. Therefore, the micas are not specifically labeled in Figures 5.4 and 5.5.

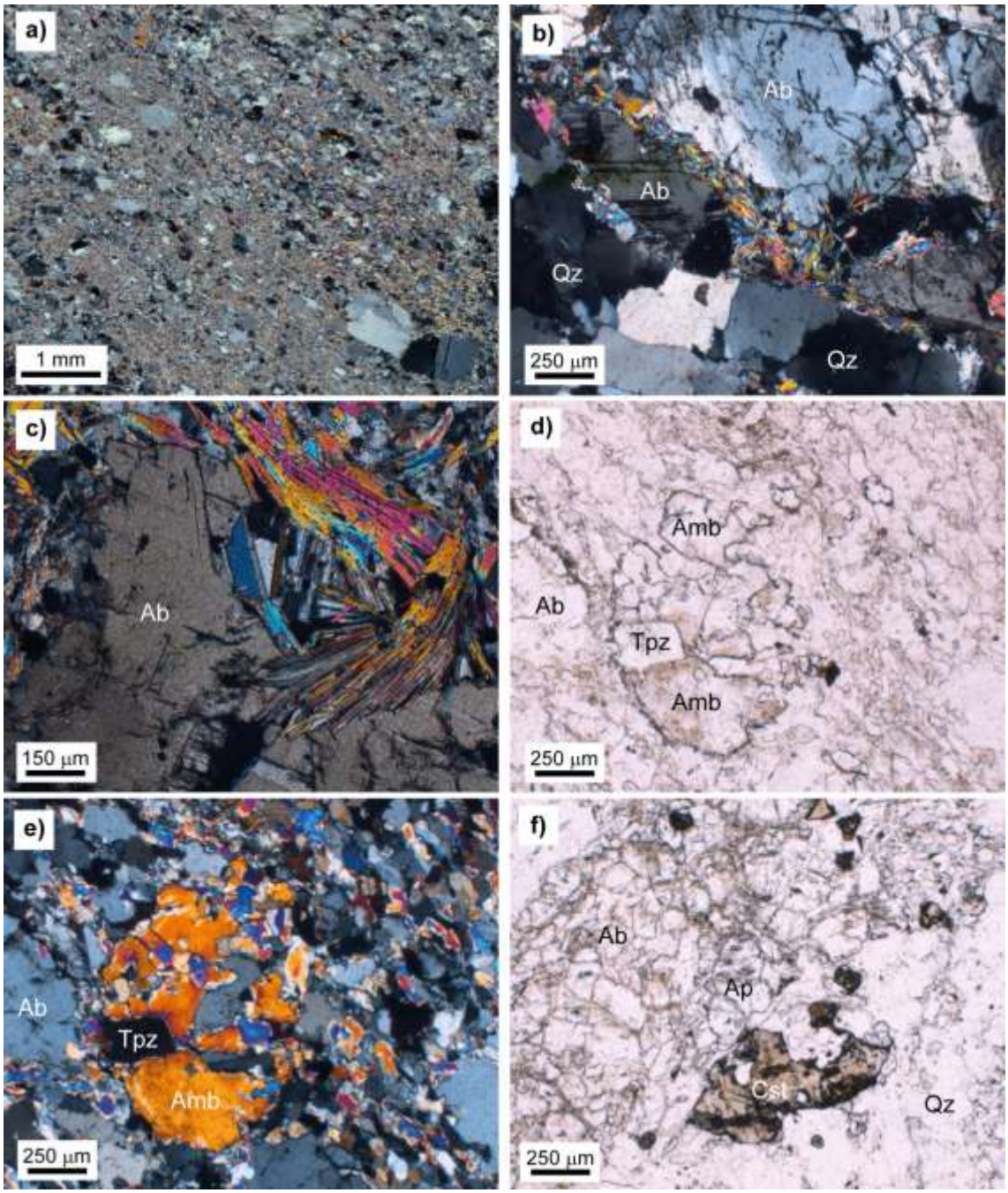

Figure 5.4. Photomicrographs of the granitic rocks from the Dong Ram area. All photographs, expect those shown in (d) and (f), were taken with crossed polarizers. a) overview showing typical appearance of the granitic rocks, where large albite and quartz crystals occur in a fine-grained matrix consisting of mostly micas, sample LAV02. b) micas forming rims around and between albite crystals as well as between albite and quartz, sample LAV03. c) close-up view of micas that appear to overgrow albite, sample LAV03. d) coexisting albite, quartz, colorless micas, and topaz, sample LAV02. e) same area as in (d), but viewed in cross-polarized light. f) coexisting albite, quartz, colorless micas, fluorapatite, and cassiterite, sample LAV05. The micas (Ms,

Lpd) are not further differentiated, because it is almost impossible to distinguish them optically. Abbreviations: Amb = amblygonite; all others according to Whitney & Evans (2010).

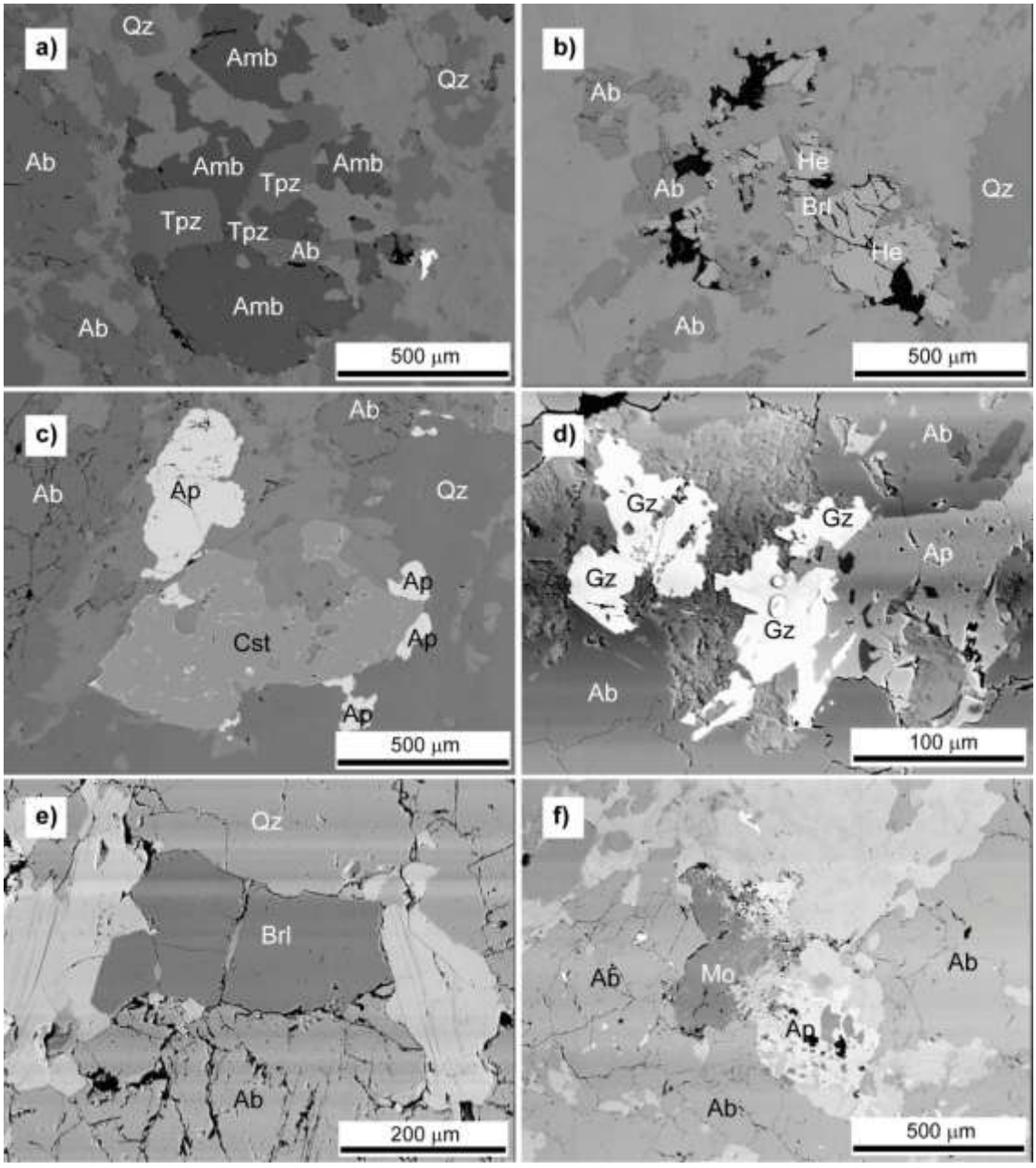

Figure 5.5. BSE images showing examples of the mineral assemblages in the granitic rocks from the Dong Ram area. a) amblygonite, associated with topaz, micas, albite, and quartz, sample LAV02. Image shows a detail of the photomicrographs displayed in Fig. 5.4d, e. b) large herderite grain surrounded by micas and associated with small beryl, albite, and quartz, sample LAV01. c) large cassiterite grain, partially rimmed apatite and associated with micas, albite, and quartz, sample LAV05. Image shows a detail of the

photomicrograph displayed in Fig. 5.4f. d) goyazite, fluorapatite, micas, and albite, sample LAV06. e) beryl associated with micas (bright), quartz, and albite, sample LAV08. f) montebrasite partially surrounded by fluorapatite and associated with micas and albite, sample LAV06. The micas (Ms, Lpd) are not further differentiated. Abbreviations: Amb = amblygonite; Gz = goyazite; He = herderite; Mo = montebrasite; all others according to Whitney & Evans (2010).

The amblygonite – montebrasite-series minerals occur typically in granite pegmatites (Dana *et al.*, 1951), and thus, it is not surprising that they were observed as minor minerals in four of six thin sections. They occur as relatively large (typically 250–700 µm across), anhedral crystals (Fig. 5.4d, e), which exhibit a dark grey contrast in BSE images (Fig. 5.5a). They exhibit a pale brownish absorption color (Fig. 5.4d) and typically a dark yellow interference color (Fig. 5.4e). These Li phosphates are in most cases associated with topaz, micas, and albite (Fig. 5.4d, e, and 5.5a), and occasionally also with fluorapatite (Fig. 5.5f). An example of the association amblygonite + topaz + albite + mica + quartz is shown as ToF-SIMS maps in Figure 5.6, where amblygonite and topaz can be distinguished easily because of the distinctly different intensities of the AlO^+, Na^+, PO^-, Li^+, and Si^+ signals. The Si^+ map mainly reveals the location of an albite crystal and several quartz grains, but in combination with the Na^+, Li^+, K^+, and Rb^+ maps also shows where mica is present (*e.g.*, upper left corner in each map of Fig. 5.6). The Li^+ map further reveals that mica exhibits lower signal intensity than amblygonite.

Herderite is present as medium-grained (150–300 µm across) and anhedral crystals, which exhibit a silver grey BSE contrast (Fig. 5.5b). This Ca-Be-phosphate mineral was found only in two thin sections (LAV01, LAV06), where it is associated with micas, quartz, albite, and beryl (Fig. 5.5b).

Fluorapatite is mostly fine-to medium-grained (10–70 µm across) and anhedral, but occasionally occurs as crystals that are up to 500 µm across (Fig. 5.4f, 5.5c). It is commonly observed as rim around, or coexisting with, other phosphate minerals (Fig. 5.5f), but is also associated with the colorless micas, albite, and cassiterite (Fig. 5.4f, 5.5c).

Topaz is typically associated with amblygonite/montebrasite. It is present as mostly euhedral crystals, which have a size of 150–250 µm. Topaz appears colorless in single-polarized light (Fig. 5.4d) and is relatively dark grey in BSE images (Fig. 5.5a).

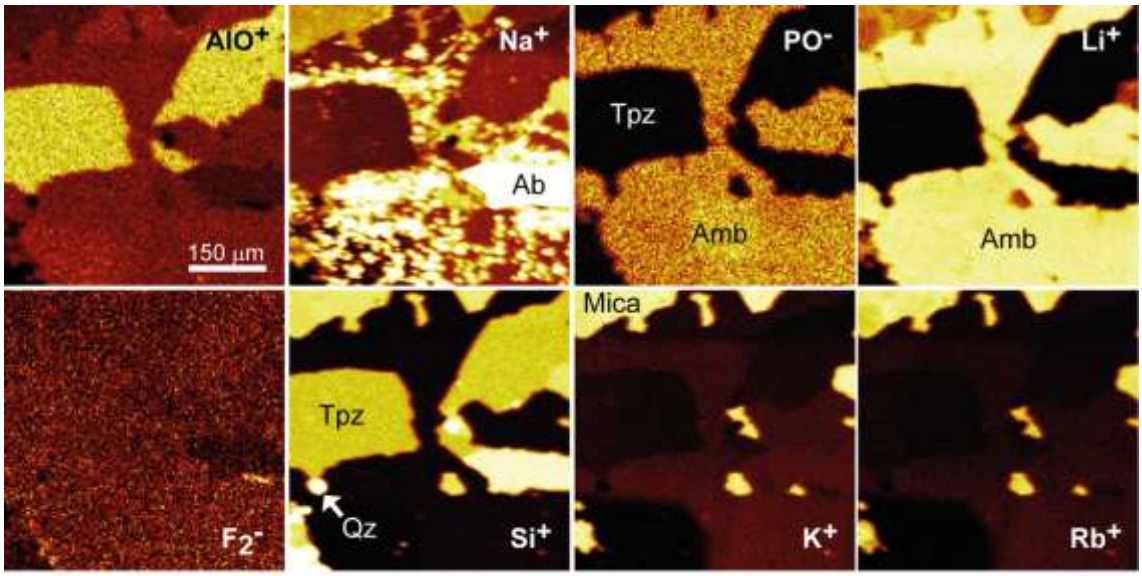

Figure 5.6. ToF-SIMS maps showing SI signal intensities, which can be assigned to mica, topaz, amblygonite, albite, and quartz. Maps show a detail of the view displayed in Figure 5.5a. Abbreviations: Amb = amblygonite; all others according to Whitney & Evans (2010).

Cassiterite is the only colored mineral observed in the thin sections, where it displays a dark brown absorption color (Fig. 5.4f). It is up to several mm across and displays an intermediate gray-scale contrast in BSE images (Fig. 5.5c). Cassiterite is only a minor mineral in the studied Li-rich granitic rocks of the Dong Ram area, in contrast to the rocks from the Nuoc Giap area, where it is one of the main minerals (Thong *et al.*, 2009). In the samples studied here, cassiterite was only observed in one thin section (LAV05).

Accessory beryl is present as medium-grained (~100 µm across), subhedral to euhedral crystals with a medium-dark grey color in BSE images (Fig. 5.5b, e).

Goyazite is a very rare accessory mineral in the Dong Ram area granites, where it was observed in only one out of ten thin sections. Here, it occurs as medium-grained (~60-100 µm across), anhedral, colorless crystals, which are associated with apatite, mica, and albite. In BSE images, goyazite displays a very bright contrast, much brighter than that of apatite (Fig. 5.5d).

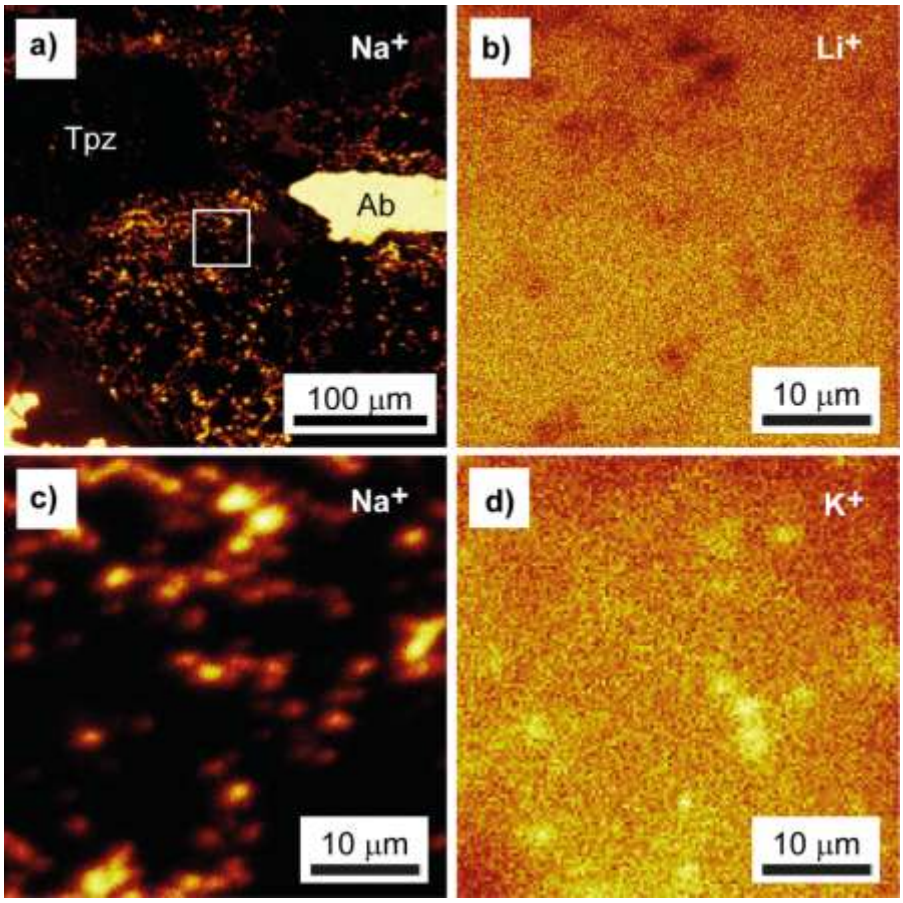

Figure 5.7. ToF-SIMS maps showing higher lateral-resolution maps for a detail of Figure 5.6. a) Overview of the area selected from Figure 5.6 (compare locations of topaz and albite crystals). White square indicates an area in amblygonite, which was mapped at even higher resolution and is shown as b) Li^+ map, c) Na^+ map, and d) K^+ map. Figure 5.10c clearly demonstrates that Na is not homogeneously distributed within amblygonite. The Na-enriched, Li-depleted domains are most probably inclusions of lacroixite. *Abbreviations:* Amb = amblygonite; all others according to Whitney & Evans (2010).

Chapter 6. Experimental Procedures for Lithium Extraction

Lithium chloride was produced from the Li-rich granites in the Dong Ram area, La Vi mining district. The process involved froth flotation to separate lithium minerals from gangue, roasting using gas-solid reaction at high temperature to extract lithium components, leaching to dissolve lithium compounds in distilled water, purification to remove other cations and anions except lithium, and recovery of LiCl from solution (Fig. 6.1)

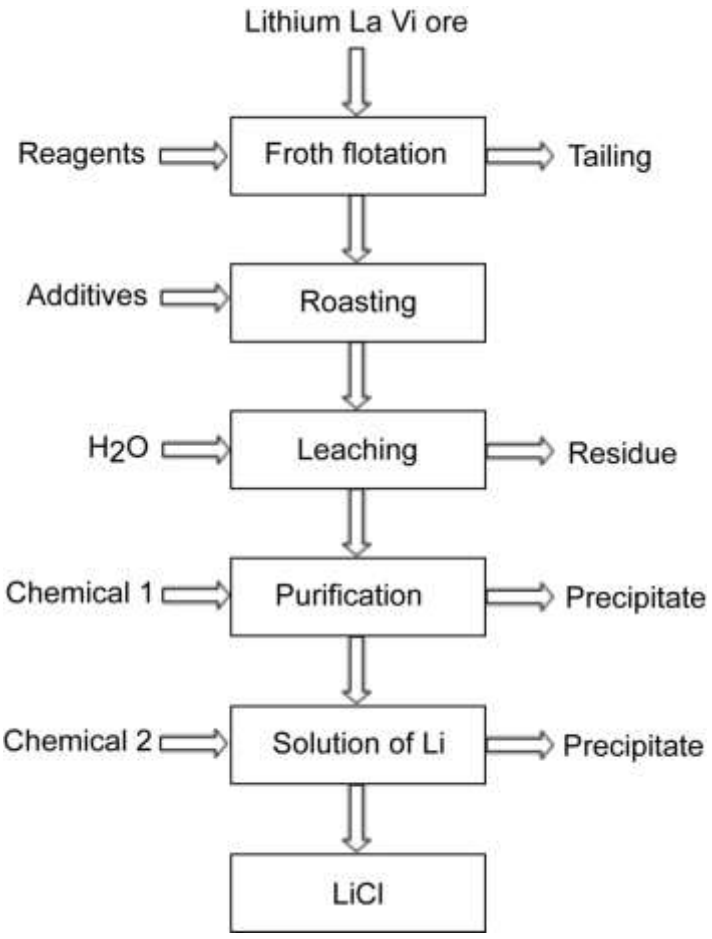

Figure 6.1. Flowchart of lithium extraction to produce LiCl from lithium La Vi ore

6.1. Recovery of lithium-mica from ore

Lepidolite concentrate was recovered from the Li-rich granites after the ore was crushed and milled, via froth flotation (Fig. 6.2). The flotation was conducted at a controlled pH using 600 g/t sodium silicate as depressant, Armax T ($C_{14}H_{31}NO_2$) collector and at a pulp density of 25 %. The slurry was first adjusted to the correct pH for 5 minutes. Then the depressant was added within 5 minutes, followed by the collector for 10 minutes and froth recovery within 10 minutes.

Cation collectors are more efficient to separate lepidolite directly via flotation than anion collectors. Armax T is a popular commercial collector which has high selectivity for lepidolite. Lithium ores from La Vi mine were milled to P90 of 75 µm, followed by flotation conducted according to the process shown in Fig 6.2. The pH of the medium was controlled at pH 3-4 by H_2SO_4.

Table 6.1 shows the chemical composition (in wt.%) of the main minerals in the concentrate products of froth flotation. In addition, a comparison between the chemical compositions of the rock samples and the products of froth flotation are shown in Table 6.2, Fig. 6.3 and Fig. 6.4. Samples MD1, MD2, TQ2 and TQ3 were recycled to previous stages, whereas TQ1 is the final concentrate (Fig. 6.2). The lepidolite concentrate contained reduced amounts of albite, quartz and topaz, but higher amounts of micas and lithium micas. The chemical data also document a significant increase in the contents of Li_2O, Al_2O_3, Fe_2O_3, K_2O and trace elements (especially Rb) of the lepidolite concentrate in comparison with the original rock samples using froth flotation for enrichment. Other components, however, decrease during this process (e.g., SiO_2, CaO, P_2O_5).

Table 6.1. Average analyses (in wt.%) and standard deviation in parentheses for concentrate samples (TQ1, TQ2, TQ3) of froth flotation (EMPA data).

Chemistry	Quartz (n = 19)	Albite (n = 17)	Topaz (n = 9)	Muscovite (n = 14)	Li-micas (n = 90)
SiO_2	100.5 (1.33)	68.9 (1.2)	32.8 (0.3)	45.8 (0.6)	51.0 (1.7)
TiO_2	n.a	n.a	n.a	0.01 (0.02)	0.01 (0.02)
Al_2O_3	n.a	20.1 (0.5)	56.4 (1.1)	37.8 (1.1)	26.1 (2.9)
FeO	n.a	0.02 (0.02)	n.a	0.04 (0.04)	0.07 (0.07)
MnO	n.a	0.01 (0.01)	n.a	0.2 (0.07)	0.8 (0.3)
MgO	n.a	n.a	n.a	0.01 (0.02)	0.01 (0.02)
CaO	n.a	0.1 (0.1)	n.a	0.01 (0.01)	0.02 (0.01)
Na_2O	n.a	11.4 (0.3)	n.a	0.6 (0.1)	0.3 (0.1)
K_2O	n.a	0.13 (0.04)	n.a	10.3 (0.3)	10.4 (0.3)
F	n.a	0.06 (0.03)	19.0 (0.4)	1.2 (0.4)	7.3 (1.5)
Cl	n.a	0.02 (0.03)	n.a	0.01 (0.01)	0.01 (0.02)
Li_2O*	n.a	n.a	n.a	0.3 (0.1)	5.1 (0.5)
H_2O*	n.a	n.a	0.91 (0.1)	4.0 (0.2)	1.3 (0.8)
O≡F, Cl	n.a	0.03	8.0	0.49	3.1
Total	100.5	100.7	101.1	99.8	99.3

* calculated after Galliski *et al.* (2012) for topaz, after Monier & Robert (1986) for muscovite, and after Tindle & Webb (1990) for Li-micas. Total Fe as FeO, n = number of points, n.a = not analyzed.

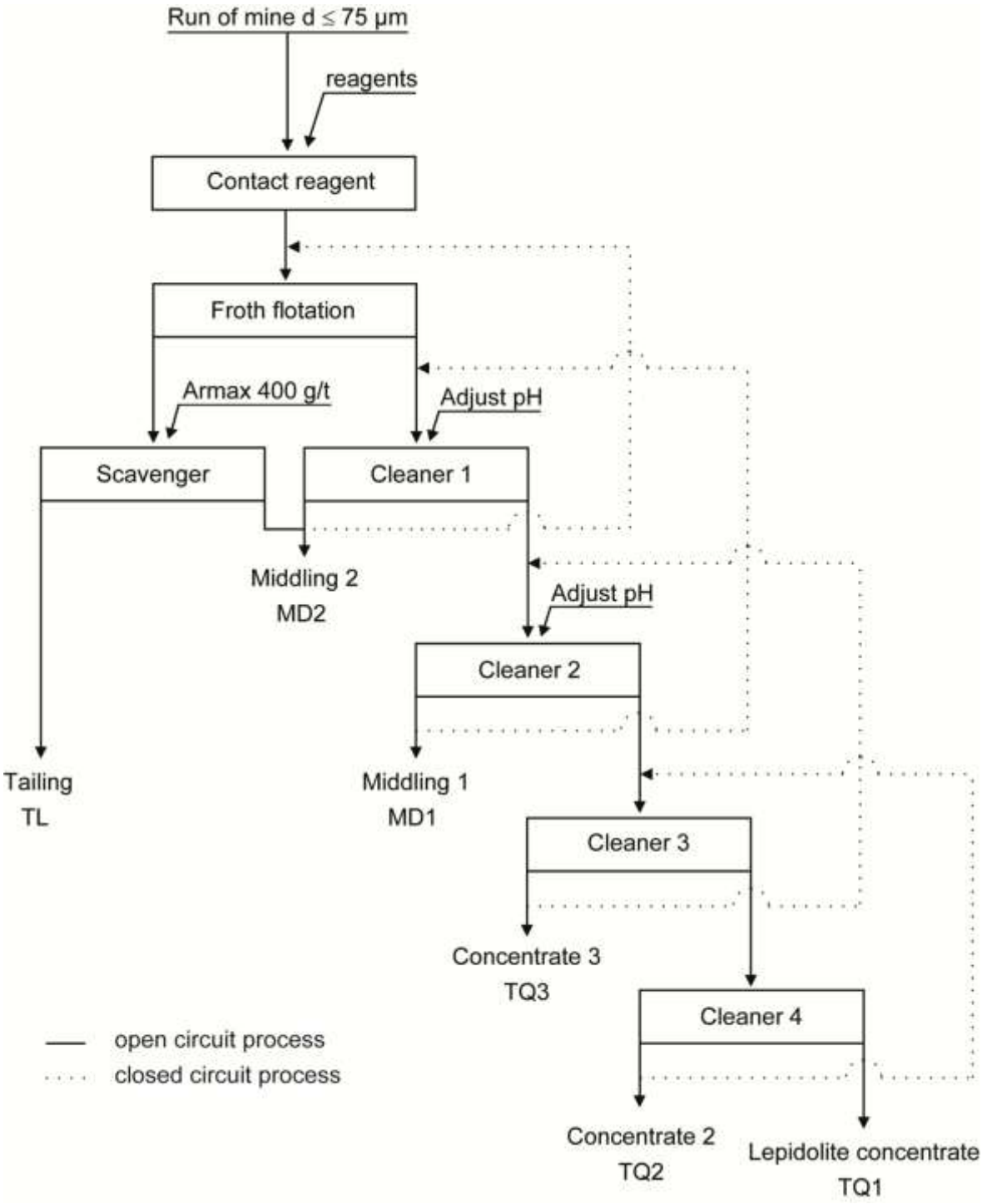

Figure 6.2. Flow-sheet of froth flotation of lithium silicates from the Dong Ram area (open and closed circuit).

Table 6.2. Bulk chemical composition (in wt.%) of major and minor elements of rock samples and products of froth flotation from the Dong Ram area in the La Vi mining District, Vietnam.

							LAV					
	TQ1	TQ2	TQ3	MD1	MD2	TL	01	02	03	04	06	08
						%						
LOI	5.49	6.20	5.00	4.75	4.51	3.03	2.17	2.54	1.54	2.49	1.50	1.66
Li_2O	3.34	3.21	3.03	2.88	2.35	1.32	1.62	1.91	0.01	1.94	0.53	0.93
SiO_2	54.67	52.99	54.91	56.28	60.25	67.71	69.51	69.20	71.97	69.29	73.14	70.87
Al_2O_3	25.10	24.40	24.95	24.61	22.60	19.03	18.08	17.96	16.68	17.95	16.17	17.77
Fe_2O_3 tot	0.35	0.37	0.38	0.38	0.32	0.22	0.10	0.08	0.06	0.10	0.06	0.09
MnO	0.50	0.48	0.44	0.41	0.33	0.18	0.19	0.20	0.07	0.21	0.08	0.11
CaO	0.08	0.07	0.11	0.13	0.18	0.19	0.14	0.15	0.42	0.10	0.17	0.07
Na_2O	1.56	1.48	1.93	2.17	3.14	4.61	4.23	3.11	2.78	3.23	5.49	5.54
K_2O	8.21	7.94	7.64	7.12	5.74	3.47	3.38	4.04	6.23	4.11	2.32	2.53
P_2O_5	0.28	0.24	0.36	0.41	0.45	0.54	0.64	0.63	0.55	0.66	0.36	0.20
						ppm						
Ga	73	70	72	66	57	40	31	24	69	23	25	29
Rb	7166	6677	7375	6096	5102	2874	32	39	11	42	10	21
Sr	38	52	39	50	56	45	25	26	19	33	23	27
Zr	15	17	14	20	21	32	29	31	68	38	21	36
Nb	78	82	82	85	79	66	64	78	39	106	32	56
Ba	58	61	56	57	45	31	59	74	21	75	26	42
U	120	116	120	104	62	38	32	39	11	42	10	21

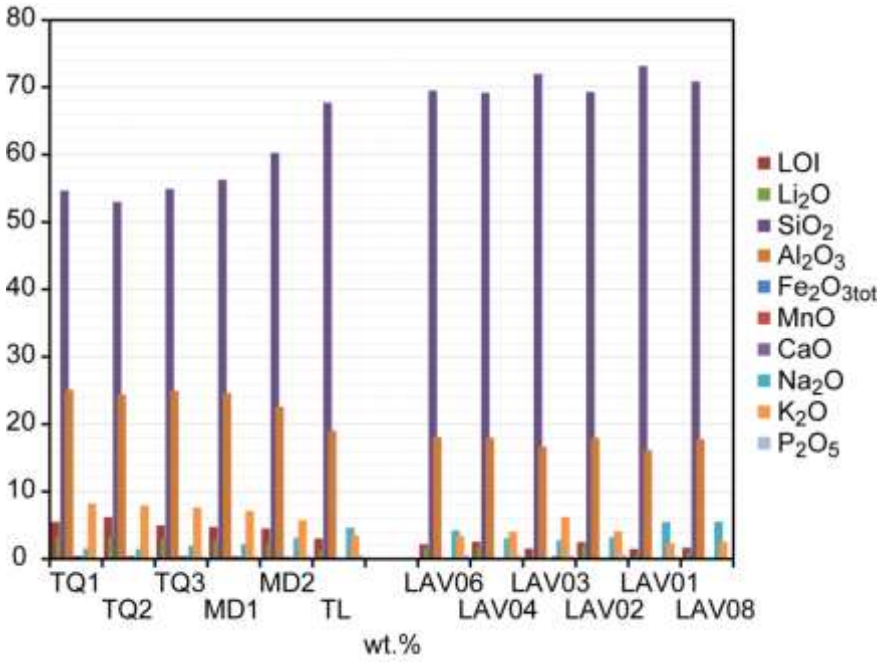

Figure 6.3. Comparison of major elements (in wt.%) of products of froth flotation and rock samples.

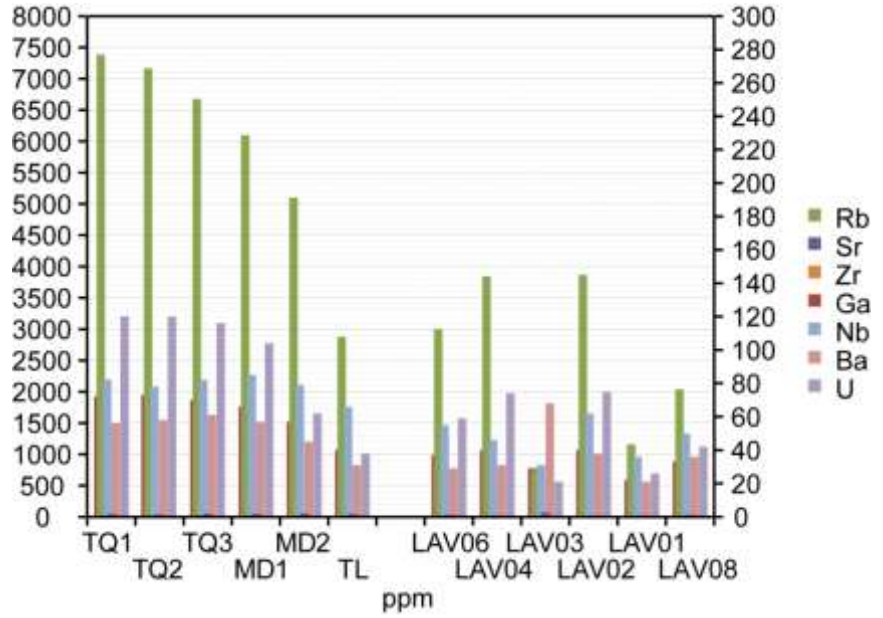

Figure 6.4. Comparison of selected trace elements (in ppm) of products of froth flotation and rock samples.

6.2. Roasting procedure

FeS and S were used to extract lithium from the lepidolite concentrate to produce lithium compounds which are easily dissolved in distilled water. A Nabertherm tube furnace with a gas trap system and gas supply was used for roasting the concentrate up to 1000 °C using ceramic crucibles.

The amounts of FeS or S were calculated based on S/Li molar ratios. CaO was added to prevent HF gas from escaping into the environment and preventing LiF formation and was tested at Ca/F molar ratios from 0.5:1 to 2:1. On the other hand, the mass of CaO used was sufficient for F removal as CaF_2. SO_2/SO_3 will react with redundant CaO to form $CaSO_4$, which will reduce the required SO_2/SO_3 for lepidolite roasting. The mixture of lepidolite and additives was roasted using ceramic crucibles in an open or closed system. The roasting temperature was chosen based on modeling results obtained from the Outotec's Chemical Reaction and Equilibrium Software HSC Chemistry (Outotec, 2011) for FeS or S, respectively.

HSC modelling indicates that roasting a lepidolite-FeS-CaO mixture should lead to the formation of $LiKSO_4$ and Li_2SO_4 as main lithium compounds, accompanied by hematite (Fe_2O_3), maghemite (Fe_2O_3(G)), $CaSO_4$, and other phases (Fig. 6.5). LiF is also generated although its amount is insignificant. Roasting lepidolite with the mixture of S and CaO resulted in $LiKSO_4$ and Li_2SO_4 as major solid compounds with a minor amount of $LiAlSiO_4$ (Fig 6.6a). In both cases, high quantities of SO_2 and SO_3 were liberated together with HF and LiF gases. Luong *et al*. (2014) suggested that SO_2/SO_3 formed during the decomposition of $FeSO_4.7H_2O$ played a key role in the extraction of lithium from lepidolite based on HSC modelling and LOI (loss on ignition) obtained from experiments. Similarly, roasting lepidolite with S or FeS would also create SO_2/SO_3 gases generated through oxidation as observed in Fig. 6.6. A gas-solid interaction of the gases with lepidolite was therefore also believed to be a factor controlling the extraction of Li in the form of $LiKSO_4$ and Li_2SO_4 in this study. The following reactions are predicted to take place during roasting of the mixture:

$$2FeS + 7/2O_2 \rightarrow Fe_2O_3 + 2SO_2 \text{ or } S + O_2 \rightarrow SO_2 \quad \text{(Eq. 6.1)}$$

$$SO_2 + 1/2O_2 \rightarrow SO_3 \quad \text{(Eq. 6.2)}$$

$$CaO + SO_3 \rightarrow CaSO_4 \quad \text{(Eq. 6.3)}$$

$$K(Li,Al)_3(Al,Si)_4O_{10}(F,OH)_2 + SO_3 \rightarrow Li_2SO_4 + LiKSO_4 + LiF \qquad \text{(Eq. 6.4)}$$

Equation (6.4) describes schematically (reaction is not balanced) the formation of the main products according to the HSC prediction (Fig. 6.5).

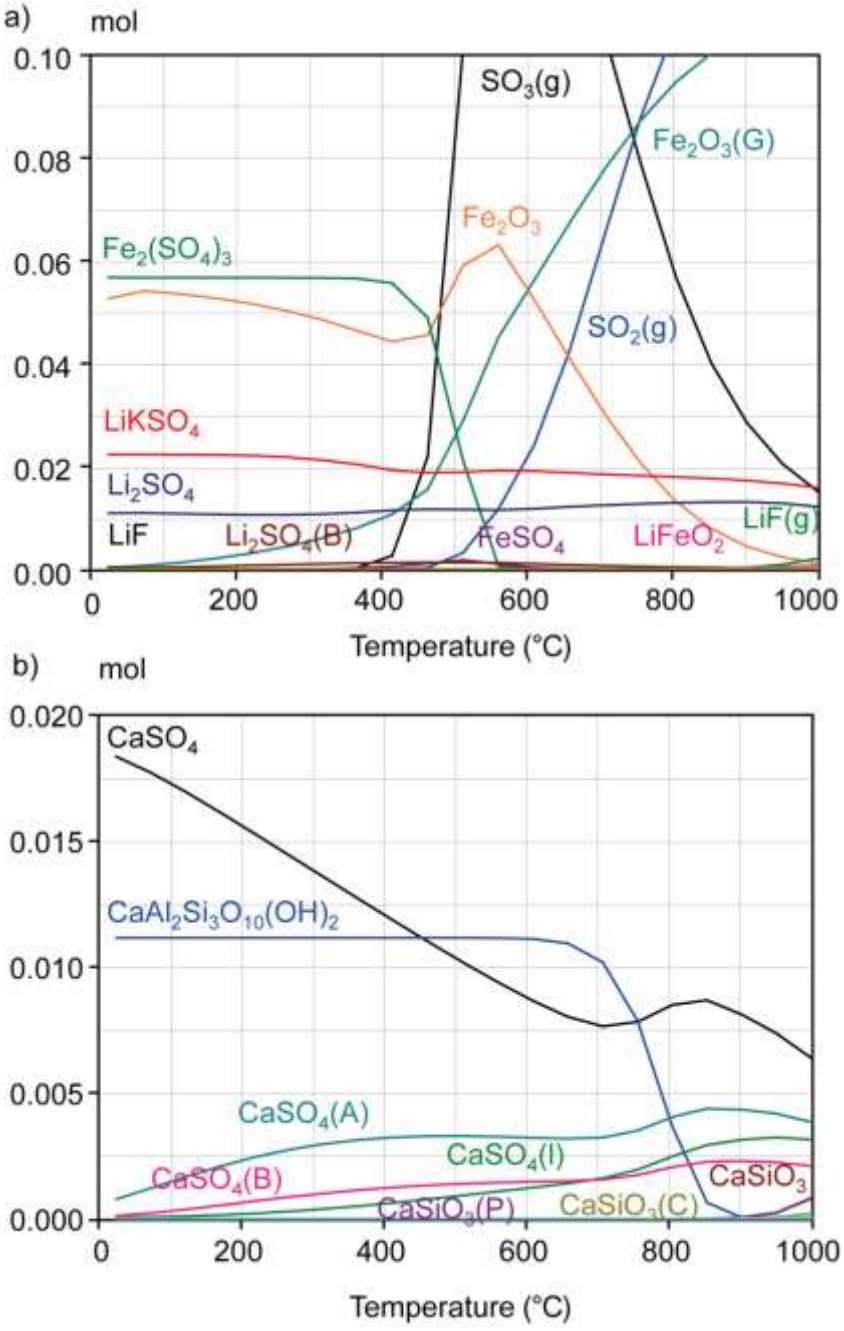

Figure 6.5. HSC models for roasting a mixture of lepidolite concentrate, FeS and CaO using FeS/Li and Ca/F molar ratios of 5:1 and 1:1, respectively. Abbreviations: A = alpha; B = beta; C = cyclowollastonite; G = gamma; g = gas; l = liquid; and P = pseudowollastonite. a) main new compounds of iron and lithium; b) new Ca compounds. Note different scales in the two diagrams.

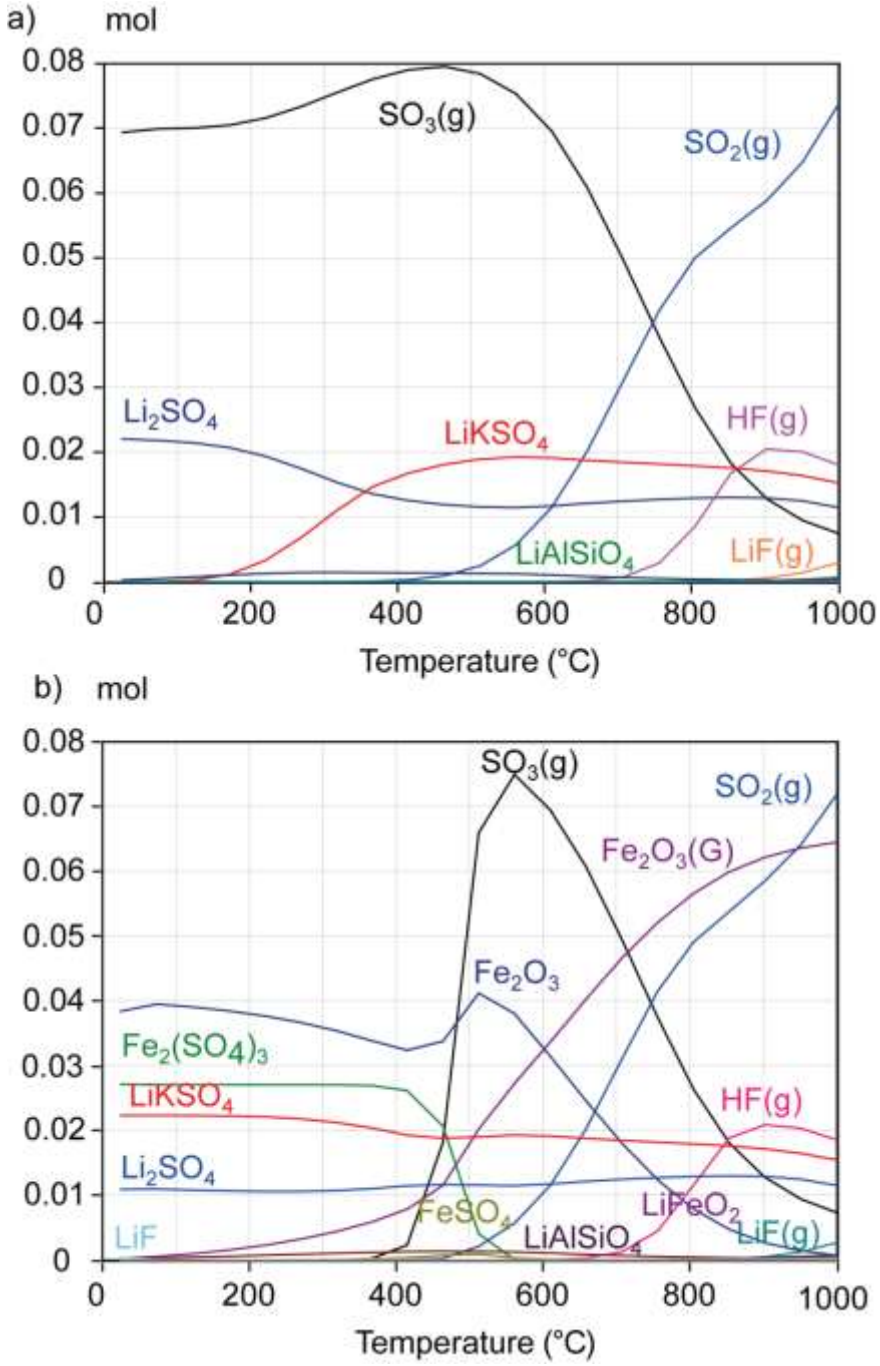

Figure 6.6. HSC models for roasting of a) lepidolite and S, b) lepidolite and FeS at S/Li molar ratio of 3/1. Abbreviation: G = gamma, g = gas.

Calcines after cooling to ambient temperature and grinding to powder for leaching step were evaluated by XRD. The masses of calcines and mixtures were weighed for mass balance.

6.3. Leaching procedure

The calcines were leached to release lithium compounds into the solution using distilled water. A magnetic stirring hotplate (operating range: 0-450 °C) was used for the leaching experiments. The slurries were contained in suitable beakers.

Known amounts of 10-50 g calcines were mixed with water based on the mass ratio of water/ calcine from 1:1 to 15:1. Reaction time (1-3 h, step 0.5 h) and temperature (ambient to 85 °C) were tested to determine the optimal conditions of leaching.

Leach liquors and residues were separated by filtering. Dried residues were weighed for mass balance while minerals in residues were identified by XRD. Li and F were analyzed by AAS and XRF. All ions (cations and anions) in the leach liquors were analyzed by IC and AAS.

6.4. Purification procedure

Purification steps were conducted to remove ions except alkaline cations in the leach liquors after water leaching. A caustic solution of 0.5 M NaOH was used to precipitate cations at controlled pH's. A 0.2 M $BaCl_2$ solution was used to remove sulphate ions as $BaSO_4$. 50-500 ml leach liquors were used for all purification tests.

Reactions were tested at different temperatures (from ambient to 60 °C) and times (0.5-3 h). Precipitates and the lithium solution were separated by filtering. Filtered precipitates were dried and then weighed for mass balance. The concentrations of remaining anions and cations in the lithium solutions were analyzed by AAS and IC.

Equation 6.5 shows the reaction between OH^- of NaOH and cations in the leach liquors for their removal via precipitation. Similarity, the reaction of $BaCl_2$ to precipitate SO_4 ions from the solution is shown in equation 6.6.

$$M^{n+}\,(aq) + nOH^-\,(aq) \leftrightarrow M(OH)_n\,(s) \qquad \text{(Eq. 6.5)}$$

$$BaCl_2\,(aq) + SO_4^{2-}\,(aq) \rightarrow BaSO_4\,(s) + 2\,Cl^- \qquad \text{(Eq. 6.6)}$$

6.5. Evaporation-Crystallization procedure

Brown *et al*. (1981c) indicated that, using solar evaporation for concentrating solutions containing lithium chloride will increase the concentration of LiCl to at least 40 wt.%. Crude salts were therefore heated preferably at 270 °C to 325 °C to reduce water to less than 0.5 wt.% before extracting with isopropanol to produce high purity lithium chloride.

The produced lithium solutions containing mainly Li and minor elements were placed in shallow glass dishes and evaporated at ambient conditions. The obtainable salts were monohydrate of alkali, which were then dried at 105 °C and 270 °C. Crude salts were weighed for mass balance and small amounts were sampled for AAS analysis.

The crude salts were leached in isopropanol based on techniques proposed by Brown *et al*. (1981b). Isopropanol leaching was conducted at ambient temperature and different times of 5-24 h, and weight ratios of isopropanol to salts were set from 5:1 to 10:1. Solids and solvents were separated by centrifugation (using Heraeus Primo centrifuge). The solvents were evaporated and dried until stable weights of lithium chloride monohydrate were achieved. Lithium chloride monohydrate was sampled to analyze ions by AAS and IC.

Chapter 7. Results and Discussion of Lithium Extraction Study

7.1. Mineral component of lepidolite concentrate

A lepidolite concentrate (90% particle size ≤ 75 μm, Fig. 7.1) containing 1.55 wt% Li with chemical composition as shown in Table 7.1 was produced using froth flotation. The XRD pattern of the concentrate indicates that it contains mainly lepidolite - $K(Li,Al)_3(Al,Si)_4O_{10}(F,OH)_2$ and albite - $NaAlSi_3O_8$ (Fig. 7.2b). The lepidolite concentrate will be used to extract lithium to produce LiCl.

Table 7.1. Chemical composition in wt.% of lepidolite concentrate.

SiO_2	Al_2O_3	Fe	Mn	Mg	Ca	Na	K	Cs	Rb	Li	P	F
54.67	25.10	0.25	0.39	0.6	0.71	1.16	6.82	0.063	0.8	1.55	0.12	2.91

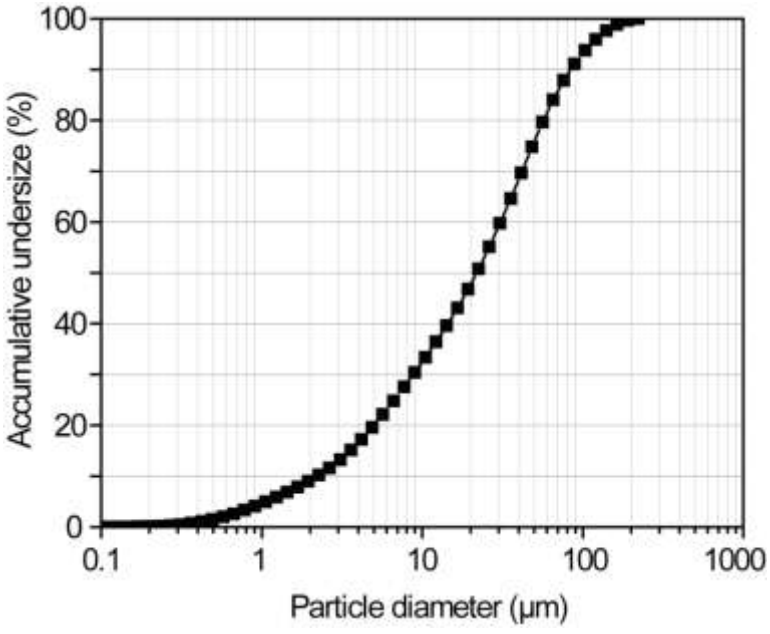

Figure 7.1. Particle size distribution of the lepidolite concentrate.

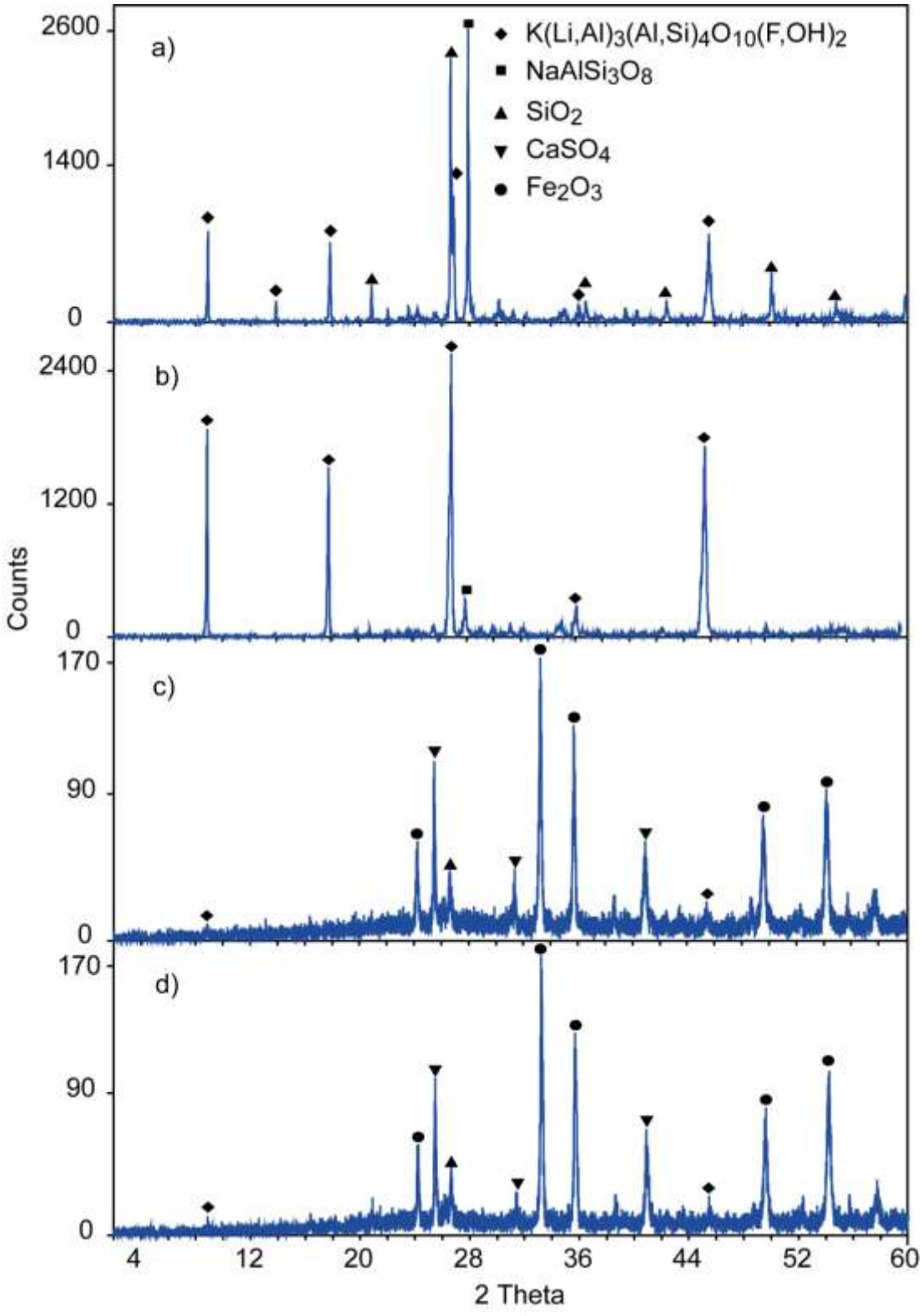

Figure 7.2. XRD patterns of a) La Vi ore; b) lepidolite concentrate; c) calcine after roasting at 750 ºC for 1.5 h and with molar FeS/Li and Ca/F ratios of 5:1 and 1:1, respectively; d) residue after leaching at 50 °C for 2 h with a water/calcine mass ratio of 10:1.

7.2. Roasting of lepidolite to extract lithium

Roasting of lepidolite-FeS-CaO mixtures destroys the lepidolite structure and converts the mix into mainly Ca sulphate, hematite and quartz, as confirmed by XRD (Fig. 7.2c, d). Optimal conditions of roasting for maximum lithium recovery during extraction will be determined in this section. Fig. 7.3 illustrates a) the mixtures of lepidolite and additives (bright) before roasting and hard calcine (red) in ceramic crucible; and b) the pulverized calcines.

Figure 7.3. Photos of calcines before and after roasted in roasting procedure a) the mixtures of lepidolite and additives (bright) and hard calcine (red) in ceramic crucible; b) the pulverized calcines.

7.2.1. Effect of FeS/Li molar ratio

The formation of SO_2/SO_3 gases during the oxidation of FeS in air is believed to be the key factor controlling the extraction of lithium from lepidolite via a gas-solid interaction as proposed by Luong *et al*. (2014) and Li *et al*. (2010&2011). The reaction of FeS and O_2 to generate these gases required the presence of large amounts of air during the roasting of the lepidolite-FeS mixture. An open-system roasting was therefore applied to promote the release of Li from lepidolite. Li_2SO_4 and $LiKSO_4$ were predicted to be the main soluble lithium compounds formed during the decomposition of lepidolite in

the presence of SO_3. Such products were also found during sulphation roasting of Li-bearing ores containing lepidolite (Luong *et al*. 2013&2014) and zinnwaldite (Jandová *et al*. 2009&2010, Siame and Pascoe 2011).

As shown in Fig. 7.4, the extraction of lithium increases sharply from ~36% to ~85% when the FeS/Li molar ratio is raised from 1:1 to 5:1. However, using a higher amount of FeS (at 7:1 molar ratio of FeS/Li) led to a decrease in the Li extraction from lepidolite.

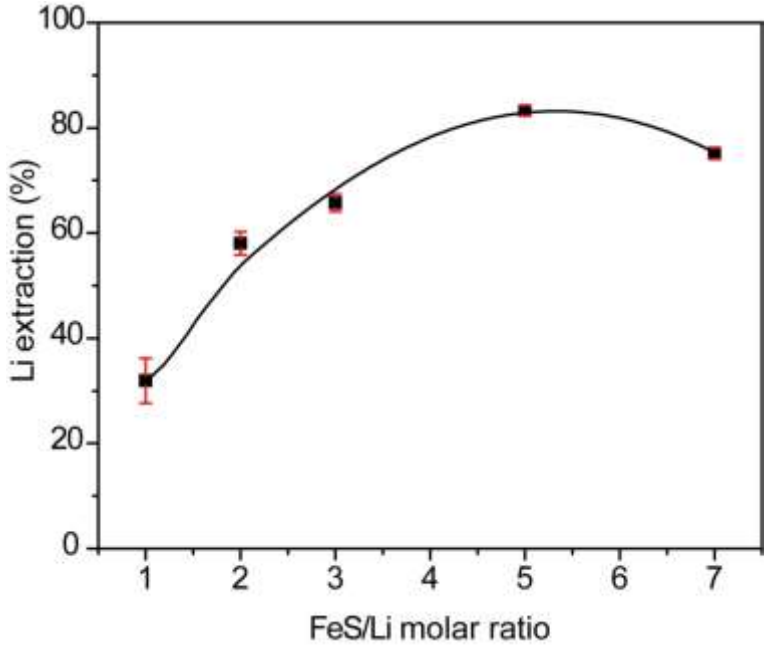

Figure 7.4. Effect of FeS/Li molar ratio on lithium extraction with the following conditions: Roasting at 750 °C, 1.5 h, Ca/F molar ratio of 1:1; and Leaching at 50 °C, 2 h, water/calcine mass ratio of 10:1. Reproducibility: ± 4%.

A mass balance based on analytical data obtained from two experiments and calculated for the feed of 100 kg lepidolite shows that the loss of Li into the gas phase is 10.7% of its initial mass (1.55 kg Li) in the feed (Fig. 7.5). In this mass balance, the amounts of gas were calculated by subtraction. A further 19.4% of the initial Li remains in the residues after leaching in these experiments. Of importance is the loss of SO_2/SO_3 from the furnace and captured in traps, which was calculated at 71.5% of the available S in the feed. The mass balance reproducibility for two experiments was ± 4% for Li, ±1% for S, and ±20% for F.

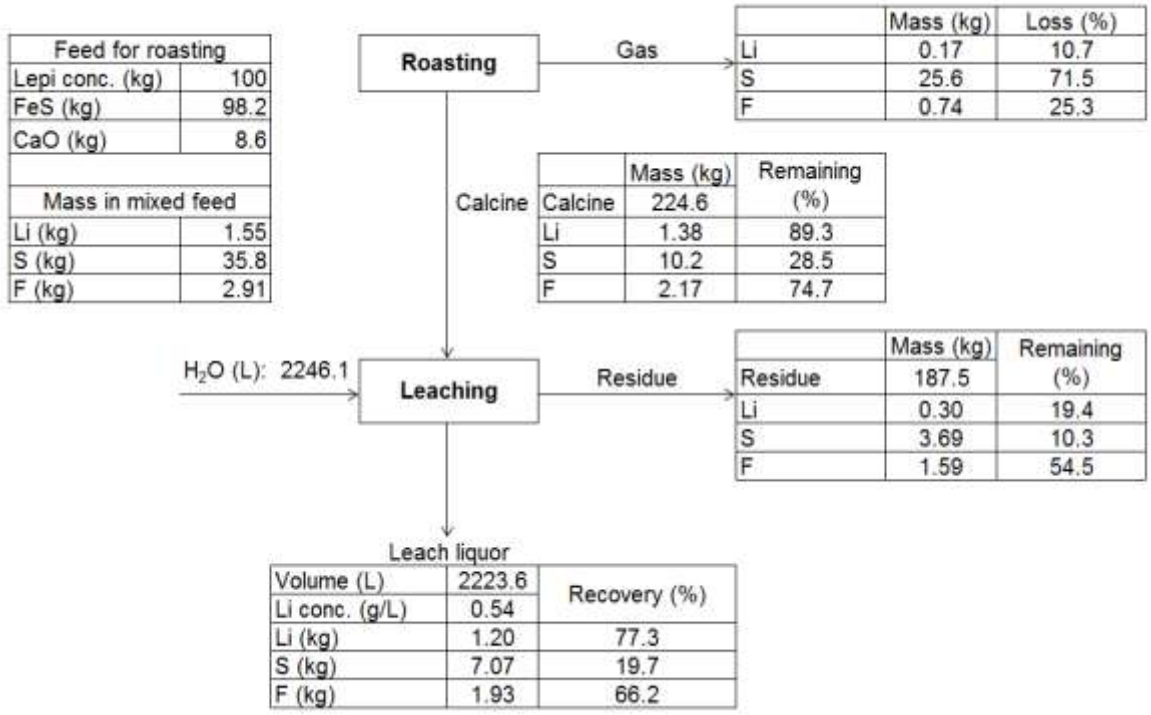

Figure 7.5. Mass balance for roasting and leaching based on 100 kg lepidolite concentrate. Roasting: 750 °C, 1.5 h, FeS/Li and Ca/F molar ratios of 5:1 and 1:1, respectively. Leaching: 50 °C, 2 h, water/calcine mass ratio of 10:1.

7.2.2. Effect of roasting temperature and time

The differential thermal analysis (DTA) profile of the lepidolite concentrate (Fig. 7.6a) shows two endothermic peaks: The first peak at 247.7 ^{o}C could correspond to the dehydration of lepidolite, whereas at the second endothermic peak (875.1 ^{o}C) a phase transformation from solid to gas could take place. This interpretation is consistent with the liberation of LiF and Li_3F_3 gases predicted by HSC modeling (Fig. 7.6b). Moreover, a total mass loss of ~3.4% was measured by thermo-gravimetric analysis (TGA) at 1000 °C (Fig. 7.6a), whereas HSC predicts that ~4.4% of the lepidolite mass could be lost due to the release of gaseous species during roasting at 1000 °C.

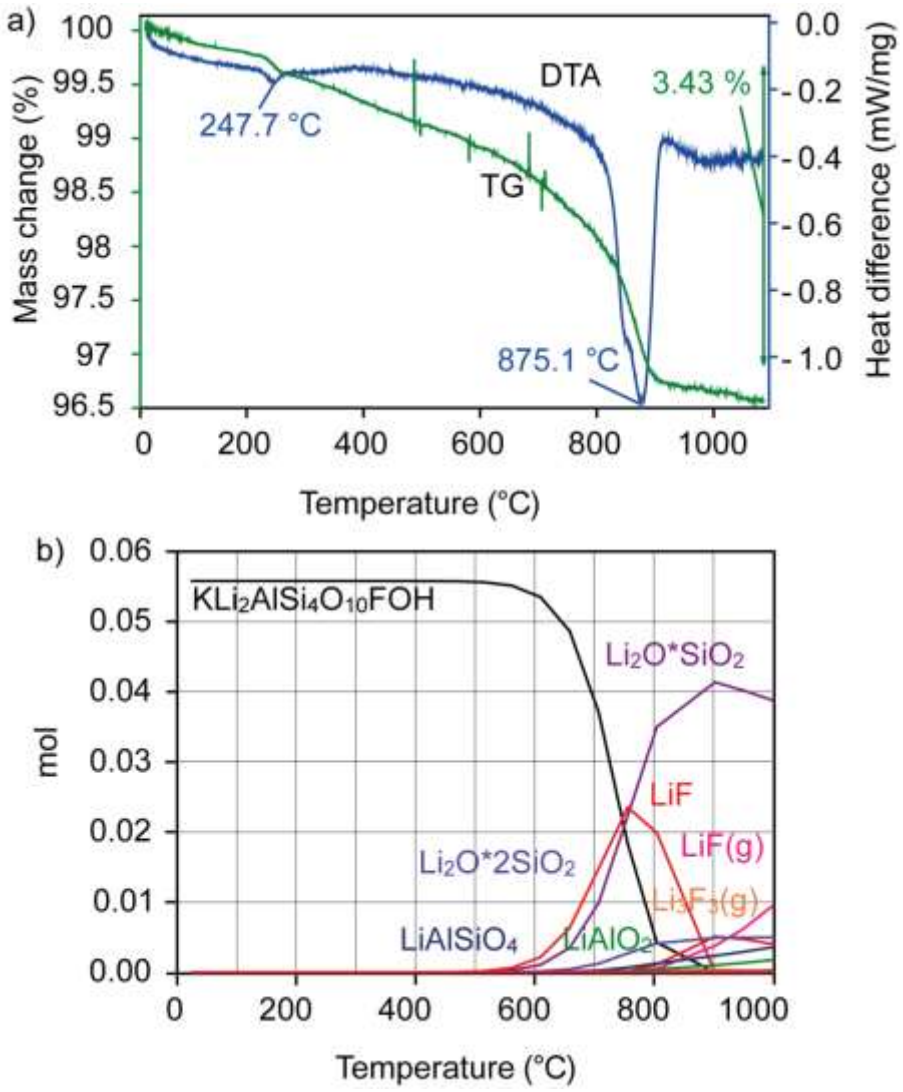

Figure 7.6. a) TGA-DTA profile and b) HSC model for roasting lepidolite concentrate without additives.

Roasting temperature is one of the major factors influencing the extraction of lithium from lepidolite. Based on the DTA profile and the HSC prediction, temperatures in the range of 700-850 ^{o}C were tested to determine the best condition for lithium extraction. Using a FeS/Li molar ratio of 5:1 and a water/calcine mass ratio of 10:1, it was found that roasting at 750 ^{o}C resulted in the highest extraction of lithium, where ~84% of Li was recovered after leaching (Fig. 7.7). Higher temperatures (800-850 ^{o}C) led to a reduction of the formation of leachable lithium compounds. This optimum temperature found in our experiments is lower than the range of 850-1000 ^{o}C required to maximize lithium extraction from lepidolite in other studies (Yan *et al*., 2012a,b&c; Luong *et al*., 2013&2014). This difference is not only caused by the different additives used, which results in different melting temperatures during roasting. It also results from differences

in the mineral concentrates, derived from different mines, because this raw material contains lepidolite of variable composition and consists of different amounts and types of minerals associated with the lepidolite. All these factors will control how efficient the Li extraction by various chemical reagents would be.

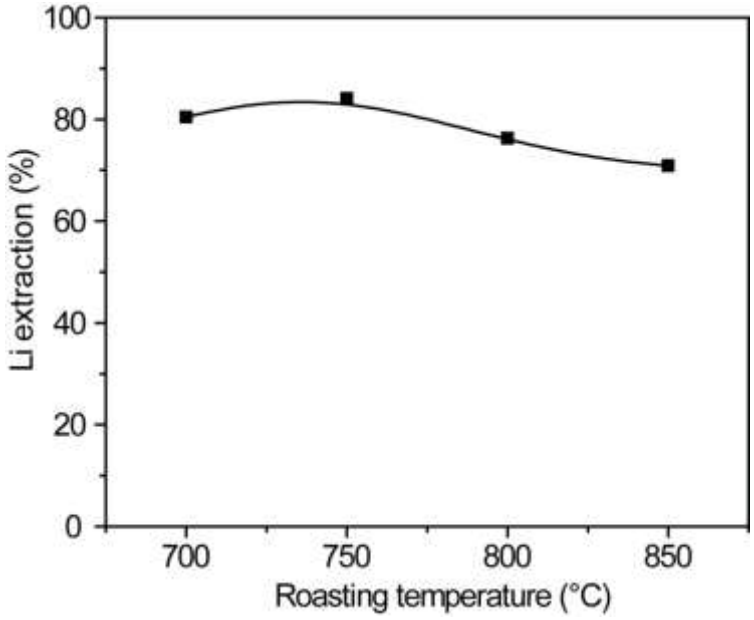

Figure 7.7. Effect of roasting temperature on lithium extraction. Roasting: 1.5 h, FeS/Li and Ca/F molar ratios of 5:1 and 1:1, respectively. Leaching: 50 °C, 2 h, water/calcine mass ratio of 10:1. Reproducibility: ± 4%.

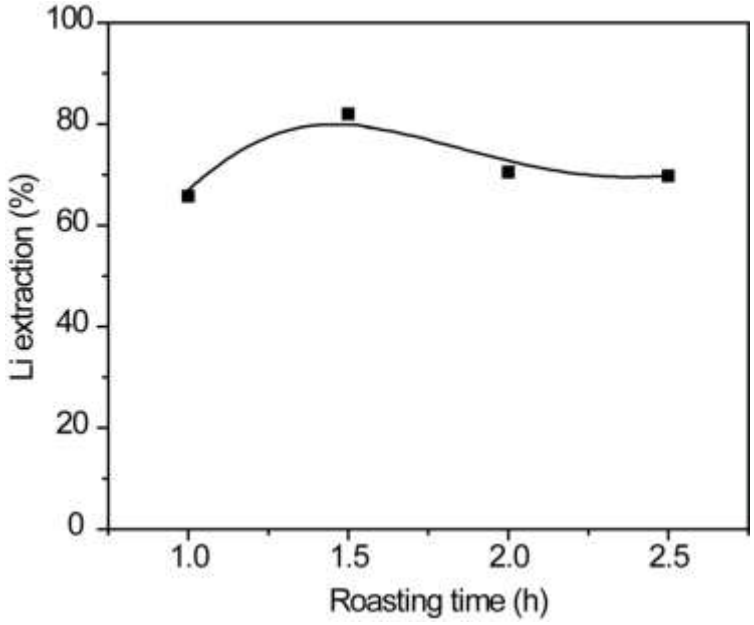

Figure 7.8. Effect of roasting time on lithium extraction. Roasting: 750 °C, FeS/Li and Ca/F molar ratios of 5:1 and 1:1, respectively. Leaching: 50 °C, 2 h, water/calcine mass ratio of 10:1. Reproducibility: ± 4%.

Roasting time of 1.5 h was noted to be the optimal duration for extracting lithium from the lepidolite concentrate (Fig. 7.8). A lithium extraction of ~82% was obtained after 1.5 h roasting, whereas only ~66% Li were extracted when lepidolite-FeS-CaO mixtures were roasted for 1 h only.

7.2.3. Effect of Ca/F molar ratio

The use of CaO to capture F has been dealt with in earlier studies (Luong *et al.*, 2013&2014). In this study, the addition of CaO in amounts >1:1 Ca/F molar ratio yielded a smaller Li recovery, possibly due to the formation of $CaSO_4$, which would reduce the SO_3 activity during roasting (Fig. 7.9).

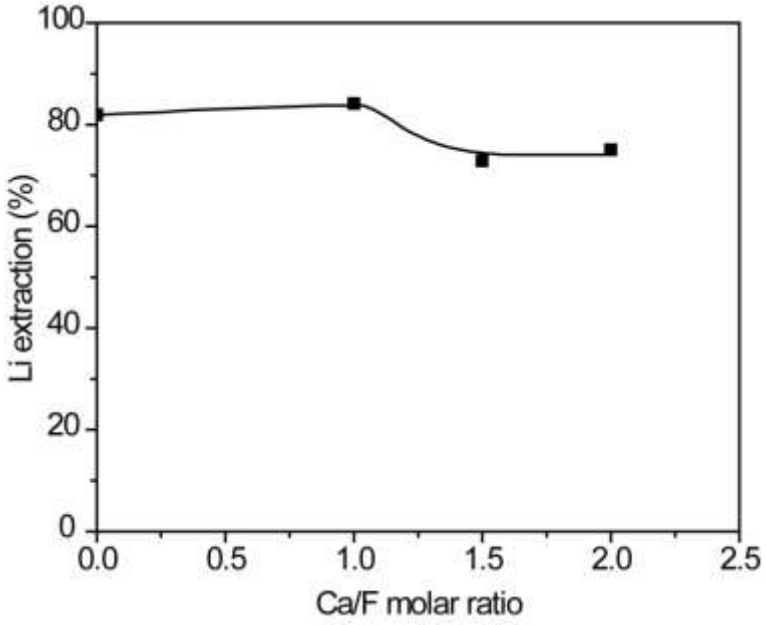

Figure 7.9. Effect of Ca/F molar ratio on lithium extraction. Roasting: 750 °C, 1.5 h, FeS/Li molar ratio of 5:1. Leaching: 50 °C, 2 h, water/calcine mass ratio of 10:1. Reproducibility: ± 4%.

The maximum lithium extraction of ~85% was obtained in roasting at 750 °C in 1.5 h with FeS/Li molar ratio of 5:1 and Ca/F molar ratio of 1:1. The main minerals in the calcines were quartz, hematite, and anhydrite. Meanwhile, $LiSO_4$ and $LiKSO_4$ were identified in the minor peaks (Fig. 7.2c).

7.2.4. Comparison of FeS with other additives

To investigate the role of SO_2/SO_3 gases on the extraction of lithium, both open and closed roasting systems were performed as described in Luong *et al*. (2014). An S/Li molar ratio of 3:1 was applied for mixtures of the concentrate with S or FeS. There was an indication that roasting in the closed system at 800-950 ^oC resulted in ~5-16 % Li extraction when S was used as the additive. The recovery of lithium was sharply increased when S was replaced by FeS, in which case ~57 % of Li was extracted at 850-900 ^oC. However, using the open system for roasting of lepidolite and the additives could greatly enhance the amount of soluble lithium compounds created as well as reduce the amount of thermal energy required for the optimal extraction of lithium. As shown in Fig. 7.10, a maximal Li recovery of ~75.4 % was attained at temperature of

750 ^{o}C after 1.5 h roasting using mixtures of lepidolite and FeS. Meanwhile, the improvement in Li extraction from lepidolite-S mixtures seemed to be negligible.

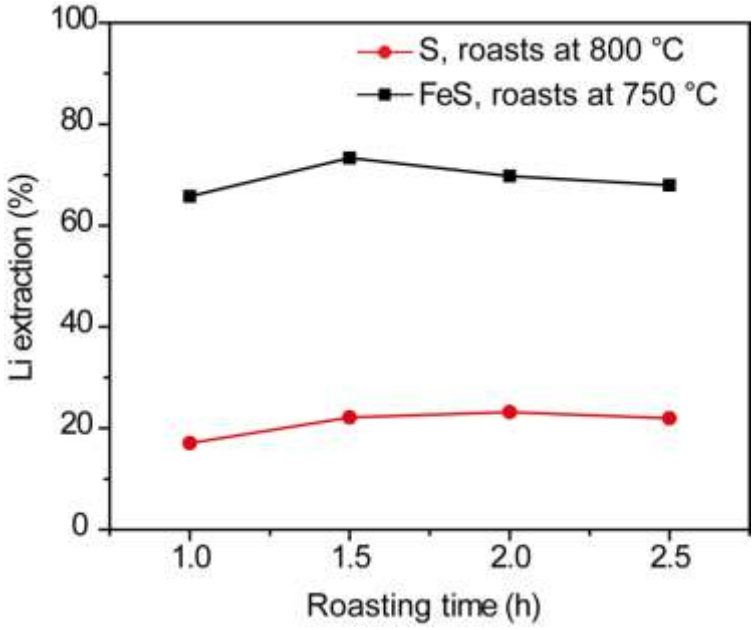

Figure 7.10. Effect of roasting time on Li extraction from lepidolite-S and lepidolite-FeS mixtures at S/Li molar ratio of 3:1. Leaching at 85 °C for 2 h, using water/calcine mass ratio of 5:1.

The effect of roasting technique on Li extraction seemed to be incompatible with that obtained from Luong *et al*. (2014), in which roasting in the closed system yielded higher extractions of Li. However, the behavior of S and FeS is different from $FeSO_4.7H_2O$ indeed. Heating of $FeSO_4.7H_2O$ could directly liberate SO_2 during its decomposition, which subsequently interacts with lepidolite to release Li. In contrast, S and FeS first needed to be oxidized to form SO_2/SO_3 that required ventilation for a supply of oxygen. On the other hand, the gases created could be rapidly lost before reacting with lepidolite if no cap was used to cover crucibles. In addition, S and FeS only work in an abundant oxygen environment. As a result, the maximal extraction of Li (at ~90 %), as obtained by Luong *et al*. (2014) when iron sulphate was utilized, could not be achieved. Finally, roasting in the open system was more suitable for mixtures of lepidolite and either S or FeS.

The use of CaO as secondary additive during sulphation roasting of lepidolite lowers the amount of HF gas liberated due to the formation of CaF_2, as also reported by Luong *et al*. (2014) and Yan *et al*. (2012b). A Ca/F molar ratio of 1:1 was found to effectively

decrease the liberation of HF gas with an insignificant influence on the lithium extraction in this study.

Microscopy and electron probe microanalysis (EPMA) were used to observe the grain morphology in the calcines obtained from roasting. Lepidolite seemed to be slightly decomposed when being roasted with S. Only the rim of lepidolite particles was metamorphosed during roasting while their surfaces were contaminated by the additives (Fig. 7.11a). In contrast, lepidolite was obviously affected by FeS roasting, causing a conversion to new compounds as shown in Fig. 7.11b.

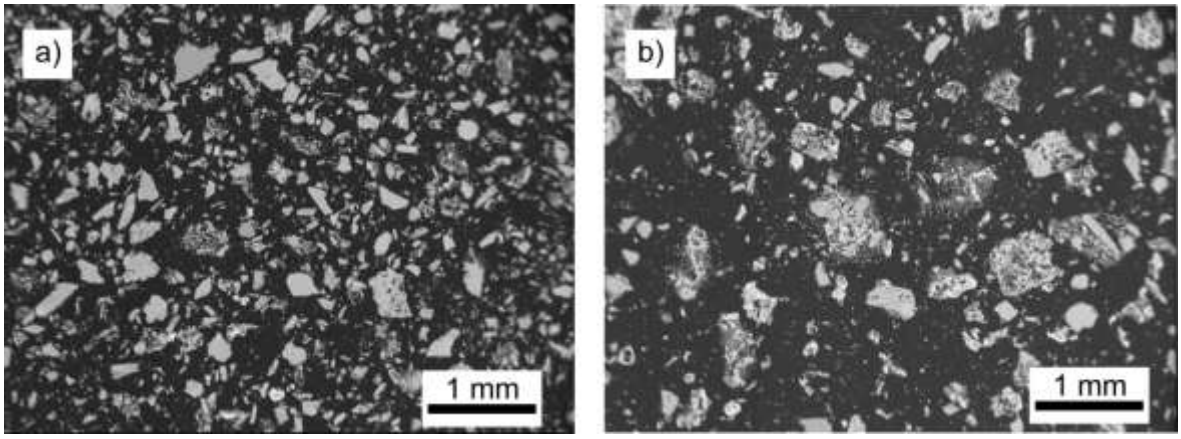

Figure 7.11. BSE images of calcines roasted at S/Li molar ratio of 5:1 and a) at 800 °C for 2 h using S; b) at 750 °C for 1.5 h using FeS.

XRD patterns of calcines obtained from roasting of lepidolite and the additives using the optimal conditions are shown in Fig. 7.12. It was noticeable that lepidolite was still present in the calcine after roasting with S as seen by its clear peaks (Fig. 7.12a). Other compounds such as CaF_2 and $CaSO_4$ were formed due to the addition of CaO. Meanwhile, lepidolite seemed to have completely disappeared when FeS was utilized, resulting the dominance of Fe_2O_3 peaks (Fig. 7.12b). The existence of Li_2SO_4 and $LiKSO_4$ in the calcines was also found, but these phases exhibit poor crystallinity. Thus, the effectiveness of FeS compared to S on the extraction of lithium from lepidolite was evident.

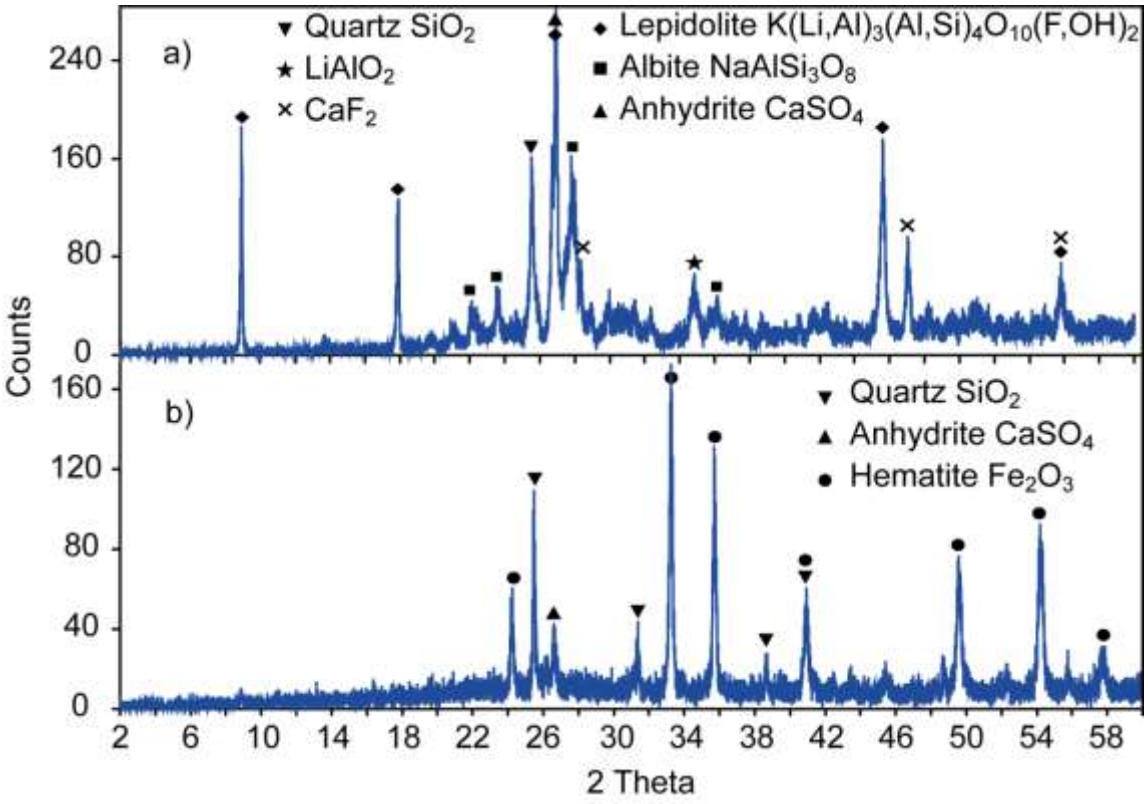

Figure 7.12. XRD patterns of a) calcine at 800 °C for 2 h using S, b) calcine at 750 °C for 1.5 h using FeS. Roast using S/Li molar ratio 5:1.

The extraction of lithium from lepidolite via sulphation roasting and water leaching was experimentally performed based on HSC thermodynamic models. It was found that using FeS as the additive could extract a maximum of ~85% Li from lepidolite in the open roasting system. Sulphur (S) was found to be an unsuitable additive for the recovery of Li due to a low extraction obtained (~23%). The usefulness of FeS compared to S was confirmed by EPMA and XRD. The role of CaO in lowering the formation of HF gas was also tested.

Comparing to the research by Luong *et al*. (2013&2014), Yan *et al*. (2012a&b) on other additives or mixture SO_2/SO_3 gases are formed and react more readily to extract lithium from lepidolite.

7.3. Leaching of lithium from calcines

The solvent used for leaching was distilled water. Parameters tested include: water/calcine mass ratio, leaching in different temperatures and times to optimize the leaching conditions.

7.3.1. Effect of water/calcine mass ratio

The water/calcine mass ratio affects the Li extraction greatly as shown in Fig. 7.13. The highest Li recovery of ~85% was obtained using a 10:1 water/calcine mass ratio. At this level, however, the Li concentration in the leach liquor was only 0.64 g/L Li (Table 7.2), compared to 1.1 g/L Li when a 5:1 water/calcine mass ratio was used for the leaching experiment.

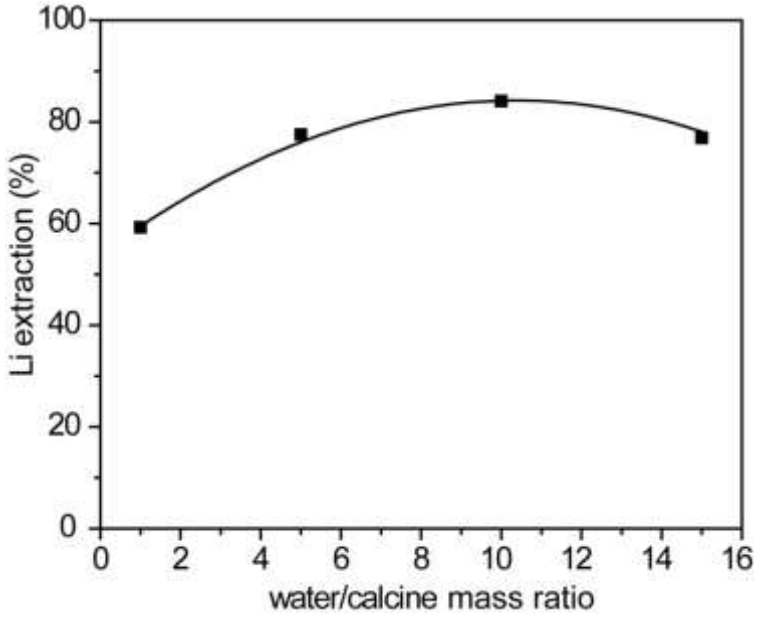

Figure 7.13. Effect of water/calcine mass ratio on lithium extraction. Roasting: 750 ^{o}C, 1.5 h, FeS/Li and Ca/F molar ratios of 5:1 and 1:1, respectively. Leaching: 50 ^{o}C, 2 h. Reproducibility: ± 4%.

Table 7.2. Composition (g/L) of leach liquor determined by IC and AAS analyses. Roasting: 750 ^{o}C, 1.5 h, FeS/Li and Ca/F molar ratios of 5:1 and 1:1, respectively. Leaching: 50 ^{o}C, 2 h, water/calcine mass ratio of 10:1.

Li	Mg	Na	K	Rb	Ca	Fe	Al	SO_4	F
0.64	0.02	0.43	1.98	0.15	0.42	0.02	0.97	12.27	1.33

7.3.2. Effect of leaching temperature and time

A leaching temperature varying between 50 ^{o}C and 85 ^{o}C seems to improve the Li extraction only slightly (Fig. 7.14). Similarly, increasing the leaching time from 1 h to 3 h seems to have little effect on Li recovery (Fig. 7.15).

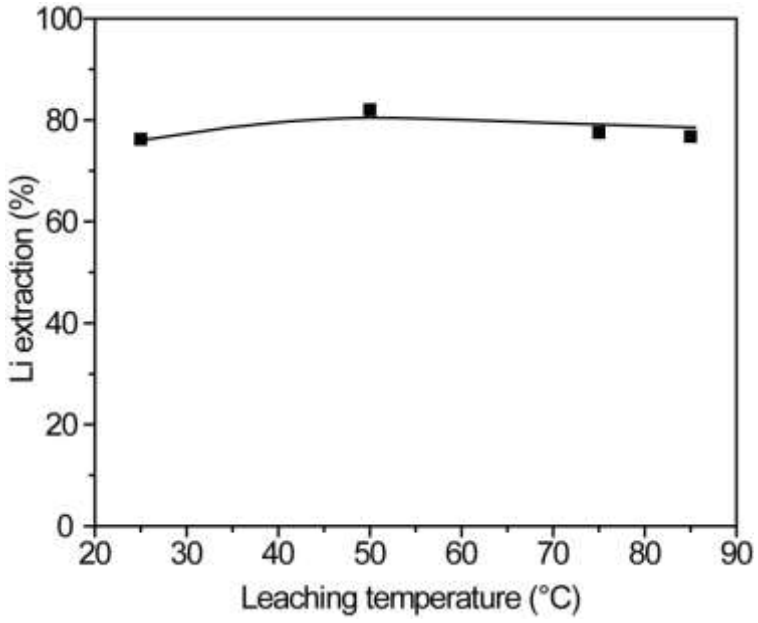

Figure 7.14. Effect of leaching temperature on lithium extraction. Roasting: 750 ^{o}C, 1.5 h, FeS/Li and Ca/F molar ratios of 5:1 and 1:1, respectively. Leaching: 2 h, water/calcine mass ratio of 10:1. Reproducibility: ± 4%.

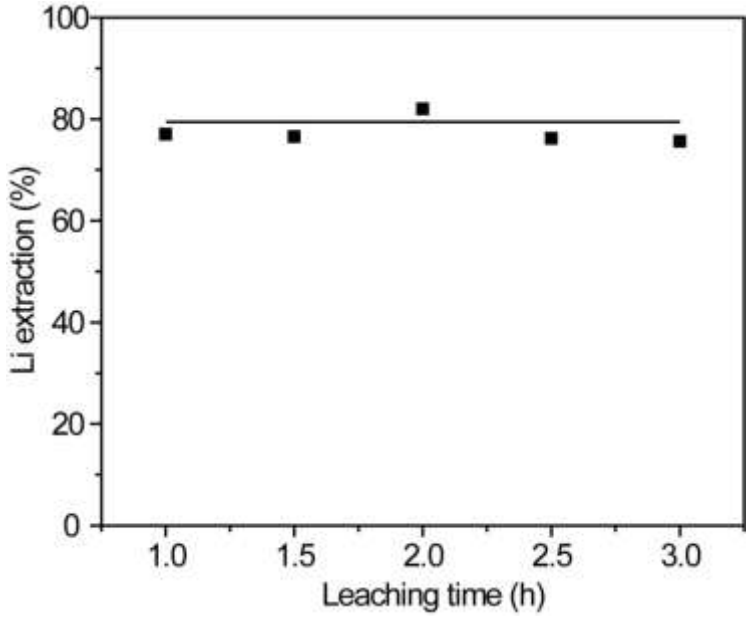

Figure 7.15. Effect of leaching time on lithium extraction. Roasting: 750 ^{o}C, 1.5 h, FeS/Li and Ca/F molar ratios of 5:1 and 1:1, respectively. Leaching: 85 ^{o}C, water/calcine mass ratio of 10:1. Reproducibility: ± 4%.

The lithium extraction will be increased when the residues are washed after filtering with small amount of distilled water. The concentration of Li in the leach liquor was 988 ppm, in 30 ml the washed water had 590 ppm Li. It is proven that washing the residue does improve the lithium recovery from leaching.

7.3.3. Comparison with other studies

Table 7.3 compares the results of our study with those reported earlier. Roasting of lepidolite with FeS-CaO seems to yield slightly lower Li recovery than roasting with Fe sulphate (Luong *et al*., 2014). Most importantly, a much higher water/calcine mass ratio (>5:1) was required to leach Li from the calcine, and additionally, it only yielded liquors containing <1 g/L Li compared to >8 g/L Li when Fe sulphate was used as an additive (Luong *et al*., 2014) and compared to 1-3 g/L Li when Na sulphate was used as an additive (Luong *et al*., 2013). This could be due to the formation of larger amounts of $LiKSO_4$ in our study. This phase is known to be only sparingly soluble compared to Li_2SO_4 (Luong *et al*., 2013&2014). The 71.5% loss of SO_2/SO_3 shown in the mass balance presented in Fig. 7.5 could be the key factor causing this inferior performance

compared to the higher Li recovery and more concentrated Li liquors yielded by the Fe sulphate roasting process. The use of FeS as an additive, however, produces an overall better calcine compared to those of other processes using Na_2SO_4 (Luong *et al*., 2013; Yan *et al*., 2012a&b), which require higher temperatures for roasting (850-1000 ^oC).

Table 7.3. Experimental profiles and results of several published studies on processing of various Li mineral sources.

	This study	Luong *et al*. (2014)	Luong *et al*. (2013)	Siame & Pascoe (2011)
Li mineral	Lepidolite	Lepidolite	Lepidolite	Zinnwaldite
Li, %	1.55	1.79	2.55	0.96
Roast temp, ^oC	750	850	1000	850
Roast time, h	1.5	1.5	0.5	1
Additives	FeS, CaO	$FeSO_4.7H_2O$, CaO	Na_2SO_4	Na_2SO_4
S or SO_4/Li, molar ratio	5:1	3:1	2:1	unstated
Additives/Li mineral, mass ratio	~0.98:0.09:1	~2.2:0.09:1	~1:1	1:2
Ca/F, molar ratio	1:1	1:1	not included	not included
Leach temp, ^oC	50	ambient	85	85
Leach time, h	1.5	1	3	0.5
H_2O/calcine, mass ratio	10:1	1:1	2-18:1	10:1
Max. Li extract., %	~85	93	~90	>90
Li conc., g/L	0.64	8.7	1-3	Expected to be ~1

Table 7.3. *(continued)*.

	Yan *et al*. (2012a)	Yan *et al*. (2012b)	Jandová *et al*. (2009)	Sitando & Crouse (2012)
Li mineral	Lepidolite	Lepidolite	Zinnwaldite	Petalite/lepidolite
Li, %	2.00	2.00	1.4	1.9
Roast temp, ^{o}C	850	880	950	1100 (1st stage)
Roast time, h	0.5	0.5	1	2
Additives	Na_2SO_4,K_2SO_4, CaO	Na_2SO_4, $CaCl_2$	$CaSO_4$, $Ca(OH)_2$	H_2SO_4 (300^{o}C, 2nd stage)
S or SO_4/Li, molar ratio	unstated	unstated	unstated	
Additives/Li mineral, mass ratio	0.5:0.1:0.1:1	0.5:0.3:1	2.1:1:3	Unstated
Ca/F, molar ratio	unstated	unstated	unstated	
Leach temp, ^{o}C	Ambient	ambient	90	50
Leach time, h	0.5	0.5	0.5	1
H_2O/calcine, mass ratio	2.5:1	0.8:1	10:1	7.5:1
Max. Li extract., %	~90	~90	96	97.3
Li conc., g/L	4.39	8.53	0.69	5.7

7.4.Purification of leach liquor

The purification experiments were conducted using beakers, stirring hotplates, and a pH controller to determine the optimum conditions of purification procedure (Fig. 7.16).

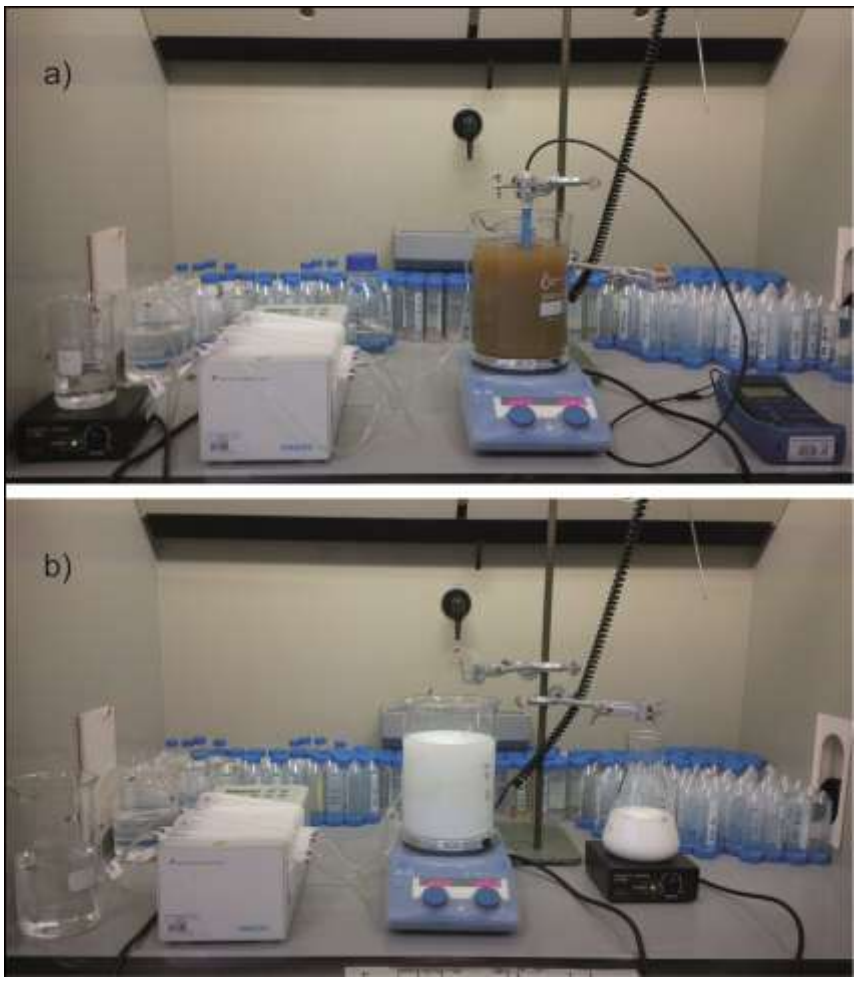

Figure 7.16. Photos of a) removal of cations; b) removal of sulphate in purification procedure.

The stages tested for purification and final product recovery are as shown in the flowsheet presented in Fig. 7.17. The process involves: (a) removal of cationic contaminants ; (b) removal of sulphate and conversion of lithium liquors from sulphate to chloride-base, and finally (c) LiCl product recovery.

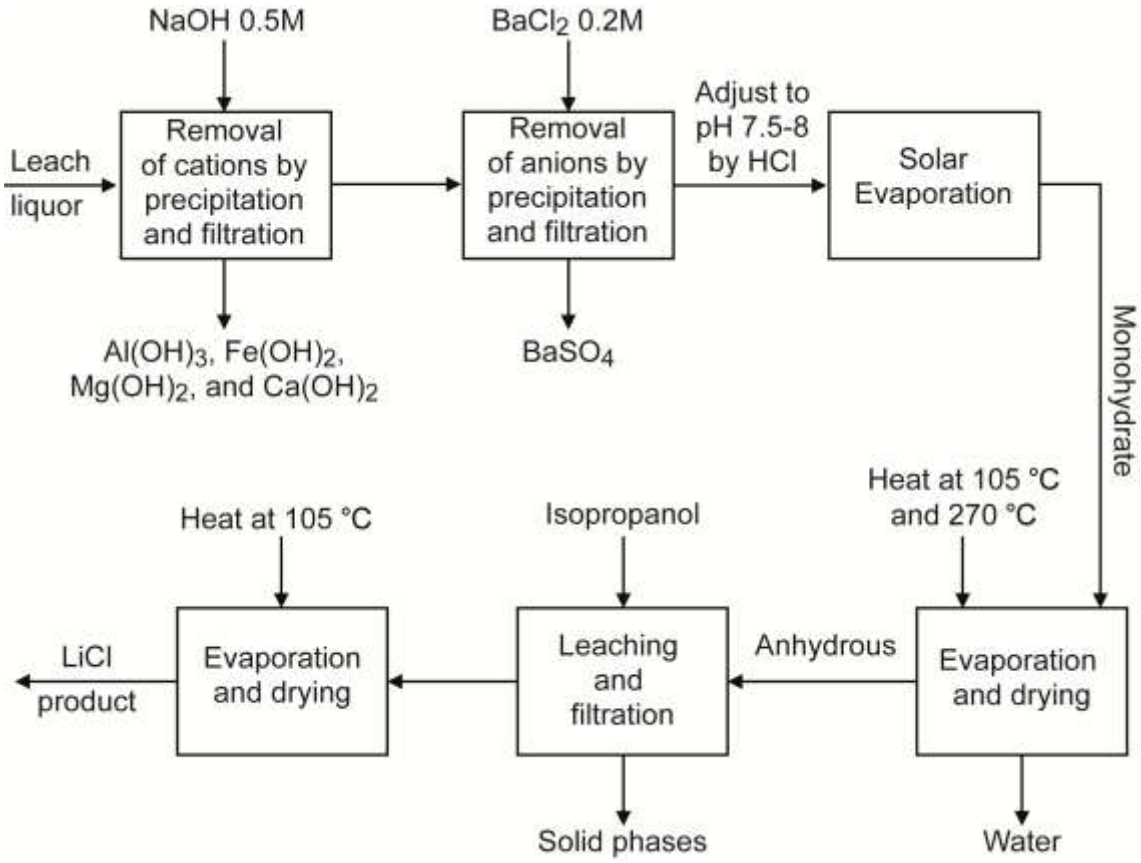

Figure 7.17. Flowsheet showing the process for LiCl recovery.

7.4.1. Removal of cations

Cations in the leach liquor are shown in the Table 7.4, which include alkaline metals (Na^+, K^+, Rb^+, Li^+) and other metals (Ca^{2+}, Mg^{2+}, Fe^{2+}, Al^{3+}). NaOH 0.5M was chosen as a reagent for precipitation of Ca^{2+}, Mg^{2+}, Fe^{2+}, and Al^{3+}. The main reactions between cations and hydroxide are illustrated by the equations below. In the presence of sulphate and fluoride other solids could co-precipitate as predicted by Stabcal modeling (Huang, 2005). The stability of various species (Al, Fe, Ca, Mg) is shown in Fig. 7.18. This modeling is based on the conditions as specified for liquor F5-4, whose composition is shown in Table 7.4, and yielded equilibrium conditions for the above cations at 25 °C.

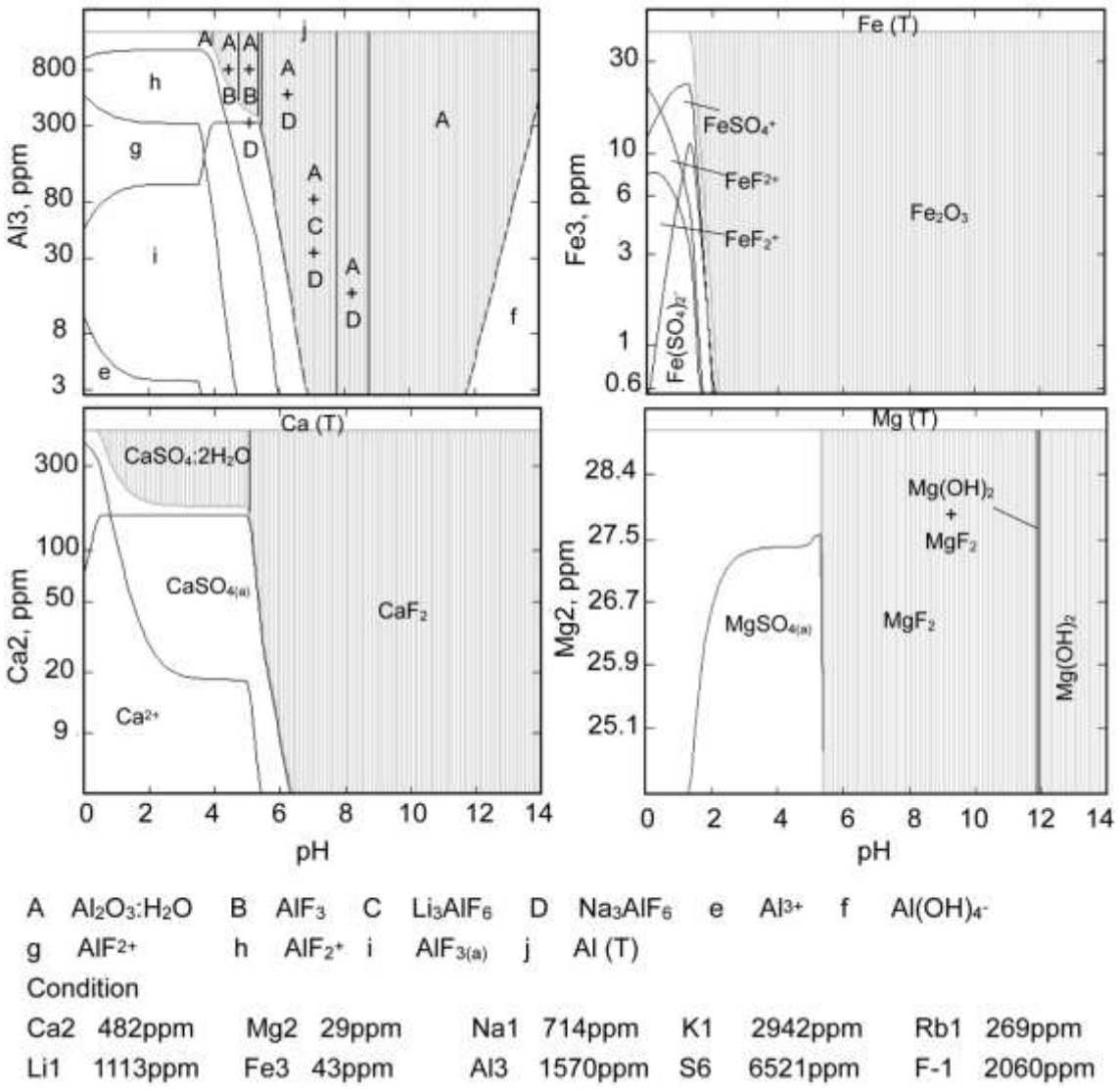

Figure 7.18. Stabcal modeling showing stability of various cations at different pH's. Input stabcal data is sample F5-4 in Table 7.4

Al^{3+} (aq) + $3OH^-$ (aq) ↔ $Al(OH)_3$ (s) (Eq. 7.1)

Fe^{2+} (aq) + $2OH^-$ (aq) ↔ $Fe(OH)_2$ (s) (Eq. 7.2)

Mg^{2+} (aq) + $2OH^-$ (aq) ↔ $Mg(OH)_2$ (s) (Eq. 7.3)

Ca^{2+} (aq) + $2OH^-$ (aq) ↔ $Ca(OH)_2$ (s) (Eq. 7.4)

Table 7.4. Chemical composition of leach liquors.

mg/L	F5-4	F6-6
Ca	482	380
Mg	29	13
Na	714	334
K	2942	1410
Rb	269	127
Li	1113	539
Fe	43	20
Al	1570	721
SO_4	19563	9520
F	2060	867

The modeling allows the pH to be adjusted by NaOH addition to remove most cations which might contaminate the final liquors. As shown in Table 7.5 Ca, Mg and Fe could be removed to <1ppm, which is very close to the equilibrium conditions predicted by Stabcal.

For aluminium, an excessive addition of NaOH would cause the precipitate to redissolve as aluminate ions (at a pH>12). In the range of pH 6-7 the equilibrium Al concentration is very sensitive to pH, varying from 30 to 300 ppm as predicted by Stabcal. The experiment yielded a liquor containing 10.8 ppm at pH 9-9.5 in the same range as what is predicted from Stabcal (Table 7.5).

Co-precipitation of Li with aluminium precipitates was observed as shown in Figure 7.19. This was also observed in other studies in the literature (Hamzaoui *et al*., 2007). Li is intercalated into the Al-hydroxide structure which causes the overall recovery of Li to decrease from 98% to 94% after 3h of Al precipitation (Fig 7.20).

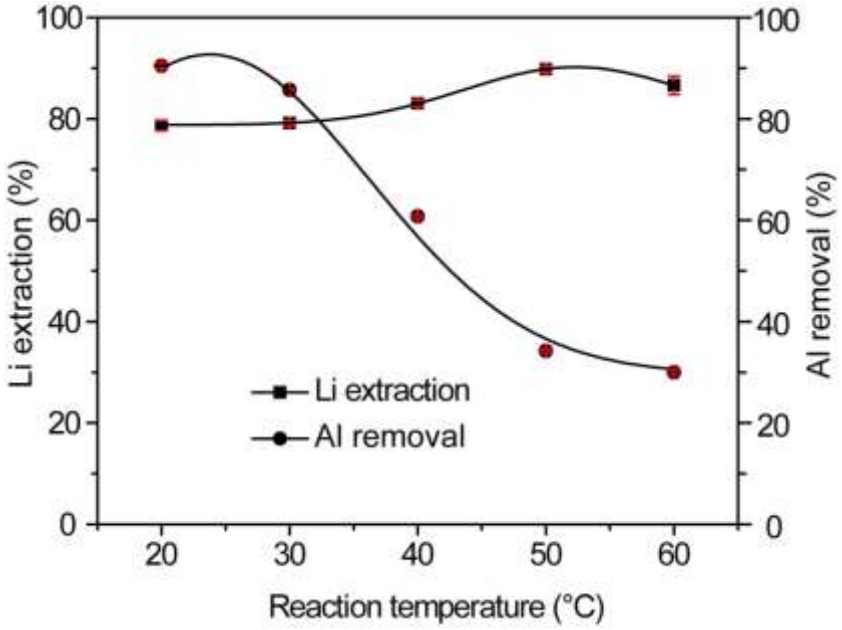

Figure 7.19. Effect of reaction temperature on lithium extraction. Reaction time: 30 minutes with NaOH 0.5M. Reproducibility: ± 2%.

Fig. 7.20 presents the tendency of decreasing lithium extraction as purification time increases. The efficiency of Al removal reaches 95-96 % range of 1.5-3 h. ~ 100 % lithium could be recovered by washing of the precipitate after filtering. The time required was acceptable based on lithium extraction and Al removal at 1.5 h with ± 2% reproducibility.

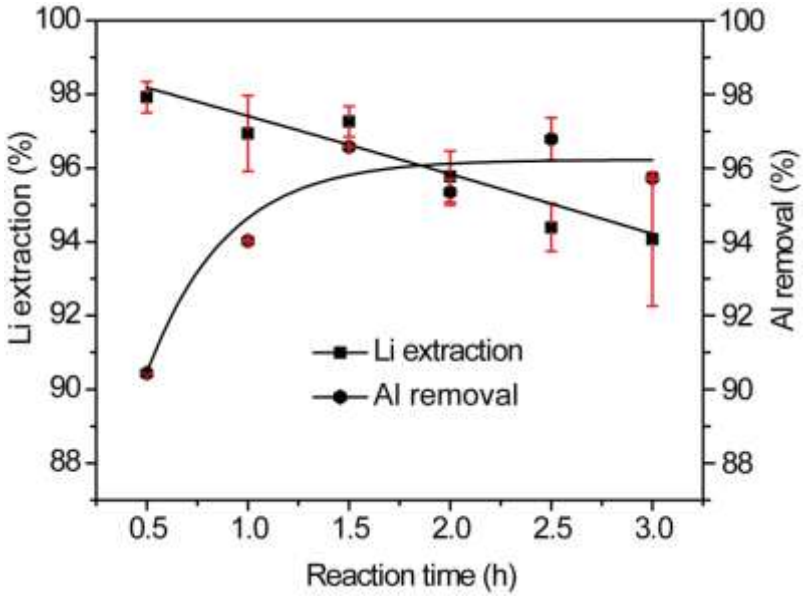

Figure 7.20. Effect of reaction time on lithium extraction and Al removal. NaOH 0.5M. Reproducibility: ± 2%.

7.4.2. Removal of sulphate

$BaCl_2$ was the reagent used to remove SO_4^{2-} from the leach liquors and at the same time convert the Li sulphate into a chloride-based liquor. Stephen. (1979) showed that the solubility of $BaSO_4$ solid is 0.0024 g/L at 20 °C and 0.00285 g/L at 30 °C.

Stabcal modeling using the conditions of the liquors after caustic precipitation indicates that sulphate could be completely removed (Fig. 7.21). At equilibrium condition and with stoichiometric addition (i.e. Ba/SO_4 molar ratio of 1:1) the concentration of SO_4 should be approximately 6 ppm (corresponding to 2 ppm S). The remaining Ba should be less than 1 ppm at these conditions.

Experimental results (Table 7.5) show that the removal of sulphate by barium chloride is nearly quantitative as at the end of the experiment, the remaining Ba and sulphate is <7.5 ppm and 92 ppm, respectively.

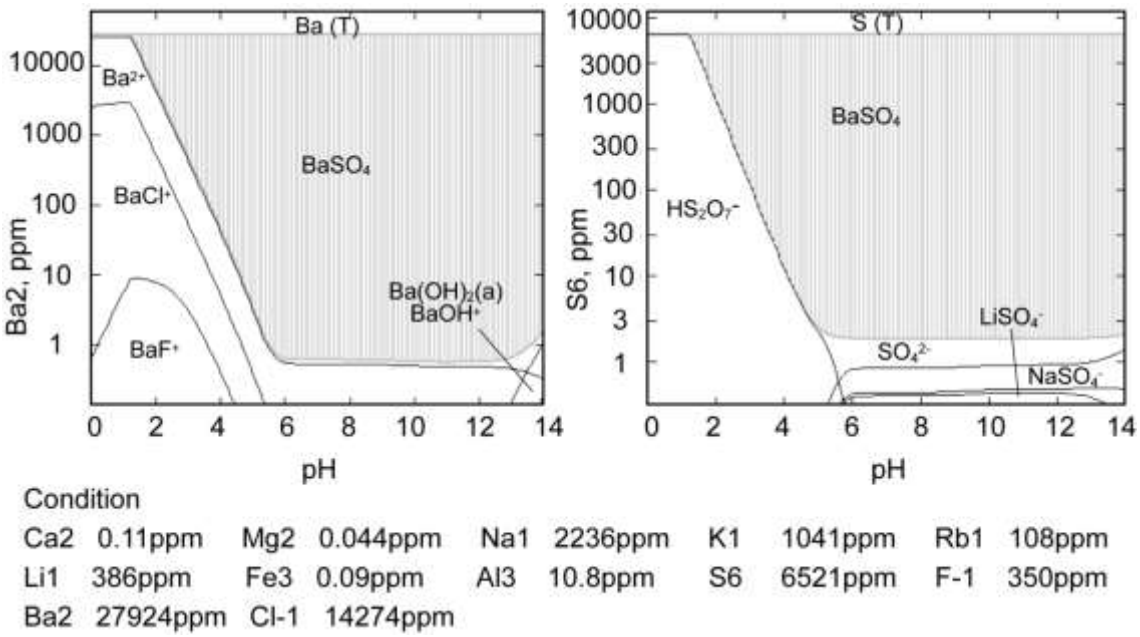

Figure 7.21. Stabcal modeling showing stability of S and Ba at different pH's. Input stabcal data is sample F5-4 in Table 7.5.

Table 7.5. Composition of the lithium solution after removal of Ca^{2+}, Mg^{2+}, Fe^{2+}, and Al^{3+} by OH^- from NaOH and SO_4 by using enough Ba^{2+}.

Analysis #	Concentration, ppm	Note
Li	386	0.24 wt.% LiCl
Rb	108	
Al	10.8	
Ca	0.11	
Fe	<0.09	
K	1041	
Mg	0.044	
Na	2236	
F	350	
SO_4	92	
Ba	<7.5	
Cl	5749	

Sulphate could be removed to >96.9% at stoichiometric addition of Ba chloride at a loss of <5% Li. An excess of Ba chloride addition would remove all sulphate but this would leave remnant Ba in the final liquor (Table 7.6).

Table 7.6. Sulphate removal and Li remaining in the liquor.

%	Average	Std Dev (n=4)	Average	Std Dev (n=5)
Li recovery	96.82	1.11	94.98	1.24
SO_4 removal	100.0	0.0	96.98	3.01
Ba used	In excess		Stoichiometric requirement	

7.5. Recovery of LiCl

As indicated by Brown *et al*. (1981a), the concentration of salts after evaporation through solar energy increase to 40 wt.% or more. To achieve this the slurry should be dried at least at 200 °C to produce anhydrous LiCl, and rather between about 270 °C and 325 °C.

The lithium solutions containing small amounts of various impurities as shown in Table 7.5 were subjected to solar evaporation, dried at 105 °C and 270 °C, respectively in order to obtain anhydrous salts rather than the monohydrate precipitate. Evaporation causes 80-90 % of mass reduction based on comparison of mass measurements of the crude salts after evaporation and lithium solution analysis before evaporation. Drying for 30 minutes at 270 °C will also decrease the moisture content to ~1 wt.%. Through this process, the concentration of lithium chloride was increased to 18.95 wt.% (Table 7.7) from the original value of 0.24 wt.% (Table 7.5).

Table 7.7. Chemical compositions of salts after solar evaporation.

Analysis #	Concentration, ppm	Note
Li	31030	18.95 wt.% LiCl
Rb	9063	
Al	104	
Ca	29.3	
Fe	<18	
K	96831	
Mg	46	
Na	215069	
F	29610	
SO_4	6002	
Ba	<1500	
Cl	569982	

The XRD result of the solid which was separated by filtering after dissolving the crude salts in water is shown in Fig. 7.22. The main peaks are for lithium fluoride which dissolves in the water at high temperature.

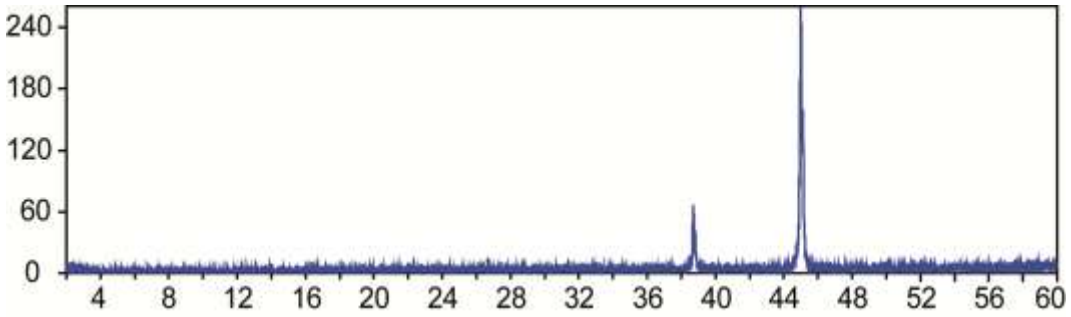

Figure 7.22. XRD pattern of precipitate remained in the lithium solution.

The major salts in the sample subjected to isopropanol leaching are mainly from alkaline metals (Table 7.7). However, the solubilities of those salts are different in isopropanol (Table 7.8), thus, lithium chloride can be separated easily from other salts by isopropanol leaching. In addition, isopropanol is a secondary alcohol and it is easy to evaporate with time and at high temperature. For that reason, the experiment will be tested at different times (5-24 h), isopropanol/salts mass ratios (5:1-10:1) and at ambient temperature.

Table 7.8 shows the solubility of different salts in isopropanol, the highest being LiCl at 13.68 and 13.95 % at 20 and 25 °C, respectively. Apart from Ca chloride solubilities of other salts of Na, K, Rb remain below 0.05 % at 25 °C.

Table 7.8. The solubility of chemical compounds in isopropanol (Stephen. 1979)

Compounds	Solubility at 20 °C, wt.%	Solubility at 25 °C, wt.%
LiCl	13.68	13.95
NaCl	0.809	0.04
Na_2SO_4	0.000886 Mol.%	0.000939 Mol.%
KCl	0.0023	0.0023
RbCl	0.015	0.015
$CaCl_2$	13.63	16.67

As a result, LiCl could be solubilized preferentially in isopropanol, leaving other salts in solid forms. The solid and liquid phases are then easily separated by centrifugation. Solar evaporation and drying at 105 °C could then be applied to recover/remove isopropanol and to extract lithium chloride from the solvent. The composition and purity of lithium chloride are determined by AAS and IC analysis.

Lithium extraction was 70 % after 3 h isopropanol leaching, which dropped slightly after 5 h leaching. Further leaching to 12 and 24 h resulted in 66 % and 53% Li extraction, respectively. Loss due to evaporation increases from 1 g of 3 h to 5 g of 24 h (Fig. 7.23) and as discussed (Table 7.8), the concentration of LiCl is reduced because small amount of other salts are dissolved in abundant isopropanol. Isopropanol leaching during a short period (3-5 h) showed a high concentration of lithium chloride (92 wt.%).

Leaching (dissolution) experiments were conducted at different conditions of isopropanol/salt mass ratio and reaction time. Figure 7.23 shows the effect of leaching time on the extraction of Li from the salt and the final LiCl grade of the product (as weight %) of LiCl in the solution.

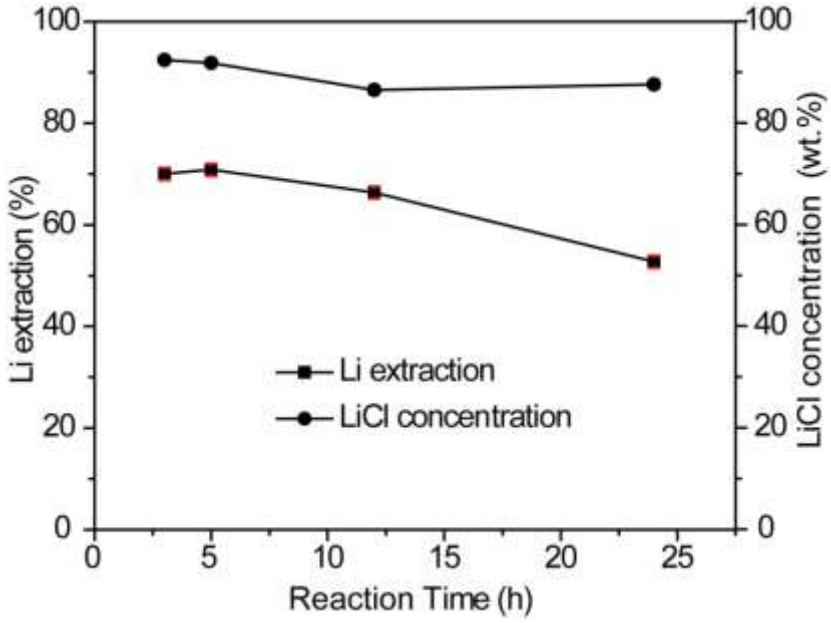

Figure 7.23. Effect of isopropanol leaching time on lithium extraction and LiCl product grade. Isopropanol/salts mass ratio of 10:1. Reproducibility: ± 1.2%.

As shown in Brown *et al*. (1981c), the amount of isopropanol should be calculated based on the isopropanol to salts mass ratios of 5:1 to 10:1, the optimum ratio being 7:1. Fig. 7.24 illustrates the effect of isopropanol/salts mass ratios to lithium from La Vi. It indicates that the lithium extraction slightly decreases when the amount of isopropanol used was larger (87 % at 5:1 to 85 % at 10:1 ratio), as is also the concentration of LiCl (96 wt.% at 5:1 *vs*. 82 wt.% at 10:1). The maximum lithium extraction was obtained at 3 h of leaching at isopropanol/salts mass ratio of 5:1.

A photo of lithium chloride product from the La Vi ore is presented in Fig. 7.25. Its composition is listed in Table 7.9.

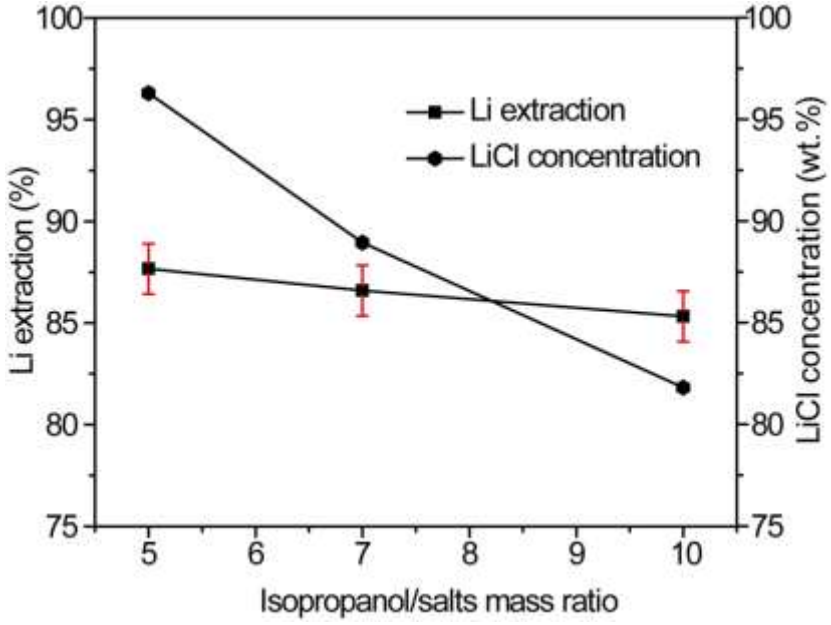

Figure 7.24. Effect of isopropanol/salts mass ratio on lithium extraction and LiCl product grade. Isopropanol leaching: 3 h. Reproducibility: ± 1.2%.

Figure 7.25. Photo of lithium chloride product.

Table 7.9. The quality of lithium chloride product.

Analysis #	Concentration, ppm	Note
Li	157665	96.26 wt.% LiCl
Rb	2335	
Al	19.5	
Ca	163	
Fe	<35	
K	556	
Mg	5.45	
Na	899	
F	770	
SO_4	<3829	
Ba	<2918	
Cl	849416	

Chapter 8. Conclusions and Recommendations

8.1. Conclusions

This study has demonstrated that lithium could be recovered from lepidolite from Li-rich granites of the La Vi mining district (Vietnam) to produce LiCl through froth flotation, roasting with iron (II) sulphide, water leaching, purification and crystallization. The following conclusions are reached based on the experimental results:

1. By using XRD, XRF, EMPA, AAS, ICP-MS, and SIMS analysis, the mineral components of La Vi ore were determined. The major minerals are as follows: quartz SiO_2, albite $NaAlSi_3O_8$, micas as muscovite $KAl_2(ALSi_3)O_{10}(OH,F)_2$, lithian-micas like muscovite and lepidolite $K(Li, Al)_3(Al,Si)_4O_{10}(OH,F)_2$. The other silicates and phosphates are minor minerals which include topaz $Al_2SiO_4(F,OH)_2$, beryl $Be_3Al_2Si_6O_{18}$, lithium phosphate such as amblygonite $(Li,Na)Al(PO_4)(F,OH)$, montebrasite $LiAl(PO_4)(F,OH)$, and other phosphate minerals, including fluorapatite $Ca_5(PO_4)_3F$, herderite $CaBe(PO_4)(OH,F)$, and goyazite $SrAl_3(PO_4)_2(OH)_5.(H_2O)$.

2. The Lithium ores in the Dong Ram area are medium- to coarse-grained and contain mainly SiO_2, Al_2O_3, Na_2O, K_2O, and Li_2O (Table 5.1). These ores were classified as between alkalic and alkali-calcic granites, which have a peraluminous bulk composition.

3. Iron sulphide (FeS) and CaO were used to convert Li into a water-soluble form by roasting the mixture with lepidolite at 700-850 ^oC for 1.5 h. Moreover, the Li extraction using water/calcine mass ratios of 10:1 at 50 ^oC for 2 h can only yield a maximum of 85% Li (at <1 g/L Li concentration) in the solution. The formation of SO_2/SO_3 gases is believed to be crucial for the extraction of lithium from lepidolite via a gas-solid interaction as introduced by Luong *et al*. (2014) and Li *et al*. (2010&2011). In addition,

CaO should be used to capture F during lepidolite roasting by forming CaF_2, which also could limit the creation of insoluble LiF.

4. Removal cations except alkali metals from leach liquor through hydroxide precipitations by NaOH was carried out at ambient temperature for 1.5 h and a controlled pH. Besides, removal SO_4^{2-} as sulphate salt precipitated by $BaCl_2$ was accomplished at ambient temperature. The efficiency of lithium extraction reached 100 % because of washing the precipitates after filtering. LiCl solutions were produced as a result.

5. The difference of the solubility of salts in isopropanol allows for selective recovery of LiCl and drying to anhydrous salts, which were subjected to isopropanol leaching. After evaporating isopropanol, LiCl products can be obtained. This was done after LiCl solutions were concentrated using solar evaporation or evaporative heating. In this study, ~90 % LiCl (96.3 wt.% LiCl) were produced using isopropanol/salts mass ratio of 5:1 at ambient temperature in 3 h.

8.2. Recommendations

Optimum processing conditions using additive FeS were determined for extracting lithium from lepidolite. However, there are many factors controlling the process that need to be further studied in order to obtain high-purity LiCl from lepidolite. Hence, recommendations to further develop this work are as follow:

1. Conduct further studies to improve the removal of sulphate before removal of cations.

2. Use $Ca(OH)_2$ for removal of cations and fluoride in the leach liquor before converting salts of sulphate to chloride.

3. Expanding the study of the extraction of valuable Rb and Cs as by-products of processing lithium from lepidolite.

4. Examining the suitability of other natural sulfur compounds such as pyrite (FeS_2) and anhydrite ($CaSO_4$).

References

Abe, M., Chitrakar, R. (1987). Synthetic inorganic ion-exchange materials. XLV. Recovery of lithium from seawater and hydrothermal water by titanium (IV) antimonate cation exchanger. *Hydrometallurgy* 19 (1), 117–128.

Abe, M., Hayashi, K. (1984). Synthetic inorganic ion-exchange materials. XXXIV. Selective separation of lithium from seawater by tin (IV) antimonate cation exchanger. *Hydrometallurgy* 12 (1), 83–93.

Amer, A.M. (2008). The hydrometallurgical extraction of lithium from egyptian montmorillonite-type clay. *JOM* 60 (10), 55–57.

An, J.W., Kang, D.J., Tran, K.T., Kim, M.J., Lim, T., Tran, T. (2012). Recovery of lithium from Uyuni salar brine. *Hydrometallurgy* 117–118 (0), 64–70.

Archambault, M., Charles, A.O., Lemay, H.P., Savard, M. (1963). Sodium-ammonium compounds process for extracting lithium from spodumene. Google Patents. http://www.google.com/patents/US3112170.

Badanina, E.V., Veksler, I.V., Thomas, R., Syritso, L.F., Trumbull, R. B. (2004). Magmatic evolution of Li–F, rare-metal granites: a case study of melt inclusions in the Khangilay complex, Eastern Transbaikalia (Russia). *Chemical Geology* 210 (1–4), 113–133.

Barbosa, L. I., Valente, G., Orosco, R. P., and González, J. A. (2014). Lithium extraction from β-spodumene through chlorination with chlorine gas. *Miner. Eng.* 56, 29–34.

Boryta, D.A. (2000). Method for removing magnesium from brine to yield lithium carbonate. Google Patents. https://www.google.com/patents/US6143260.

Botton, R., Delgrange, J.P., Steinmetz, A. (1965). Method of recovering lithium from lepidolite. Google Patents. http://www.google.com/patents/US3189407.

Breiter, K., Fryda, J., Seltmann, R., Thomas, R. (1997). Mineralogical evidence for two magmatic stages in the evolution of an extremely fractionated P-rich rare-metal granite: the Podlesi stock, Krusne Hory, Czech Republic. *Journal of Petrology* 38, 1723–1739.

Breiter, K., Kronz, A. (2004). Phosphorus-rich topaz from fractionated granites (Podlesí, Czech Republic). *Mineralogy and Petrology* 81 (3-4), 235–247.

Breiter, K., Sokolová, M., Sokol, A. (1991). Geochemical specialization of the tin-bearing granitoid massifs of NW Bohemia. *Mineralium Deposita* 26 (4), 298–306.

Brown, P.M., Beckerman, S.J. (1990). Production of lithium metal grade lithium chloride from lithium-containing brine. Google Patents. http://www.google.com/patents/US4980136.

Brown, P.M., Boryta, D.A. (1993). Production of low boron lithium carbonate from lithium-containing brine. Google Patents. http://www.google.com/patents/US5219550.

Brown, P. M., Jacob, S. R., Boryta, D. A. (1981a). Process for purification of lithium chloride. *US pattern 4274834*.

Brown, P. M., Jacob, S. R., Boryta, D. A. (1981b). Process for solar concentration of lithium chloride brine. *US pattern 4243392*.

Brown, P. M., Jacob, S. R., Boryta, D. A. (1981c). Production of highly pure lithium chloride from impure brines, 9 pp.

Büyükburç, A., Köksal, G. (2005). An attempt to minimize the cost of extracting lithium from boron clays through robust process design. *Clays and Clay Minerals* 53 (3), 301–309.

Cau, D.V., Cong, N.C., Huy, P.L., Long, T.V. (2004). Geological mapping and minerals prospecting of Ba To group sheets in ratio 1: 50000., South Vietnam Geological Mapping Division. http://diachatnv.vn/.

Černá, I., Černý, P., Selway, J.B., Chapman, R. (2002). Paragenesis and origin of secondary beryllophosphates: beryllonite and hydroxyllhederite from the BEP granitic pegmatite, southeastern Manitoba, Canada. *The Canadian Mineralogist* 40 (5), 1339–1345.

Cerný, P. (2002). Mineralogy of Beryllium in Granitic Pegmatites. *Reviews in Mineralogy and Geochemistry* 50 (1), 405–444.

Černý, P., Ercit, T.S. (2005). The classification of granitic pegmatites revisited. *The Canadian Mineralogist* 43 (6), 2005–2026.

Černý, P., London, D., Novák, M. (2012). Granitic Pegmatites as Reflections of Their Sources. *Elements* 8 (4), 289–294.

Charoy, B., Noronha, F. (1999). Rare-element (Li-rich) granitic and pegmatitic plutons: a primary or superimposed signature? *Revista Brasileira de Geociências* 29, 3–8.

Charoy, B., Noronha, F., Lima, A. (2001). Spodumene – petalite – eucryptite: mutual relationships and pattern of alteration in Li-rich aplite-pegmatite dykes from Northern Portugal. *The Canadian Mineralogist* 39 (3), 729–746.

Chen, Y., Tian, Q., Chen, B., Shi, X., Liao, T. (2011). Preparation of lithium carbonate from spodumene by a sodium carbonate autoclave process. *Hydrometallurgy* 109 (1-2), 43–46.

Chen, Y., Tian, Q., Chen, B., Shi, X., and Liao, T. (2011). Preparation of lithium carbonate from spodumene by a sodium carbonate autoclave process. *Hydrometallurgy* 109, 43–45.

Chitrakar, R., Makita, Y., Ooi, K., Sonoda, A. (2013). Magnesium-doped manganese oxide with lithium ion-sieve property: Lithium adsorption from salt lake brine. *Bull. Chem. Soc. Jpn.* 87 (7), 850–855.

Chitrakar, R., Makita, Y., Ooi, K., Sonoda, A. (2014). Lithium recovery from salt lake brine by H_2TiO_3. *Dalton Trans* 43 (23), 8933–8939.

Chubb, P.A. (1963). Treatment of lithium ores. Google Patents. http://www.google.com/patents/US3073673.

Coleman, J.H., Jaffa, N.E. (1935). Recovering lithium compounds. Google Patents. http://www.google.com/patents/US2024026.

Cox, K., Bell, J., Pankhurst, R. (1979). *The Interpretation of Igneous Rocks.* Unwin Hyman.

Crocker, L., Lien, R.H., May, J.T., Witkowsky, D.S., Seidel, D.C. (1988). *Lithium and Its Recovery from Low-grade Nevada Clays.* U.S. Government Printing Office.

Cuney, M., Marignac, C., Weisbrod, A. (1992). The Beauvoir topaz-lepidolite albite granite (Massif Central, France); the disseminated magmatic Sn-Li-Ta-Nb-Be mineralization. *Economic Geology* 87 (7), 1766–1794.

Cunningham, G.L. (1953). Preparation of lithium chloride from spodumene. Google Patents. http://www.google.com/patents/US2627452.

Dana, J., Dana, E., Palache, C., Frondel, C., Berman, H. (1951). *Halides, nitrates, borates, carbonates, sulfates, phosphates, arsenates, tungstates, molybdates, etc.* J. Wiley & Sons.

Deer, W., Howie, R., Zussman, J. (1986). *Rock-forming Minerals: Disilicates and ring silicates. Vol. 1B.* Longman.

Dwyer, T.E. (1957). Recovery of lithium from spodumene ores. Google Patents. http://www.google.com/patents/US2801153.

Ebensperger, A., Maxwell, P., Moscoso, C. (2005). The lithium industry: Its recent evolution and future prospects. *Resources Policy* 30 (3), 218–231.

Ellestad, R.B., Leute, K.M. (1950). Method of extracting lithium values from spodumene ores. Google Patents. http://www.google.com/patents/US2516109.

Förster, H.-J., Tischendorf, G., Trumbull, R. B., Gottesmann, B. (1999). Late-Collisional Granites in the Variscan Erzgebirge, Germany. *Journal of Petrology* 40 (11), 1613–1645.

Fransolet, A.M. (1989). The problem of Na-Li substitution in primary Li-Al phosphates: new data on lacroixite , a relatively widespread mineral. *The Canadian Mineralogist* 27, 211–217.

Fransolet, A.M., Fontan, F., Parseval, P.d. (2007). Natromontebrasite, a discredited mineral species. *The Canadian Mineralogist* 45, 391–396.

Frevel, L.K., Kressley, L.J. (1962). Separation of lithium from lithium bearing micas and amblygonite. Google Patents. https://www.google.com/patents/US3032389.

Frost, B., Barnes, C., Collins, W., Arculus, R., Ellis, D., Frost, C. (2001). A Geochemical Classification for Granitic Rocks. *Journal of Petrology* 42 (11), 2033–2048.

Galaxy Resources Ltd, 2011. Jiangsu Lithium Carbonate Plant. Accessed 2 November 2011.

Galaxy Resources Ltd, 2012. Galaxy sells first lithium carbonate from Jiangsu. Accessed 3 August, 2014.

Galli, D.E., Humana, D., de las Mercedes Otaiza, M., Cachagua, C.R., Santillan, R.E. (2014). Process for recovering lithium from a brine. Google Patents. http://www.google.com/patents/US8641992.

Galliski, M.A., Cerny, P., Marquez-Zavalia, M.F., Chapman, R. (2012). An association of secondary Al-Li-Be-Ca-Sr phosphates in the San Elias pegmatite, San Luis, Argentina. *The Canadian Mineralogist* 50 (4), 933–942.

Garrett, D.E. (2004). *Handbook of lithium and natural calcium chloride. Their deposits, processing, uses and properties*, 1st ed. Elsevier Academic Press, Amsterdam, Boston.

Goodenough, R.D., Stenger, V.A. (1961). Recovery of lithium from lithium bearing ores. Google Patents. http://www.google.com/patents/US2980499.

Groat, L.A., Raudsepp, M., Hawthorne, F.C., Ercit, T.S., Sherriff, B.L., Hartman, J.S. (1990). The amblygonite-montebrasite series; characterization by single-crystal structure refinement, infared spectroscopy, and multinuclear MAS-NMR spectroscopy. *American Mineralogist* 75 (9-10), 992–1008.

Hamzaoui, A.H., Hammi, H., M'nif, A. (2007). Operating conditions for lithium recovery from natural brines. *Russian Journal of Inorganic Chemistry* 52 (12), 1859–1863.

Han, Y., Kim, H., Park, J. (2012). Millimeter-sized spherical ion-sieve foams with hierarchical pore structure for recovery of lithium from seawater. *Chemical Engineering Journal* 210 (0), 482–489.

Hawthorne, F.C., Cerný, P. (1977). The alkali-metal positions in Cs-Li beryl. *The Canadian Mineralogist* 15 (3), 414–421.

Hayes, E.T., Williams, F.P., Sternberg, W.M. (1950). Production of lithium chloride from spodumene. Google Patents. http://www.google.com/patents/US2533246.

Heinrich, E.W., Salotti, C.A., Giardini, A.A. (1978). Hydrogen-mineral reactions and their application to the removal of iron from spodumene. *Energy* 3 (3), 273–279.

Huang, H.H. (2005). Stabcal software. Montana Tech of the University of Montana, USA.
https://www.mtech.edu/academics/mines/metallurgy/bios/Huang%20Resume1.pdf

Jandová, J., Dvořák, P., Vu, H.N. (2010). Processing of zinnwaldite waste to obtain Li2CO3. *Hydrometallurgy* 103 (1-4), 12–18.

Jandová, J., Vu, H.N., Belková, T., Dvorák, P., Kondás, J. (2009). Obtaining Li_2CO_3 from zinnwaldite wastes. *Ceramics – Silikáty* 53 (2), 108–112.

Kalenowski, L.H., Runke, S.M. (1952). *Recovery of lithium from spodumene-amblygonite mixtures.* U.S. Dept. of the Interior, Bureau of Mines.

Kawata, M., Tanaka, H., Mitsuhashi, K., Kawarabuki, R., Yamamoto, Y., Kamiyama, K., Moriya, A., and Sakai, N. (2013). Method for producing lithium carbonate. Google Patents. http://www.google.com/patents/US20130251610.

Kepfer, R.J., Pfanstiel, R. (1935). Recovery of lithium values from lithium bearing ores. Google Patents. http://www.google.com/patents/US2022003.

Kesler, S.E., Gruber, P.W., Medina, P.A., Keoleian, G.A., Everson, M.P., and Wallington, T.J. (2012). Global lithium resources: Relative importance of pegmatite, brine and other deposits. *Ore Geology Reviews* 48, 55–69.

Kondás J., Jandová J. (2006). Lithium extraction from zinnwaldite wastes after gravity dressing of Sn-W ores. *Acta Metallurgica Slovaca* 12, 197–202.

Kretz, R., Loop, J., Hartree, R. (1989). Petrology and Li-Be-B geochemistry of muscovite-biotite granite and associated pegmatite near Yellowknife, Canada. *Mineralogy and Petrology* 102 (2), 174–190.

Kuznetsova, L.G., Prokof'ev, V. (2009). Petrogenesis of extremely lithium-rich spodumene aplites of the Tastyg deposit, Sangilen Highland, Tyva Republic. *Doklady Earth Sciences* 429 (1), 1262–1266.

Leavens, P.B., Dunn, P.J., Gaines, R.V. (1978). Compositional and refractive index variations of the herderite-hydroxyl-herderite series. *American Mineralogist* 63, 913–917.

Li, E.Y., Grichuk, D.V., Shilobreeva, S.N., Chareev, D.A. (2011). Interaction between (alumino) silicates and SO2 – containing gas: experiment and thermodynamic model. *Vestnik Otdelenia nauk o Zemle RAN* 3 (NZ6064).

Lide, D.R. (2005). *CRC Handbook of chemistry and physics*, 86th ed ed. Taylor & Francis, Boca Raton [etc.].

Linnen, R.L., van Lichtervelde, M., Černý, P. (2012). Granitic Pegmatites as Sources of Strategic Metals. *Elements* 8 (4), 275–280.

Löf, G. O. G., Lewis, W.K. (1942). Lithium chloride from lepidolite. *Ind. Eng. Chem.* 34 (2), 209–216.

Luong, V.T., Kang, D.J., An, J.W., Dao, D.A., Kim, M.J., Tran, T. (2014). Iron sulphate roasting for extraction of lithium from lepidolite. *Hydrometallurgy* 141, 8–16.

Luong, V.T., Kang, D.J., An, J.W., Kim, M.J., Tran, T. (2013). Factors affecting the extraction of lithium from lepidolite. *Hydrometallurgy* 134–135, 54–61.

Manning, D. (1986). Contrasting styles of Sn-W mineralisation in peninsular Thailand and SW England. *Mineralium Deposita* 21 (1), 44–52.

Mazza, H., Cohen, S.L., Schafer, G.H. (1960). Process for recovering alkali metal values from lepidolite. Google Patents. http://www.google.com/patents/US2940820.

Medina, L.F., El-Naggar, M. M. A. A. (1984). An alternative method for the recovery of lithium from spodumene. *Metall. Trans. B* 15 (4), 725–726.

Monier, G., Robert, J.L. (1986). Evolution of the miscibility gap between muscovite and biotite solid solutions with increasing lithium content: an experimental study in the system K_2O-Li_2O-MgO-FeO-Al_2O_3-SiO_2-H_2O-HF Evolution of the miscibility gap

between muscovite and biotite solid solutions with increasing lithium content: an experimental study in the system K_2O-Li_2O-MgO-FeO-Al_2O_3-SiO_2-H_2O-HF at 600°C, 2 kbar P_{H2O}: comparison with natural lithium micas. *Mineralogical Magazine* 50, 641–651.

Mulja, T., Williams-Jones, A.E., Wood, S.A., Boily, M. (1995). The rare-element-enriched monzogranite-pegmatite-quartz vein systems in the Preissac-Lacorne Batholith, Quebec; II, Geochemistry and petrogenesis. *The Canadian Mineralogist* 33 (4), 817–833.

Neiva, A.M.R., Ramos, J.M.F. (2010). Geochemistry of granitic aplite-pegmatite sills and petrogenetic links with granites, Guarda-Belmonte area, central Portugal. *European Journal of Mineralogy* 22 (6), 837–854.

Nichoson, C.M. (1946). Production of lithium compounds. Google Patents. http://www.google.com/patents/US2413644.

Outotec (2011). HSC chemistry software, version 7.1.

Pan Global Resources (2015). Lithium & Borates, Applications of Lithium.

Paukov, I.E., Kovalevskaya, Y.A., Kiseleva, I.A., Shuriga, T.N. (2010). A low-temperature heat capacity study of natural lithium micas. *Journal of Thermal Analysis and Calorimetry*. 99 (2), 709–712.

Peiró, T.L., Méndez, V.G., Ayres, R.U. (2013a). Lithium: Sources, Production, Uses, and Recovery Outlook. *JOM* 65 (8), 986–996.

Peiró, T.L., Méndez, V.G., Ayres, R.U. (2013b). Lithium: Sources, Production, Uses, and Recovery Outlook. *JOM* 65 (8), 986–996.

Peterson, J.A. (1960). Process for recovering lithium values. Google Patents. http://www.google.com/patents/US2924507.

Peterson, J.A., Gloss, G.H. (1959). Lithium values recovery process. Google Patents. http://www.google.com/patents/US2893828.

Pollard, P.J., Taylor, R. P. (1991). *Petrogenetic and metallogenetic implications of the occurrence of topaz-Li-mica granite at the Yichun Ta-Nb-Li mine, Jiangxi Province,*

south China, Pagel, M. & Leroy ed. Source, transport and deposition of metals, Balkema, Amsterdam.

Raimbault, L. (1998). Composition of complex lepidolite-type granitic pegmatites and of constituent columbite-tantalite, Chedeville, Massif Central, France. *The Canadian Mineralogist* 36 (2), 563–583.

Robinson, G.P. (1961). Recovery of lithium from ore. Google Patents. http://www.google.com/patents/US2983576.

Rockwood Lithium (2015). Applications.

Rosales, G.D., Ruiz, M.C., Rodriguez, M.H. (2014). Novel process for the extraction of lithium from β-spodumene by leaching with HF. *Hydrometallurgy* 147-148, 1–6.

Roskill Information Services Ltd. (2009). *The Economics of Lithium,* 11th ed., United Kingdom.

Roskill Information Services Ltd. (2010). The Lithium markets: 2009 review and outlook.

Roskill Information Services Ltd. (23-25th 2012). Vehicle electrification and other lithium end-uses: How big and how quickly? 4th Lithium supply & Markets Conference.

Roskill Information Services Ltd. (2013). *Lithium: Market outlook to 2017,* 12th ed., United Kingdom.

Rudnick, R.L., Gao, S. (2003). Composition of the continental crust 3, 1–64.

Schieffelin, W.J., Cappon, T.W. (1908). The manufacture of lithia from lepidolite. *J. Soc. Chem. Ind.* 27 (11), 549–550.

Siame, E., Pascoe, R.D. (2011). Extraction of lithium from micaceous waste from china clay production. *Minerals Engineering* 24 (14), 1595–1602.

Sitando, O., Crouse, P.L. (2012). Processing of a Zimbabwean petalite to obtain lithium carbonate. *International Journal of Mineral Processing* 102–103 (0), 45–50.

Slegens, H., Roder, O. (1936). Process for the production of lithium salts and metallic lithium. Google Patents. https://www.google.com/patents/US2059750.

Stephen, H., Stephen, T. (1979). *Solubilities of inorganic and organic compounds.* Pergamon press.

Stewart, D.B. (1978). Petrogenesis of lithium-rich pegmatites. *American Mineralogist* 63 (9-10), 970–980.

Talison Lithium Limited. Annual information form for the year ended June 30, 2012.

Taylor, R. P. (1992). Petrological and geochemical characteristics of the Pleasant Ridge zinnwaldite-topaz granite, southern New Brunswick, and comparisons with other topaz-bearing felsic rocks. *The Canadian Mineralogist* 30 (3), 895–921.

Thong, P.V., Vinh, N.C., Ngoc, T.B., Doan, B., Huong, N., Huu, D.L., Nho, N.C., Quan, N.D., Tam, T., Thu, G.T.M., Vien, N.T. (2009). Report of prospect estimation of tin minerals and rare earth elements (Ta, Li, Be), La Vi area, Quang Ngai Province., Mid-Centre Geological Division, 1–155. http://dgmv.gov.vn/default.aspx?tabid=138&ItemID=294.

Tindle, A.G., Webb, P.C. (1990). Estimation of lithium contents in trioctahedral micas using microprobe data; application to micas from granitic rocks. *European Journal of Mineralogy* 2 (5), 595–610.

Tinh, D.N. (2011). *Metallization features of lithium in La Vi area, Quang Ngai Province*. *Master's thesis*. Master.

Tischendorf, G., Förster, H.-J., Gottesmann, B. (2001). Minor- and trace-element composition of trioctahedral micas: a review. *Mineralogical Magazine* 65 (2), 249–276.

Tischendorf, G., Gottesmann, B., Foerster, H.-J., Trumbull, R.B. (1997). On Li-bearing micas; estimating Li from electron microprobe analyses and an improved diagram for graphical representation. *Mineralogical Magazine* 61 (6), 809–834.

USGS (2012). Lithium use in batteries. *USGS, Virginia.*

USGS (2013). Mineral Commodity Summaries 2013: Lithium. *USGS, Virginia.*, 94–95.

USGS (2014). Mineral Commodity Summaries 2014: Lithium. *USGS, Virginia.*, 94–95.

Vickerman, J., Briggs, D. (2001). *ToF-SIMS: Surface Analysis by Mass Spectrometry*. IM.

Vikström, H., Davidsson, S., Höök, M. (2013). Lithium availability and future production outlooks. *Applied Energy* 110, 252–266.

Vu, H., Bernardi, J., Jandová, J., Vaculíková, L., and Goliáš, V. (2013). Lithium and rubidium extraction from zinnwaldite by alkali digestion process: Sintering mechanism and leaching kinetics. *Int. J. Miner. Process.* 123, 9–17.

Wallace, R.B. (2012). Lithium, a strategic element for energy in the world market.

Wang, R.C., Che, X.D., Zhang, W.L., Zhang, A.C., Zhang, H. (2009). Geochemical evolution and late re-equilibration of Na–Cs-rich beryl from the Koktokay #3 pegmatite (Altai, NW China). *European Journal of Mineralogy* 21 (4), 795–809.

Webster, J.D., Thomas, R., Rhede, D., Förster, H., Seltmann, R. (1997). Melt inclusions in quartz from an evolved peraluminous pegmatite: Geochemical evidence for strong tin enrichment in fluorine-rich and phosphorus-rich residual liquids. *Geochimica et Cosmochimica Acta* 61 (13), 2589–2604.

Whitney, D.L., Evans, B.W. (2010). Abbreviations for names of rock-forming minerals. *American Mineralogist* 95 (1), 185–187.

Yan, Q., Li, X., Wang, Z., Wu, X., Guo, H., Hu, Q., Peng, W., Wang, J. (2012a). Extraction of valuable metals from lepidolite. *Hydrometallurgy* 117–118 (0), 116–118.

Yan, Q., Li, X., Wang, Z., Wu, X., Wang, J., Guo, H., Hu, Q., Peng, W. (2012b). Extraction of lithium from lepidolite by sulfation roasting and water leaching. *International Journal of Mineral Processing* 110–111, 1–5.

Yan, Q., Li, X., Yin, Z., Wang, Z., Guo, H., Peng, W., Hu, Q. (2012c). A novel process for extracting lithium from lepidolite. *Hydrometallurgy* 121-124, 54–59.

Yan, Q.X., Li, X.H., Wang, Z.X., Wang, J.X., Guo, H.J., Hu, Q.Y., Peng, W.J., Wu, X.F. (2012d). Extraction of lithium from lepidolite using chlorination roasting–water leaching process. *Transactions of Nonferrous Metals Society of China* 22 (7), 1753–1759.

Yin, L., Pollard, P.J., Hu Shouxi, Taylor, R.G. (1995). Geologic and geochemical characteristics of the Yichun Ta-Nb-Li deposit, Jiangxi Province, South China. *Economic Geology* 90 (3), 577–585.

Zbranek, V., Bertolli, S., Vargas, P. (2013). Production of lithium and potassium compounds. Google Patents. http://www.google.com/patents/US8431005.

Appendix

Appendix 1

EMPA results

Table 1. Representative EPMA data (in wt. %) for **albite** in the granitic rocks from the Dong Ram area in the La Vi mining District, Vietnam.

Analysis #	Ab 1-13	Ab 1-16	Ab 6-2	Ab 6-4	Ab 1-1
SiO_2	68.2	67.2	68.0	68.1	68.2
Al_2O_3	20.4	20.4	20.2	20.5	20.6
FeO	0.01	<0.01	0.02	0.04	0.01
MnO	<0.01	0.01	0.04	0.02	0.03
CaO	0.21	0.31	0.07	0.14	0.12
Na_2O	11.68	11.30	11.40	11.51	11.41
K_2O	0.08	0.07	0.09	0.12	0.12
P_2O_5	0.6	0.9	0.3	0.1	1.0
F	<0.01	0.06	<0.01	0.07	<0.01
Cl	<0.01	0.03	0.01	<0.01	<0.01
O≡F, Cl		0.03		0.03	
Total	101.2	100.3	100.1	100.6	101.5
Formula calculated on the basis of 8 oxygen atoms					
Si	2.9434	2.9270	2.9639	2.9593	2.9301
P	0.0118	0.0161	0.0051	0.0017	0.0176
Al^{IV}	0.0448	0.0569	0.0310	0.0390	0.0523
Σ	3.0000	3.0000	3.0000	3.0000	3.0000
Al	0.9898	0.9891	1.0069	1.0108	0.9893
Fe	0.0004	-	0.0007	0.0015	0.0004
Mn	-	0.0004	0.0015	0.0007	0.0011
Σ	0.9902	0.9895	1.0091	1.0130	0.9908
Ca	0.0097	0.0163	0.0033	0.0065	0.0055
Na	0.9769	0.9537	0.9631	0.9692	0.9500
K	0.0044	0.0061	0.0050	0.0066	0.0066
Σ	0.9910	0.9761	0.9714	0.9823	0.9621
F	-	0.0083	-	0.0096	-
Cl	-	0.0022	0.0007	-	-
Σ		0.0105	0.0007	0.0096	

Total Fe as FeO, Ab = albite**,** *n* = number of points**.**

Table 1. *Continued*.

Analysis #	Ab 1-8	Ab 3-4	Ab 5-5	**Albite**	
				Average (n = 56)	Std Dev
SiO_2	69.1	68.3	68.1	68.3	0.6
Al_2O_3	20.1	20.4	20.7	20.3	0.3
FeO	0.03	<0.01	<0.01	0.02	0.01
MnO	<0.01	0.02	0.04	0.02	0.02
CaO	0.05	0.08	0.22	0.2	0.1
Na_2O	11.57	11.19	11.64	11.4	0.2
K_2O	0.10	0.07	0.06	0.10	0.03
P_2O_5	<0.01	0.05	0.1	0.5	0.4
F	0.01	0.05	0.11	0.05	0.03
Cl	0.01	<0.01	0.01	0.01	0.01
O≡F, Cl	0.01	0.02	0.05	0.02	
Total	101.0	100.1	101.0	100.9	
Formula calculated on the basis of 8 oxygen atoms					
Si	2.9845	2.9737	2.9513	2.9569	
P	-	0.0008	0.0017	0.0094	
Al^{IV}	0.0155	0.0255	0.0470	0.0337	
Σ	3.0000	3.0000	3.0000	3.0000	
Al	1.0091	1.0208	1.0108	1.0008	
Fe	0.0011	-	-	0.0003	
Mn	-	0.0007	0.0015	0.0003	
Σ	1.0102	1.0215	1.0123	1.0014	
Ca	0.0023	0.0037	0.0102	0.0078	
Na	0.9688	0.9442	0.9781	0.9595	
K	0.0055	0.0039	0.0033	0.0053	
Σ	0.9766	0.9518	0.9916	0.9726	
F	0.0014	0.0069	0.0151	0.0061	
Cl	0.0007	-	0.0007	0.0006	
Σ	0.0021	0.0069	0.0158	0.0067	

Total Fe as FeO, Ab = albite**,** n = number of points**.**

Table 2. Representative EPMA data (in wt. %) for **muscovite** in the granitic rocks from the Dong Ram area in the La Vi mining District, Vietnam.

Analysis #	Ms 2-5	Ms 4-4	Ms 5-1	Ms 2-8	Ms 5-4
SiO_2	46.0	45.8	45.7	46.4	46.8
TiO_2	0.02	0.02	0.02	0.03	0.01
Al_2O_3	37.6	38.8	38.1	35.2	37.5
FeO	0.34	0.17	0.14	0.22	0.05
MnO	0.18	0.15	0.34	0.98	0.55
MgO	0.02	0.02	0.01	0.01	0.01
CaO	0.02	0.01	0.04	0.04	0.07
Na_2O	0.54	0.45	0.56	0.44	0.54
K_2O	9.88	10.65	10.36	10.55	9.91
Li_2O*	0.08	0.06	0.07	0.47	0.29
H_2O*	4.3	4.4	4.3	3.6	4.0
F	0.51	0.43	0.48	1.75	1.18
Cl	<0.01	<0.01	0.01	<0.01	0.01
O≡F, Cl	0.21	0.18	0.2	0.74	0.5
Total	99.3	100.8	99.9	99.0	100.4
Formula calculated on the basis of 22 oxygen atoms					
Si	6.0988	6.0006	6.0334	6.2147	6.1282
Al^{IV}	1.9012	1.9994	1.9666	1.7853	1.8718
Σ	8.0000	8.0000	8.0000	8.0000	8.0000
Al^{VI}	3.9698	3.9948	3.9693	3.7714	3.9214
Ti	0.0020	0.0020	0.0020	0.0030	0.0010
Fe	0.0377	0.0186	0.0155	0.0247	0.0055
Mn	0.0202	0.0167	0.0380	0.1113	0.0610
Mg	0.0040	0.0039	0.0020	0.0020	0.0020
Li	0.0442	0.0306	0.0391	0.2529	0.1536
Σ	4.0779	4.0666	4.0659	4.1653	4.1445
Ca	0.0028	0.0014	0.0057	0.0057	0.0098
Na	0.1389	0.1144	0.1435	0.1144	0.1372
K	1.6712	1.7809	1.7458	1.8043	1.6563
Σ	1.8129	1.8967	1.895	1.9244	1.8033
OH	3.7861	3.8217	3.7972	3.2579	3.5088
F	0.2139	0.1783	0.2006	0.7421	0.4890
Cl	-	-	0.0022	-	0.0022
Σ	4.0000	4.0000	4.0000	4.0000	4.0000

* calculated after Tindle & Webb (1990). Total Fe as FeO, Ms = muscovite**,** *n* = number of points**.**

Table 2. *Continued*.

Analysis #	Ms_6-2	Ms_4-5	Ms_1-5	Muscovite	
				Average (n = 32)	Std Dev
SiO_2	45.9	45.4	46.1	45.9	0.7
TiO_2	0.07	0.03	<0.01	0.1	0.2
Al_2O_3	36.2	37.4	37.9	37.5	1.1
FeO	0.14	0.14	0.21	0.3	0.4
MnO	0.67	0.02	0.08	0.3	0.3
MgO	<0.01	0.01	0.01	0.2	0.2
CaO	<0.01	0.05	<0.01	0.05	0.09
Na_2O	0.36	0.63	0.44	0.6	0.2
K_2O	10.86	10.04	10.06	10.3	0.4
Li_2O*	0.2	0.33	0.04	0.2	0.1
H_2O*	4.1	3.9	4.4	4.2	0.2
F	0.89	1.31	0.37	0.7	0.4
Cl	<0.01	0.02	<0.01	0.02	0.00
O≡F, Cl	0.37	0.56	0.16	0.3	
Total	99.0	98.7	99.5	100.1	
Formula calculated on the basis of 22 oxygen atoms					
Si	6.1495	6.0563	6.0951	6.0655	
Al^{IV}	1.8505	1.9437	1.9049	1.9345	
Σ	8.0000	8.0000	8.0000	8.0000	
Al^{VI}	3.8610	3.9419	4.0026	3.9445	
Ti	0.0070	0.0030	-	0.0012	
Fe	0.0157	0.0156	0.0232	0.0163	
Mn	0.0760	0.0023	0.0090	0.0364	
Mg	-	0.0020	0.0020	0.0023	
Li	0.1083	0.1783	0.0209	0.0964	
Σ	4.068	4.1431	4.0577	4.0971	
Ca	-	0.0072	-	0.0058	
Na	0.0934	0.1631	0.1127	0.1313	
K	1.8542	1.7102	1.6951	1.7470	
Σ	1.9476	1.8805	1.8078	1.8841	
OH	3.6232	3.4422	3.8454	3.6534	
F	0.3768	0.5533	0.1546	0.3454	
Cl	-	0.0045	-	0.0012	
Σ	4.0000	4.0000	4.0000	4.0000	

* calculated after Tindle & Webb (1990). Total Fe as FeO, Ms = muscovite**,** n = number of points**.**

Table 3. Representative EPMA data (in wt.%) for **lepidolite** in the granitic rocks from the Dong Ram area in the La Vi mining District, Vietnam.

Analysis #	Lpd 1-19	Lpd 1-21	Lpd 4-2	Lpd 1-4	Lpd 5-2
SiO_2	50.6	48.0	50.1	52.6	50.2
TiO_2	0.01	0.06	0.03	0.05	0.04
Al_2O_3	26.2	32.6	29.4	25.3	28.1
FeO	0.1	0.04	0.04	0.06	0.02
MnO	0.48	0.15	0.39	0.55	0.62
MgO	0.05	0.01	0.01	0.09	0.01
CaO	0.24	0.04	0.01	0.08	0.06
Na_2O	0.28	0.43	0.31	0.26	0.42
K_2O	10.32	10.24	10.11	10.32	10.2
Li_2O*	4.96	4.23	4.81	5.56	4.86
H_2O*	0.9	2.7	1.6	0.7	1.4
F	7.51	4.15	6.29	8.13	6.62
Cl	<0.01	0.01	<0.01	0.02	<0.01
O≡F, Cl	3.16	1.75	2.65	3.43	2.79
Total	98.5	100.9	100.5	100.3	99.8
Formula calculated on the basis of 22 oxygen atoms					
Si	6.7390	6.2381	6.5211	6.8631	6.5995
Al^{IV}	1.2610	1.7619	1.4789	1.1369	1.4005
Σ	8.0000	8.0000	8.0000	8.0000	8.0000
Al^{VI}	2.8505	3.2222	3.0284	2.7434	2.9449
Ti	0.0010	0.0059	0.0029	0.0049	0.0040
Fe	0.0111	0.0043	0.0044	0.0065	0.0022
Mn	0.0542	0.0165	0.0430	0.0607	0.0690
Mg	0.0099	0.0019	0.0019	0.0175	0.0020
Li	2.6604	2.2100	2.5219	2.9133	2.5703
Σ	5.5871	5.4608	5.6025	5.7463	5.5924
Ca	0.0343	0.0056	0.0014	0.0112	0.0084
Na	0.0723	0.1083	0.0783	0.0657	0.1070
K	1.7538	1.6968	1.6802	1.7162	1.7094
Σ	1.8604	1.8107	1.7599	1.7931	1.8248
OH	0.8355	2.2928	1.4081	0.6433	1.2492
F	3.1645	1.7050	2.5919	3.3523	2.7508
Cl	-	0.0022	-	0.0044	-
Σ	4.0000	4.0000	4.0000	4.0000	4.0000

* calculated after Tindle & Webb (1990). Total Fe as FeO, Lpd = lepidolite, *n* = number of points**.**

Table 3. *Continued*.

Analysis #	Lpd 4-5	Lpd 3-2	Lpd 1-2	**Lepidolite**	
				Average (n = 91)	Std Dev
SiO_2	52.9	49.5	49.9	50.8	1.6
TiO_2	0.01	0.02	0.03	0.03	0.02
Al_2O_3	23.5	27.7	27.1	27.3	2.9
FeO	0.01	0.05	0.14	0.1	0.1
MnO	0.82	0.87	0.48	0.6	0.5
MgO	0.04	0.03	0.03	0.03	0.02
CaO	0.05	0.03	0.02	0.05	0.08
Na_2O	0.29	0.33	0.24	0.3	0.1
K_2O	10.59	10.37	10.9	10.5	0.3
Li_2O*	5.64	4.65	4.77	5.0	0.5
H_2O*	0.3	1.4	1.4	1.3	0.8
F	8.88	6.61	6.55	6.9	1.6
Cl	<0.01	<0.01	0.01	0.01	0.01
O≡F, Cl	3.74	2.78	2.76	2.9	
Total	99.3	98.8	98.8	100.0	
Formula calculated on the basis of 22 oxygen atoms					
Si	6.9862	6.5960	6.6459	6.6703	
Al^{IV}	1.0138	1.4040	1.3541	1.3297	
Σ	8.0000	8.0000	8.0000	8.0000	
Al^{VI}	2.6477	2.9422	2.9057	2.8914	
Ti	0.0010	0.0020	0.0030	0.0015	
Fe	0.0011	0.0056	0.0156	0.0076	
Mn	0.0917	0.0982	0.0542	0.0657	
Mg	0.0079	0.0060	0.0060	0.0033	
Li	2.9945	2.4925	2.5538	2.6521	
Σ	5.7439	5.5465	5.5383	5.6216	
Ca	0.0071	0.0043	0.0029	0.0055	
Na	0.0742	0.0853	0.0620	0.0825	
K	1.7825	1.7633	1.8521	1.7504	
Σ	1.8638	1.8529	1.9170	1.8384	
OH	0.2939	1.2132	1.2382	1.1202	
F	3.7061	2.7868	2.7595	2.8775	
Cl	-	-	0.0023	0.0023	
Σ	4.0000	4.0000	4.0000	4.0000	

* calculated after Tindle & Webb (1990). Total Fe as FeO, Lpd = lepidolite, n = number of points.

Table 4. Representative EPMA data (in wt.%) for the **amblygonite-montebrasite**-series minerals in the granitic rocks from the Dong Ram area in the La Vi mining District, Vietnam.

Analysis #	4-8	4-10	6-39	6-25	6-42	6-46	6-21
Al_2O_3	33.4	35.1	35.0	31.7	34.5	35.2	33.7
FeO	0.02	0.01	0.03	<0.01	0.04	0.03	0.05
MnO	0.04	0.01	0.02	0.11	0.02	0.01	0.03
CaO	0.03	0.03	0.06	1.86	0.45	0.04	0.07
Na_2O	1.07	0.02	0.79	3.26	0.69	0.04	1.13
K_2O	0.02	0.01	0.01	0.01	0.03	<0.01	<0.01
P_2O_5	48.7	48.4	45.6	47.1	47.0	47.9	48.8
F	7.72	6.91	6.38	8.49	7.01	7.35	8.11
Li_2O*	9.64	10.23	9.52	8.44	9.72	10.16	9.68
H_2O*	2.5	2.9	2.9	2.0	2.7	2.6	2.3
O≡F	3.25	2.91	2.69	3.58	2.95	3.1	3.41
Total	99.9	100.7	97.6	99.4	99.2	100.2	100.5
Formula calculated on the basis of 4 oxygens and F, OH ions							
Al	0.9623	1.0035	1.0356	0.9278	1.0040	1.0133	0.9655
Fe	0.0004	0.0002	0.0006	-	0.0008	0.0006	0.0010
Σ	0.9627	1.0037	1.0362	0.9278	1.0048	1.0139	0.9665
Ca	0.0008	0.0008	0.0016	0.0495	0.0119	0.0010	0.0018
Na	0.0508	0.0009	0.0385	0.1570	0.0331	0.0019	0.0533
K	0.0006	0.0006	0.0003	0.0003	0.0009	-	-
Li	0.9486	0.9984	0.9612	0.8427	0.9660	0.9981	0.9467
Σ	1.0008	1.0007	1.0016	1.0495	1.0119	1.0010	1.0018
P	1.0096	0.9940	0.9694	0.9894	0.9837	0.9910	1.0050
F	0.5974	0.5303	0.5066	0.6670	0.5481	0.5679	0.6237
OH	0.4026	0.4697	0.4921	0.3313	0.4515	0.4308	0.3763
Σ	1.0000	1.0000	0.9987	0.9983	0.9996	0.9988	1.0000

* calculated after Groat *et al.* (1990). Total Fe as FeO**.**

Table 4. *Continued*.

Analysis #	4-1	4-12	6-41	6-44	6-31	Range (n = 65)	
						Min	Max
Al_2O_3	34.7	33.2	34.0	34.2	34.2	31.7	35.4
FeO	<0.01	0.05	0.07	0.02	0.05	<0.01	0.35
MnO	0.04	<0.01	0.02	0.01	0.03	0.01	0.1
CaO	0.02	0.28	0.6	0.05	<0.01	0.01	1.86
Na_2O	<0.01	3.8	0.14	1.93	0.32	<0.01	5.3
K_2O	0.01	0.03	0.03	0.03	0.02	<0.01	0.06
P_2O_5	48.3	48.4	46.0	46.6	47.4	44.2	51.0
F	6.4	6.24	2.02	6.2	6.18	1.2	8.5
Li_2O*	10.18	8.44	9.77	9.08	9.87	7.6	10.5
H_2O*	3.1	3.2	5.0	3.1	3.1	2.0	5.4
O≡F	2.69	2.63	0.85	2.61	2.6		
Total	100.1	101.0	96.8	98.6	98.6		
Formula calculated on the basis of 4 oxygens and F, OH ions							
Al	0.9990	0.9464	1.0108	1.0010	1.0003		
Fe	-	0.0010	0.0015	0.0004	0.0010		
Σ	0.9990	0.9474	1.0123	1.0014	1.0013		
Ca	0.0005	0.0073	0.0162	0.0013	-		
Na	-	0.1782	0.0069	0.0928	0.0154		
K	0.0003	0.0009	0.0010	0.0009	0.0006		
Li	0.9997	0.8280	0.9922	0.9062	0.9840		
Σ	1.0005	1.0144	1.0163	1.0012	1.0000		
P	0.9988	0.9909	0.9826	0.9784	0.9942		
F	0.4941	0.4775	0.1613	0.4865	0.4848		
OH	0.5059	0.5225	0.8387	0.5131	0.5152		
Σ	1.0000	1.0000	1.0000	0.9996	1.0000		

* calculated after Groat *et al.* (1990). Total Fe as FeO**.**

Table 5. Representative EPMA data (in wt. %) for **herderite** in the granitic rocks from the Dong Ram area in the La Vi mining District, Vietnam.

Analysis #	He 7-3	He 7-6	He 7-15	He 7-23	He 7-24
BeO*	13.65	13.49	13.42	13.55	13.29
SiO_2	0.01	0.08	0.25	2.62	0.19
FeO	0.04	<0.01	0.05	0.04	<0.01
MnO	0.02	0.01	0.02	0.04	0.01
CaO	33.8	33.5	33.9	34.0	34.1
Na_2O	0.11	0.04	0.4	0.09	0.26
K_2O	0.02	0.01	0.03	0.57	0.01
SrO	0.14	0.48	0.46	0.03	0.47
P_2O_5	44.6	44.0	43.2	40.5	42.6
F	6.34	7.19	6.64	5.82	6.66
H_2O*	1.9	1.5	1.7	2.1	1.6
O≡F	2.67	3.03	2.8	2.45	2.8
Total	98.0	97.3	97.3	96.9	96.4
Formula calculated on the basis of 5 anions					
Ca	1.1052	1.1071	1.1263	1.0548	1.1431
Na	0.0065	0.0024	0.0241	0.0054	0.0158
K	0.0008	0.0004	0.0012	0.0223	0.0004
Be	1.0000	1.0000	1.0000	1.0000	1.0000
Sr	0.0025	0.0086	0.0083	0.0005	0.0085
Σ	2.115	2.1185	2.1599	2.083	2.1678
P	1.1522	1.1505	1.1335	1.0524	1.1311
F	0.6116	0.7018	0.6516	0.5656	0.6600
OH	0.3879	0.2982	0.3468	0.4339	0.3400
Σ	1.0000	1.0000	1.0000	1.0000	1.0000

* calculated after Galliski *et al.* (2012). Total Fe as FeO, He = Herderite, *n* = number of points**.**

Table 5. *Continued*.

Analysis #	He 6-11	He 6-14	He 7-18	Herderite	
				Average (n = 32)	Std Dev
BeO*	12.7	13.08	13.82	13.3	0.4
SiO_2	0.17	0.14	0.49	0.4	0.7
FeO	0.05	<0.01	0.01	0.03	0.02
MnO	0.02	<0.01	<0.01	0.04	0.03
CaO	33.9	34.3	33.3	34.0	0.8
Na_2O	0.06	0.18	0.01	0.1	0.1
K_2O	0.02	0.01	0.09	0.1	0.2
SrO	0.63	0.17	0.57	0.4	0.2
P_2O_5	40.1	41.7	44.9	43.0	1.7
F	5.86	6.29	5.73	6.4	0.5
H_2O*	1.8	1.7	2.3	2.0	0.2
O≡F	2.47	2.65	2.41	2.7	
Total	92.8	94.9	98.8	97.1	
Formula calculated on the basis of 5 anions					
Ca	1.1895	1.1701	1.0763	1.1293	
Na	0.0038	0.0111	0.0006	0.0058	
K	0.0008	0.0004	0.0035	0.0026	
Be	1.0000	1.0000	1.0000	1.0000	
Sr	0.0120	0.0031	0.0100	0.0059	
Σ	2.2061	2.1847	2.0904	2.1436	
P	1.1130	1.1239	1.1446	1.1264	
F	0.6073	0.6330	0.5460	0.6272	
OH	0.3927	0.3670	0.4540	0.3724	
Σ	1.0000	1.0000	1.0000	0.9996	

* calculated after Galliski *et al.* (2012). Total Fe as FeO, He = Herderite, n = number of points**.**

Table 6. Representative EPMA data (in wt.%) for **fluorapatite, topaz,** in the granitic rocks from the Dong Ram area in the La Vi mining District, Vietnam.

Analysis #	Ap 4-19	Ap 4-25	**Fluorapatite** Average (n = 85)	Std Dev	Tpz_1	Tpz_3	**Topaz** Average (n = 9)	Std Dev
SiO_2	0.25	0.04	0.1	0.2	31.6	32.0	32.3	0.4
Al_2O_3	0.15	0.01	0.1	0.2	57.2	57.2	57.2	0.2
FeO	0.05	<0.01	0.04	0.03	n.a.	n.a.	n.a.	
MnO	2.96	3.12	2.4	1.0	n.a.	n.a.	n.a.	
CaO	52.5	52.5	52.9	1.0	n.a.	n.a.	n.a.	
Na_2O	<0.01	<0.01	0.04	0.04	n.a.	n.a.	n.a.	
K_2O	<0.01	<0.01	0.05	0.06	n.a.	n.a.	n.a.	
SrO	n.a.	n.a.	n.a.		n.a.	n.a.	n.a.	
P_2O_5	41.3	41.5	41.3	1.1	n.a.	n.a.	n.a.	
F	4.12	3.71	4.2	0.4	19.3	18.8	19.1	0.2
Cl	0.06	0.03	0.02	0.01	n.a.	n.a.	n.a.	
H_2O*	n.a.	n.a.	n.a.		0.73	0.99	0.9	0.1
$O \equiv F$	1.75	1.57	1.79		8.11	7.92	8.0	
Total	99.6	99.3	99.4		100.7	101.1	101.5	
Formula calculated on the basis of 12 oxygens for fluorapatite, 5 oxygens and F, OH atoms for topaz.								
Si	0.0204	0.0033	0.0055		0.9611	0.9669	0.9737	
Al	0.0144	0.0010	0.0029		2.0518	2.0413	2.0338	
Fe	0.0034	-	0.0013		-	-	-	
Mn	0.2045	0.2152	0.1609		-	-	-	
Σ	0.2223	0.2162	0.1651		2.0518	2.0413	2.0338	
Ca	4.5914	4.5807	4.6485		-	-	-	
Na	-	-	-		-	-	-	
K	-	-	-		-	-	-	
Sr	-	-	-		-	-	-	
Σ	4.5914	4.5807	4.6485					
P	2.8551	2.8777	2.8665		-	-	-	
F	1.0630	0.9555	1.0989		1.8523	1.7995	1.8201	
Cl	0.0083	0.0041	0.0020		-	-	-	
OH	-	-			0.1477	0.2005	0.1796	
Σ	1.0713	0.9596	1.1009		2.0000	2.0000	1.9997	

Tpz: topaz; Ap: fluorapatite; Total Fe as FeO, n.a. = not analyzed, n = number of points**.**

Table 7. Representative EPMA data (in wt.%) for **beryl**, and **goyazite** in the granitic rocks from the Dong Ram area in the La Vi mining District, Vietnam.

Analysis #	Brl_5	Brl_8	**Beryl** Average (n = 10)	**Beryl** Std Dev	**Gz** 6-19	**Gz** 6-20
Li_2O*	0.34	0.33	0.34	0.04	n.a.	n.a.
BeO*	13.36	13.33	13.4	0.1	n.a.	n.a.
SiO_2	67.0	66.7	67.0	0.3	0.04	0.07
Al_2O_3	18.5	18.5	18.6	0.3	32.1	31.7
FeO	n.a.	n.a.	n.a.		0.02	0.03
MnO	n.a.	n.a.	n.a.		<0.01	0.01
CaO	n.a.	n.a.	n.a.		0.25	0.32
Na_2O	0.68	0.67	0.7	0.1	<0.01	0.01
K_2O	0.05	0.02	0.04	0.02	0.04	0.01
SrO	n.a.	n.a.	n.a.		20.3	20.4
P_2O_5	n.a.	n.a.	n.a.		28.3	27.7
F	n.a.	n.a.	n.a.		4.5	3.6
Cl	n.a.	n.a.	n.a.		n.a.	n.a.
H_2O*	n.a.	n.a.	n.a.		7.6	8.0
O ≡ F					1.89	1.53
Total	99.9	99.6	100.1		91.3	90.3
Formula calculated on the basis of 6 silicons for beryl, 14 oxygens and OH atoms for goyazite.						
Si	5.9995	5.9995	5.9995		0.0043	0.0075
Al	1.9507	1.9618	1.9636		4.1051	4.0178
Fe	-	-	-		0.0018	0.0027
Mn	-	-	-		0.0000	0.0046
Σ	1.9507	1.9618	1.9636		4.1069	4.0251
Ca	-	-	-		0.0291	0.0368
Na	0.1181	0.1169	0.1178		0.0000	0.0021
K	0.0057	0.0023	0.0033		0.0055	0.0014
Sr	-	-	-		1.2798	1.2703
Σ	0.1238	0.1202	0.1211		1.3144	1.3106
Li	0.1239	0.1192	0.1211		-	-
Be	2.8761	2.8808	2.8789		-	-
Σ	3.0000	3.0000	3.0000			
P	-	-	-		2.6015	2.5177
F	-	-	-		1.5374	1.2369
Cl	-	-	-		-	-
OH					3.4626	3.7631
Σ					5.0000	5.0000

Brl: beryl; Gz: goyazite. Total Fe as FeO, n.a. = not analyzed, n = number of points**,** * calculated after Wang *et al.* (2009) for beryl.

Table 8. Representative EPMA data (in wt.%) for **biotite** in the country rock from the Dong Ram area in the La Vi mining District, Vietnam.

Analysis #	Bt 1-5	Bt 1-9	Bt 1-10	Bt 2-1	**Biotite**	
					Average (n = 9)	Std Dev
SiO_2	35.5	36.0	35.9	35.8	35.8	0.2
TiO_2	2.09	2.14	2.08	2.12	2.10	0.03
Al_2O_3	20.1	20.0	19.9	20.0	20.0	0.1
FeO	18.92	18.51	18.72	18.5	18.7	0.2
MnO	0.12	0.22	0.19	0.22	0.19	0.05
MgO	9.74	9.74	9.68	9.66	10.00	0.04
CaO	0.02	<0.01	<0.01	<0.01	0.01	0.01
Na_2O	0.21	0.29	0.25	0.23	0.25	0.03
K_2O	8.36	8.71	8.94	8.49	8.7	0.3
Li_2O*	0.14	0.14	0.14	0.14	0.14	0.00
H_2O*	3.7	3.7	3.7	3.7	3.7	0.0
F	0.53	0.59	0.6	0.55	0.60	0.03
Cl	0.07	0.04	0.09	0.06	0.07	0.02
O≡F, Cl	0.24	0.26	0.27	0.25	0.3	
Total	99.3	99.8	99.9	99.2	100.0	
Formula calculated on the basis of 22 oxygen atoms						
Si	5.3534	5.3926	5.3898	5.3894	5.3813	
Al^{IV}	2.6466	2.6074	2.6102	2.6106	2.6187	
Σ	8.0000	8.0000	8.0000	8.0000	8.0000	
Al^{VI}	0.9190	0.9261	0.9110	0.9351	0.9228	
Ti	0.2370	0.2409	0.2346	0.2403	0.2382	
Fe	2.3862	2.3169	2.3479	2.3318	2.3457	
Mn	0.0153	0.0279	0.0241	0.0281	0.0239	
Mg	2.1895	2.1731	2.1640	2.1702	2.1742	
Li	0.0835	0.0828	0.0840	0.0847	0.0837	
Σ	5.8305	5.7677	5.7656	5.7902	5.7885	
Ca	0.0032	0.0000	0.0000	0.0000	0.0008	
Na	0.0614	0.0842	0.0727	0.0672	0.0714	
K	1.6080	1.6628	1.7101	1.6321	1.6533	
Σ	1.6726	1.7470	1.7828	1.6993	1.7255	
OH	3.7293	3.7106	3.6925	3.7225	3.7137	
F	0.2528	0.2793	0.2846	0.2622	0.2697	
Cl	0.0179	0.0101	0.0229	0.0153	0.0166	
Σ	4.0000	4.0000	4.0000	4.0000	4.0000	

* calculated after Tischendorf *et al.* (1997). Total Fe as FeO, Bt = biotite, n = number of points.

Table 9. Representative EPMA data (in wt.%) for **biotite** and **muscovite** in the country rock from the Dong Ram area in the La Vi mining District, Vietnam.

Analysis #	Ms 1-11	Ms 1-6	Ms 2-3	Ms 3-1	Ms 3-2	Ms 4-2	**Muscovite**	
							Average (n = 6)	Std Dev
SiO_2	45.3	45.8	45.7	46.4	46.3	44.0	45.6	0.9
TiO_2	0.42	0.36	0.46	0.22	0.21	0.28	0.3	0.1
Al_2O_3	35.3	35.9	36.5	36.5	36.7	34.8	36.0	0.8
FeO	2.46	0.81	0.9	0.75	0.79	0.8	1.1	0.7
MnO	<0.01	<0.01	<0.01	<0.01	0.02	<0.01	0.02	0.00
MgO	0.67	0.48	0.56	0.54	0.54	0.62	0.6	0.1
CaO	<0.01	0.05	0.01	0	0.01	0.04	0.02	0.02
Na_2O	0.72	0.75	0.96	0.74	0.83	0.85	0.8	0.1
K_2O	9.96	9.43	10.03	10.31	10.15	9.61	10	0.3
Li_2O*								
H_2O*	4.4	4.4	4.4	4.5	4.5	4.3	4.4	0.1
F	0.12	0.14	0.16	0.11	0.11	0.12	0.13	0.02
Cl	<0.01	0.02	0.02	0.01	<0.01	0.03	0.02	0.01
O≡F, Cl	0.05	0.06	0.07	0.05	0.05	0.06	0.06	
Total	99.3	98.1	99.6	100.0	100.1	95.4	98.9	
Formula calculated on the basis of 22 oxygen atoms								
Si	6.0880	6.1490	6.0706	6.1386	6.1132	6.1025	6.1103	
Al^{IV}	1.9120	1.8510	1.9294	1.8614	1.8868	1.8975	1.8897	
Σ	8.0000	8.0000	8.0000	8.0000	8.0000	8.0000	8.0000	
Al^{VI}	3.6755	3.8348	3.7909	3.8224	3.8285	3.7990	3.7918	
Ti	0.0424	0.0364	0.0460	0.0219	0.0209	0.0292	0.0328	
Fe	0.2764	0.0910	0.1001	0.0829	0.0873	0.0928	0.1218	
Mn	0.0000	0.0000	0.0000	0.0000	0.0022	0.0000	0.0004	
Mg	0.1342	0.0962	0.1110	0.1064	0.1064	0.1282	0.1137	
Li								
Σ	4.1285	4.0584	4.0480	4.0336	4.0453	4.0492	4.0605	
Ca	0.0000	0.0072	0.0014	0.0000	0.0014	0.0059	0.0027	
Na	0.1876	0.1955	0.2474	0.1897	0.2126	0.2287	0.2102	
K	1.7070	1.6167	1.7006	1.7383	1.7105	1.7008	1.6956	
Σ	1.8946	1.8194	1.9494	1.9280	1.9245	1.9354	1.9085	
OH	3.9490	3.9359	3.9282	3.9518	3.9540	3.9403	3.9432	
F	0.0510	0.0595	0.0673	0.0460	0.0460	0.0527	0.0537	
Cl	0.0000	0.0046	0.0045	0.0022	0.0000	0.0071	0.0031	
Σ	4.0000	4.0000	4.0000	4.0000	4.0000	4.0001	4.0000	

* calculated after after Tindle & Webb (1990). Total Fe as FeO, Ms = muscovite, n = number of points.

Appendix 2

SIMS results

Microscope images of sample

ifos

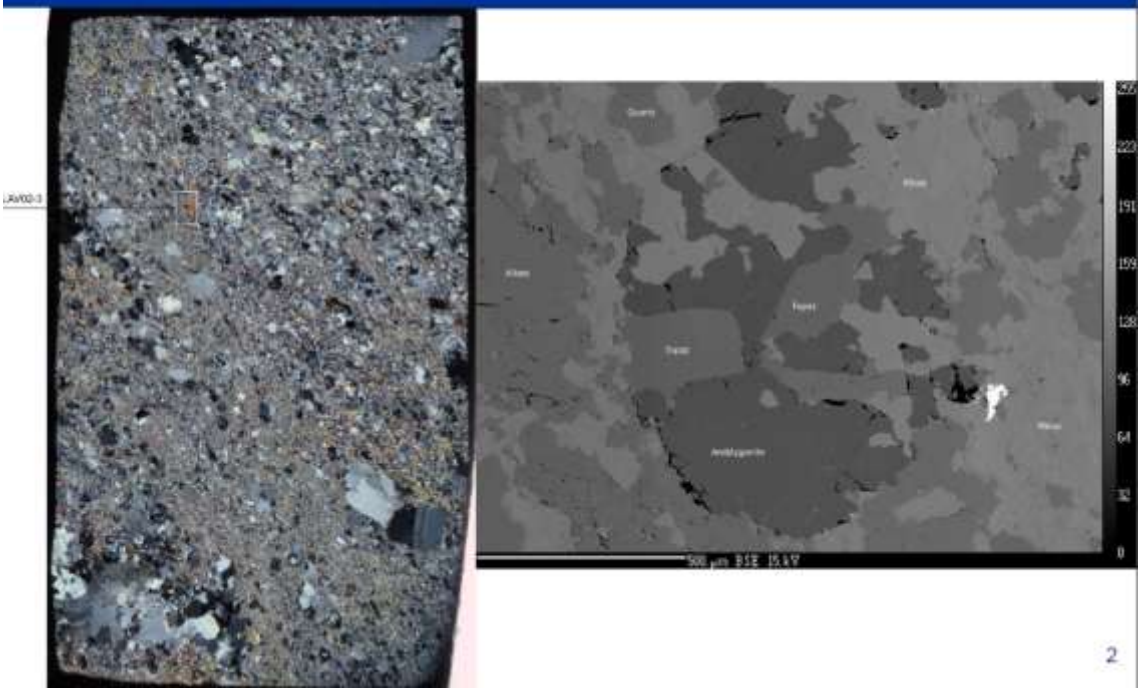

2

Selected ToF-SIMS Mappings

ifos

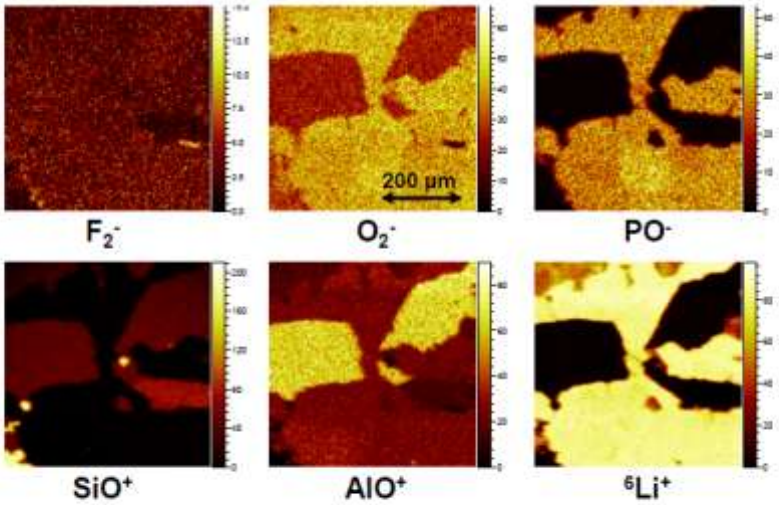

Analysis Position 1

4

Quantified XPS-Mapping

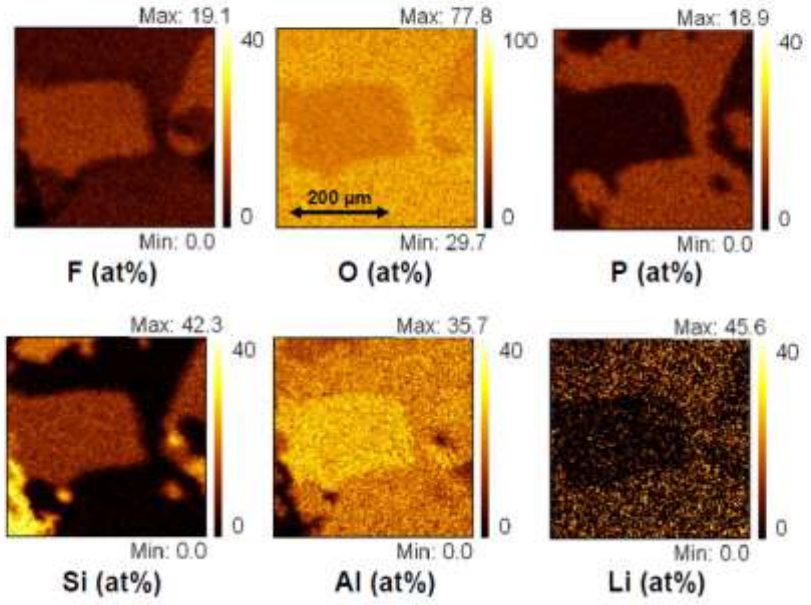

Analysis Position 1

5

XPS Spectra
(Spotanalysis in the center of the amblygonite)

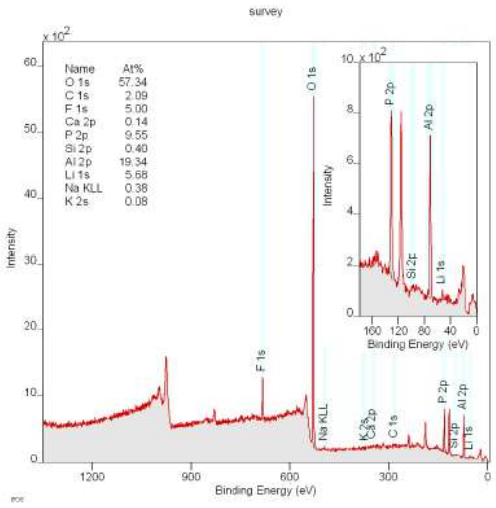

6

XPS Spectra
(analysis over a larger area)

ifos

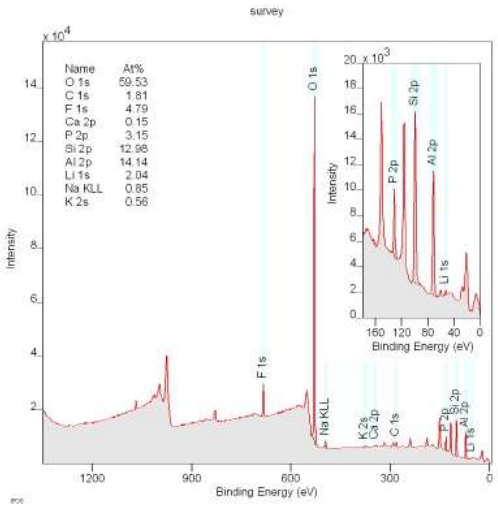

Comparisation of quantified composition
of the different areas

ifos

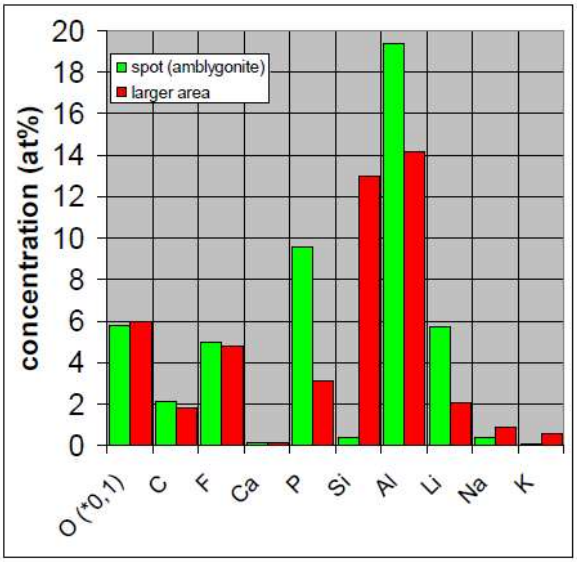

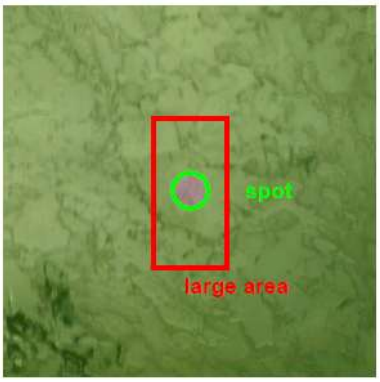

The Li concentration in the area
of the amplygonite is of the size of 5 at%

Image taken with the video-camera of the ToF-SIMS:

ifos

Analysis Position 1

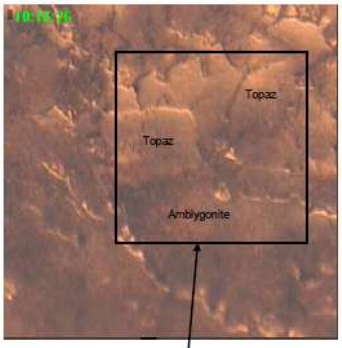

Area mapped in the following images

12

Lateral intensity distribution of selected positive secondary ions:

ifos

Positiv

Analysis Position 1

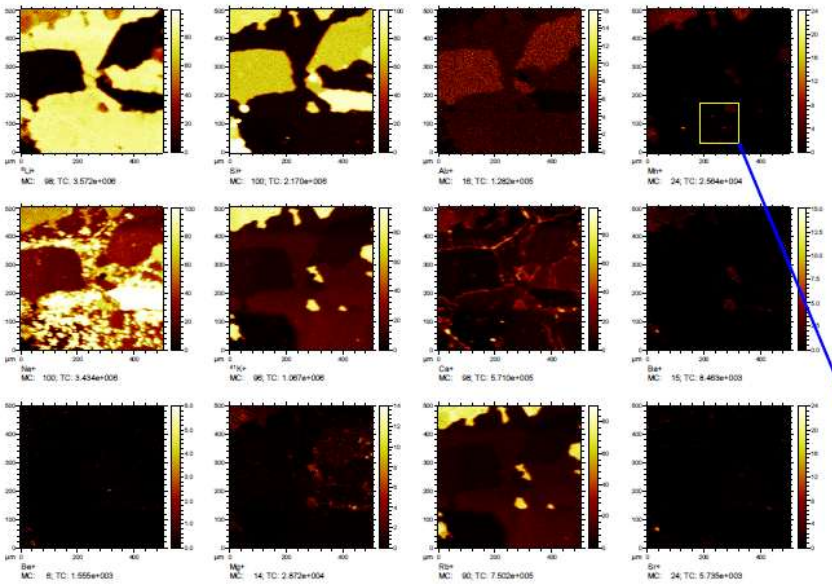

See page 8-9

13

Al was detected via the Al_2+ molecule because the Al^+ - intensity saturated the counter.

Lateral intensity distribution of selected positive secondary ions:

Positive

Analysis Position 1

minor elements and Cs

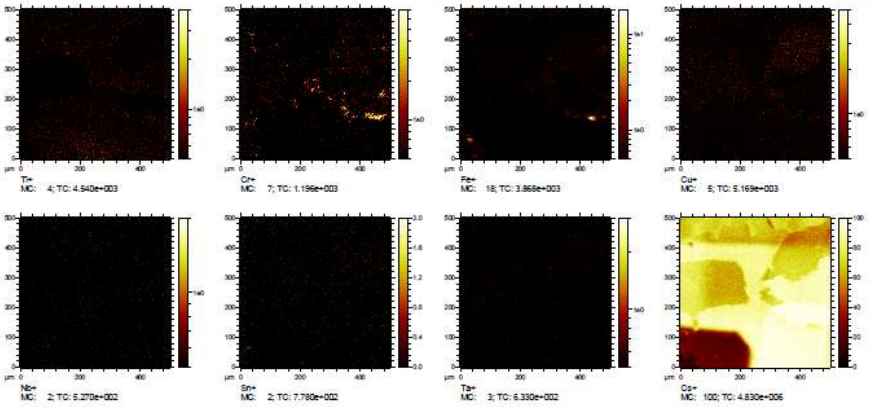

Logarithmic scales for Ti, Cr, Fe, Cu, Nb, Sn and Ta.
The ToF-SIMS apparatus is equipped with a Cs-sputtergun, therefore Cs might be superimposed by a background from the system although the gun was not applied for the present measurements.

14

Lateral intensity distribution of selected positive secondary ions:

Positiv

Zoom Analysis Position 1

„Zoom“ of the area marked on page 6

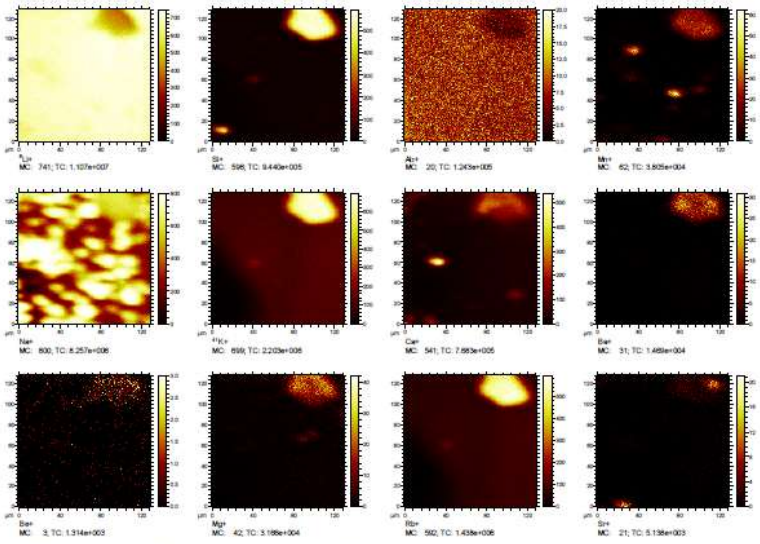

Al was detected via the Al_2+ molecule because the Al^+ - intensity saturated the counter.

15

Lateral intensity distribution of selected positive secondary ions:

ifos

Positive

„Zoom“ of the area marked on page 6, minor elements and Cs

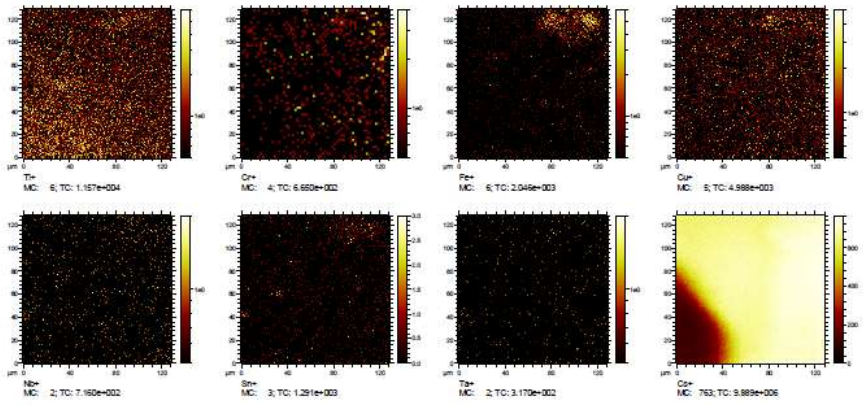

Logarithmic scales for Ti, Cr, Fe, Cu, Nb, Sn and Ta.
The ToF-SIMS apparatus is equipped with a Cs-sputtergun, therefore Cs might be superimposed by a background from the system although the gun was not applied for the present measurements.

Zoom Analysis Position 1

16

Lateral intensity distribution of selected negative secondary ions:

ifos

Negative

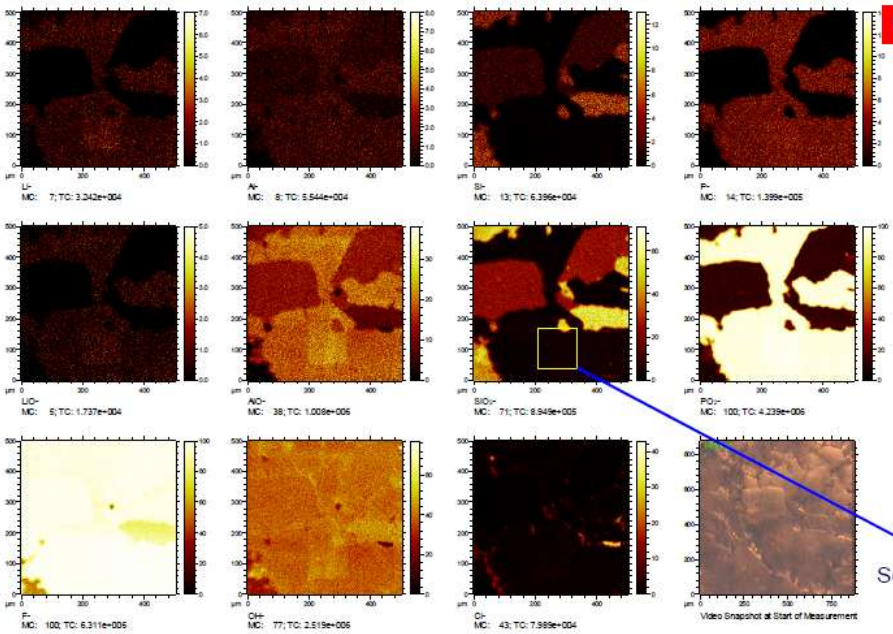

See next page

Analysis Position 1

17

Lateral intensity distribution of selected negative secondary ions:

Negative

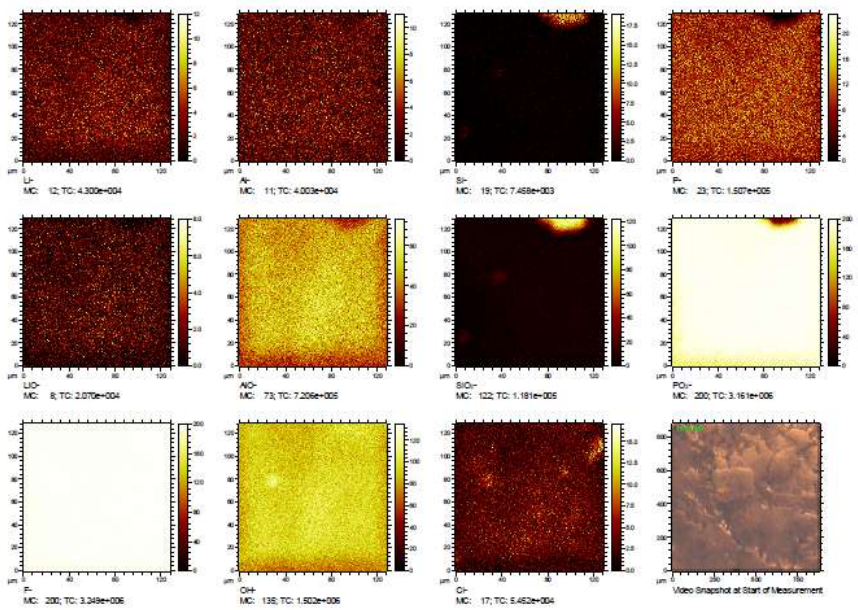

Zoom Analysis Position 1

18

Image taken with the video-camera of the ToF-SIMS:

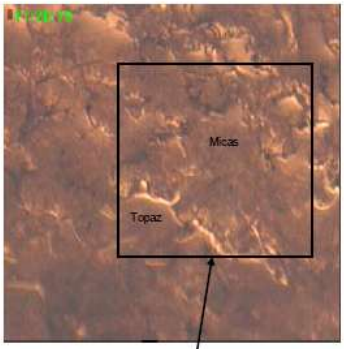

Area mapped in the following images

Analysis Position 2

19

Lateral intensity distribution of selected positive secondary ions:

ifos

Positive

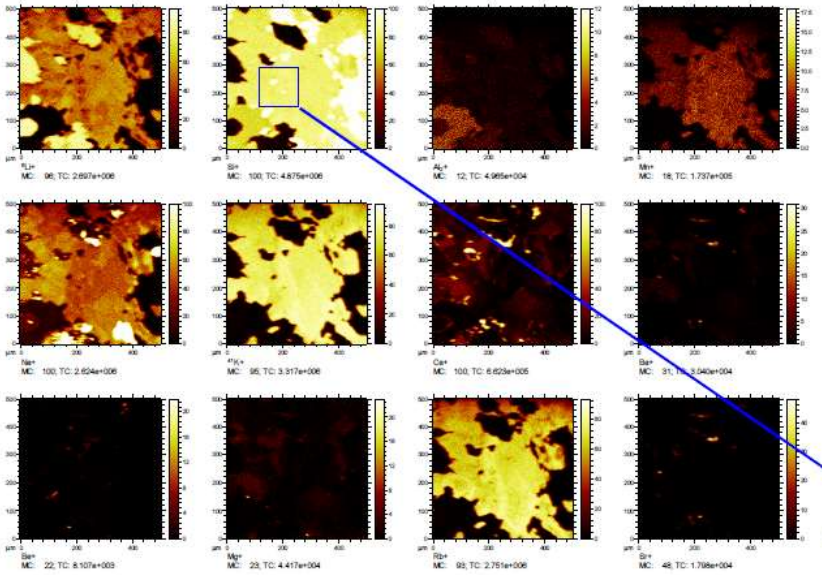

Analysis Position 2

See page 15-16

Al was detected via the Al_2+ molecule because the Al^+ - intensity saturated the counter.

20

Lateral intensity distribution of selected positive secondary ions:

ifos

Positive

minor elements and Cs

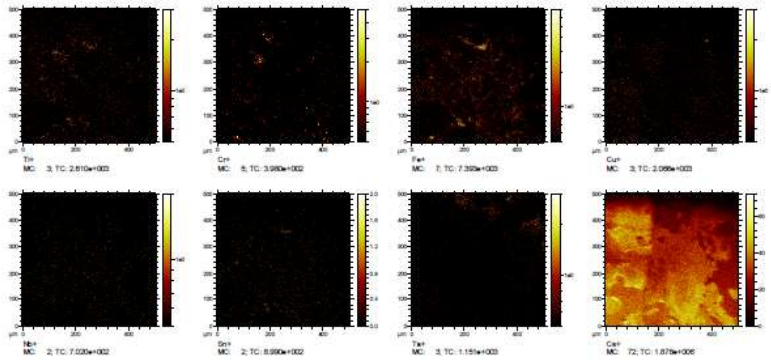

Analysis Position 2

Logarithmic scales for Ti, Cr, Fe, Cu, Nb, Sn and Ta.
The ToF-SIMS apparatus is equipped with a Cs-sputtergun, therefore Cs might be superimposed by a background from the system although the gun was not applied for the present measurements.

21

Lateral intensity distribution of selected positive secondary ions:

ifos

„Zoom“ of the area marked on page 13

Positive

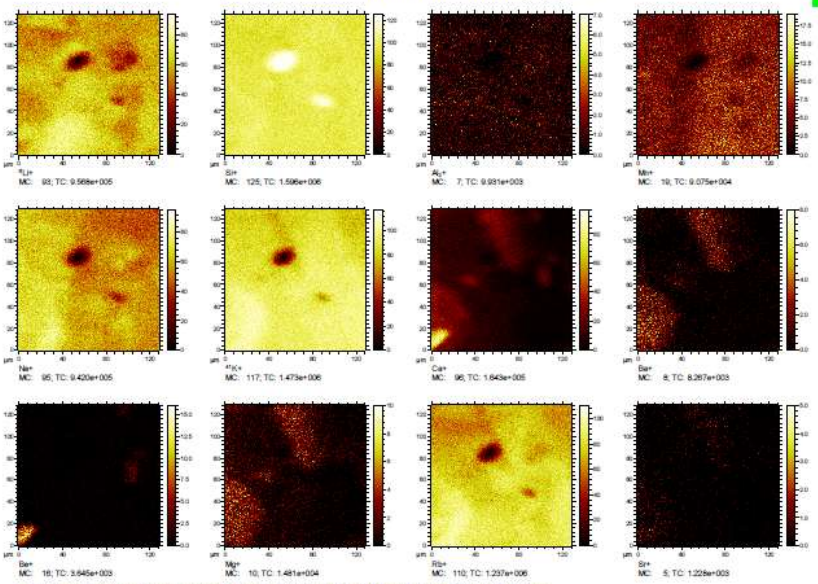

Al was detected via the Al_2+ molecule because the Al^+ - intensity saturated the counter.

Zoom Analysis Position 2

22

Lateral intensity distribution of selected positive secondary ions:

ifos

„Zoom“ of the area marked on page 13, minor elements and Cs

Positive

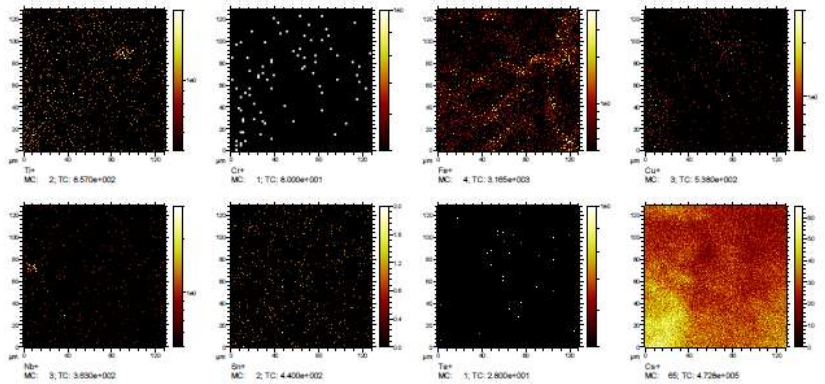

Logarithmic scales for Ti, Cr, Fe, Cu, Nb, Sn and Ta.
The ToF-SIMS apparatus is equipped with a Cs-sputtergun, therefore Cs might be superimposed by a background from the system although the gun was not applied for the present measurements.

Zoom Analysis Position 2

23

Lateral intensity distribution of selected negative secondary ions:

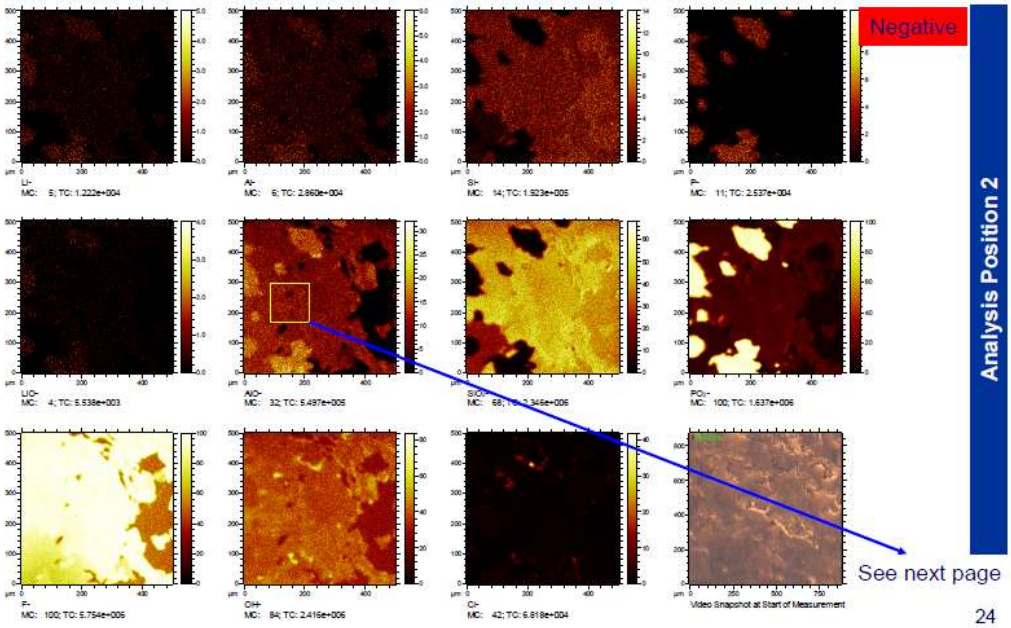

24

Lateral intensity distribution of selected negative secondary ions:

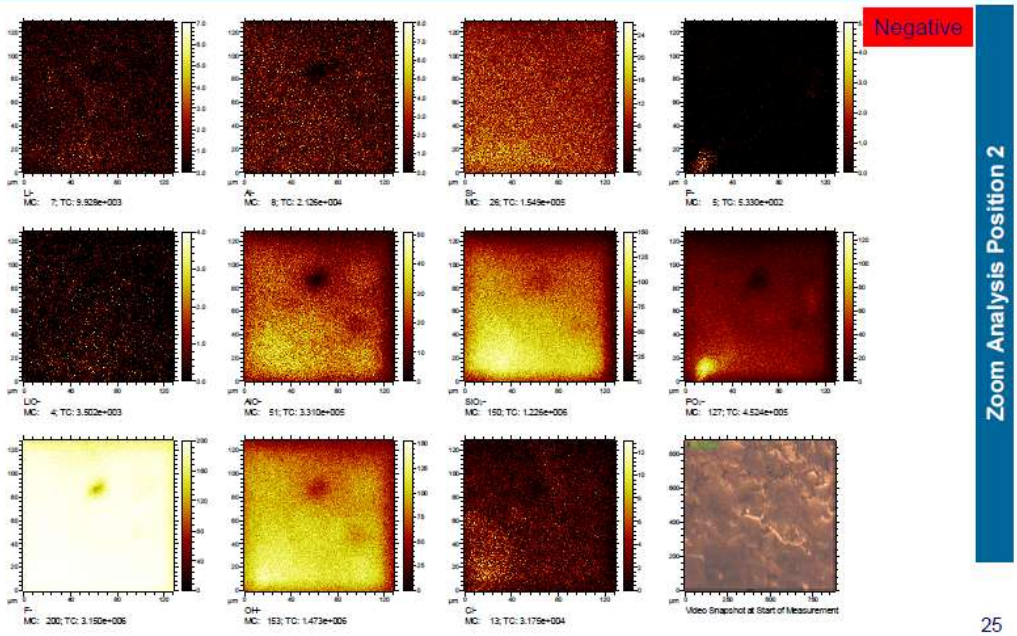

25

Results obtained:

ifos

positive

- Position 1:

The Amblygonite and Topaz can be disguished by the Li- and Al-distribution.
Na is inhomogeneously distributed in the Amblygonite-region
K and Rb appear characteristic for the Micas
Ca is detected with enhanced intensity in the boundaries between the different minerals
Be, Ba, Sr, Mg, Mn, Cr, Ti, Cu and Fe are detected in traces.
The intensities of Nb, Sn and Ta are too low to have a clear detection.

- Position 2:

In the region with the Micas, high intensities of K and Rb are detected.
Li, Mn and Na are also detected, Na is homogeneously distributed.
Be, Mg, Ba, Sr, Ti, Cr, Cu and Fe are detected in traces.
The intensities of Nb, Sn and Ta are too low to have a clear detection.

Negative

- Position 1:

In the Amblygonite region high intensities of P and POx are detected.
The F-intensity saturates the counter.
Cl is detected in traces.
The intensities of Li, LiO, Al and AlO are low because their low negative ion-yield.

- Position 2:

No P is detected in the Micas region.
The F-intensity saturates the counter.
Cl is detected in traces.
The intensities of Li, LiO, Al and AlO are low because their low negative ion-yield.

26

Higher lateral resolution, positive secondary ions

ifos

For the images presented below, the instrument was operated with a setting which provides a higher lateral resolution, but with the drawback of a lower mass-resolution and a lower detection sensitivity.

Positive

standard lateral resolution (3 – 5 µm)

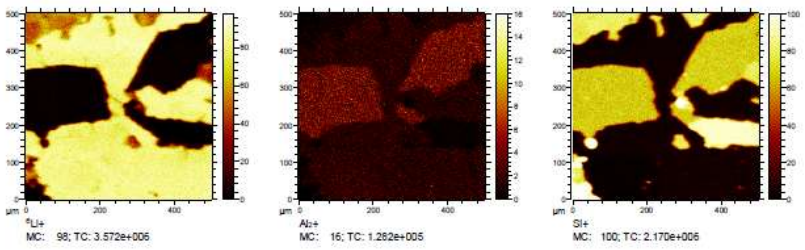

enhanced lateral resolution (0,5 µm)

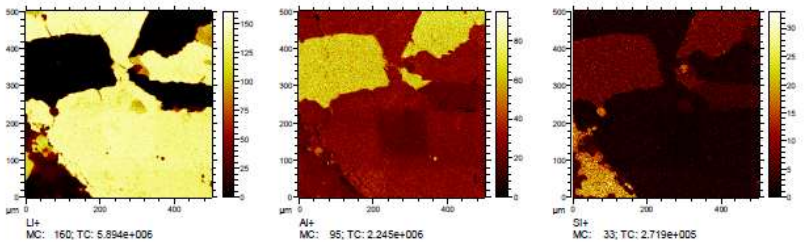

Analysis Position 1

Comparison of images obtained with standard and enhanced lateral resolution

27

Higher lateral resolution, positive secondary ions

ifos

Positive

standard lateral res. (3 – 5 µm)

enhanced lateral res. (0,5 µm)

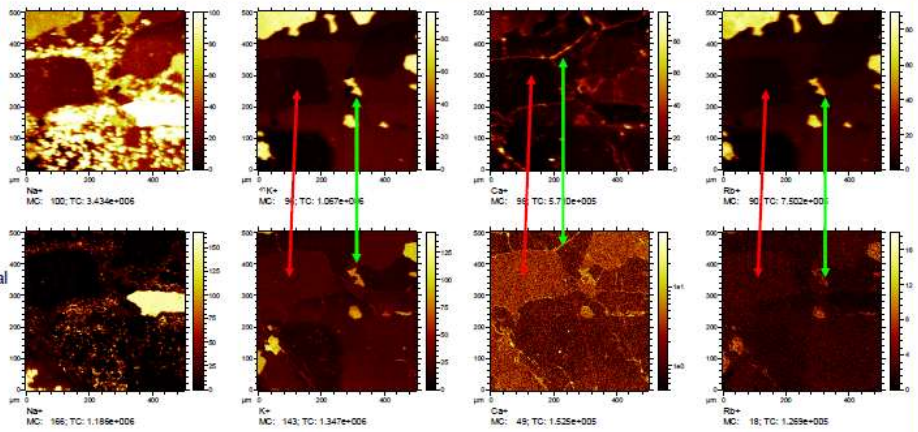

Analysis Position 1

Comparison of images obtained with standard and enhanced lateral resolution

Clearly, the Na-distribution in the Amblygonite area is better resolved.
In case of K, Ca and Rb, some structures are found in both resolution modes (green arrows), but there are also some deviations in the images (red arrows). In some areas a low intensity is detected with the standard mode while with the enhanced mode an increased intensity is found in the same area. The reason for this is the lower mass resolution of the enhanced setting which leads to mass interferences accounting for the increased intensity.
Due to the lower sensitivity of the enhanced mode, the detection of trace elements is not possible.

28

Higher lateral resolution, positive secondary ions

ifos

Positive

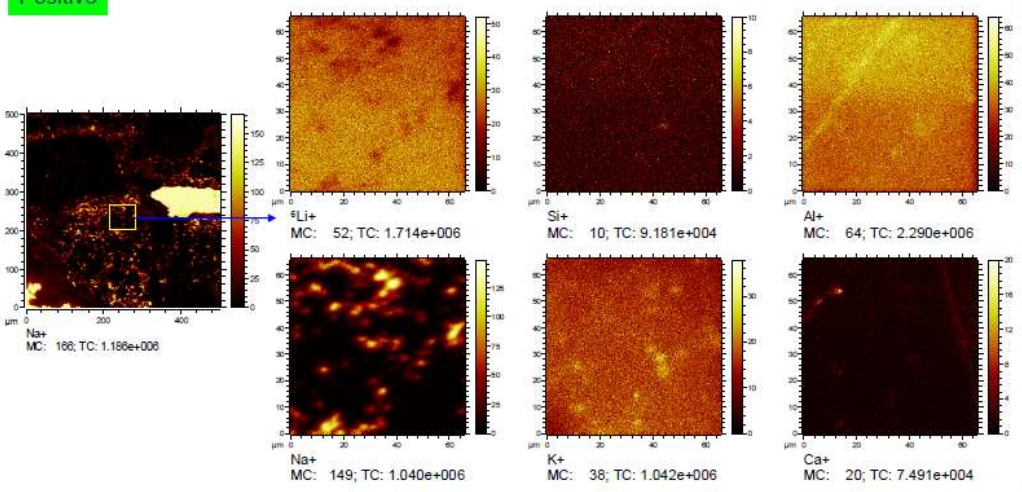

Zoom Analysis Position 1

29

Remarks:

ifos

Example: Lateral intensity distribution of a secondary ion

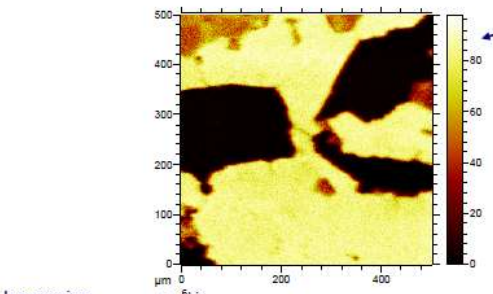

Intensity scale, individually scaled for each image
The intensities cannot be directly converted into concentrations!

Ion species → $^{6}Li+$
MC: 98; TC: 3.572e+006

TC=Total Counts: sum of the intensity of all pixels

MC=Maximum Counts: Intensity of the most intense pixel

30

Appendix 3

Master size of flotation products

Table 10. Particle size analysis of flotation products by Malvern Mastersizer.

Particle diameter, μm	Accumulative undersize, %			
	TQ1	TQ2	TQ3	MD1
0.0582	0	0	0	0.00084
0.0679	0	0	0	0.00295
0.0791	0	0	0	0.00716
0.0921	0	0	0	0.01499
0.1073	0	0	0	0.0289
0.125	0.00256	0	0	0.0526
0.1456	0.01319	0	0	0.09114
0.1697	0.0384	0.01053	0.00675	0.15114
0.1977	0.08716	0.04927	0.03922	0.24103
0.2303	0.1708	0.13337	0.11446	0.37087
0.2683	0.30179	0.28206	0.2517	0.55068
0.3125	0.49096	0.51269	0.46947	0.78734
0.3641	0.74616	0.83755	0.78243	1.08463
0.4242	1.07679	1.26866	1.20401	1.45136
0.4941	1.49673	1.82083	1.74709	1.90514
0.5757	2.01299	2.49822	2.41594	2.45671
0.6707	2.62777	3.29655	3.20607	3.11359
0.7813	3.34255	4.2084	4.10583	3.88557
0.9103	4.1282	5.18626	5.04986	4.75148
1.0604	4.97981	6.22576	6.02457	5.70741
1.2354	5.8912	7.32445	7.00939	6.74809
1.4393	6.85767	8.48685	7.98414	7.86631
1.6767	7.88507	9.73665	8.9435	9.06498
1.9534	8.99822	11.12787	9.90979	10.37323
2.2757	10.23712	12.73817	10.9289	11.84093
2.6512	11.64564	14.64815	12.05931	13.52093
3.0887	13.26805	16.93411	13.37078	15.47316
3.5983	15.13294	19.64239	14.92469	17.74107
4.192	17.24977	22.77331	16.76532	20.34735
4.8837	19.59828	26.26504	18.89986	23.27481
5.6895	22.1354	30.00165	21.2906	26.47019
6.6283	24.81003	33.84094	23.86869	29.85675
7.7219	27.58515	37.66079	26.56449	33.36356
8.996	30.44049	41.36866	29.31044	36.92505
10.4804	33.3782	44.919	32.05732	40.49215
12.2096	36.42839	48.32382	34.79595	44.04598
14.2242	39.63983	51.63971	37.55273	47.5926
16.5712	43.06902	54.94986	40.38445	51.15604

Table 10: *continued.*

Particle diameter, µm	Accumulative undersize, %			
	TQ1	TQ2	TQ3	MD1
19.3055	46.7735	58.35049	43.37671	54.77653
22.4909	50.78933	61.91996	46.61541	58.4858
26.2019	55.12489	65.71363	50.17563	62.30492
30.5252	59.75223	69.75969	54.09964	66.23731
35.5618	64.61167	74.06261	58.37953	70.27066
41.4295	69.63607	78.42756	62.95625	74.39119
48.2654	74.77178	82.638	67.7223	78.37877
56.2292	79.63438	86.48268	72.56842	82.08795
65.507	84.03529	89.79384	77.4044	85.40589
76.3157	87.86374	92.5027	81.90523	88.29583
88.9077	91.0922	94.63818	85.98328	90.78905
103.5775	93.7538	96.29394	89.59274	92.94945
120.6678	95.90621	97.58249	92.69632	94.83261
140.578	97.60703	98.59737	95.25229	96.4618
163.7733	98.85627	99.33858	97.26064	97.83687
190.7959	99.65393	99.80612	98.72137	98.91731
222.2773	100	99.99999	99.63448	99.63836
258.953			99.99997	100.00001

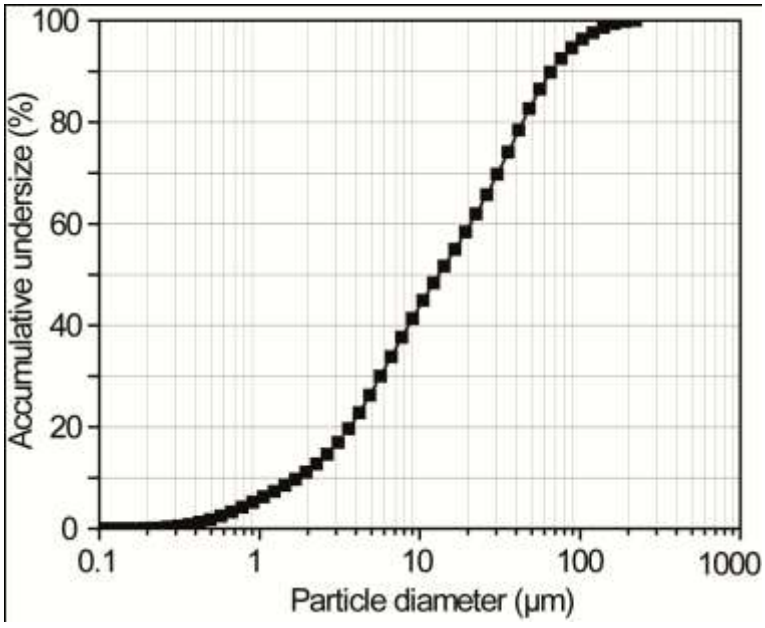

Figure 1. Particle size distribution of TQ2.

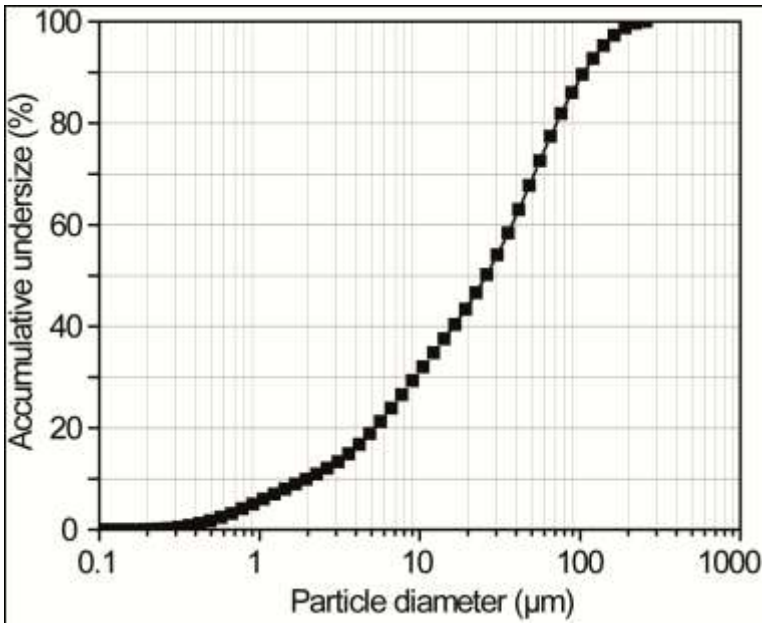

Figure 2. Particle size distribution of TQ3

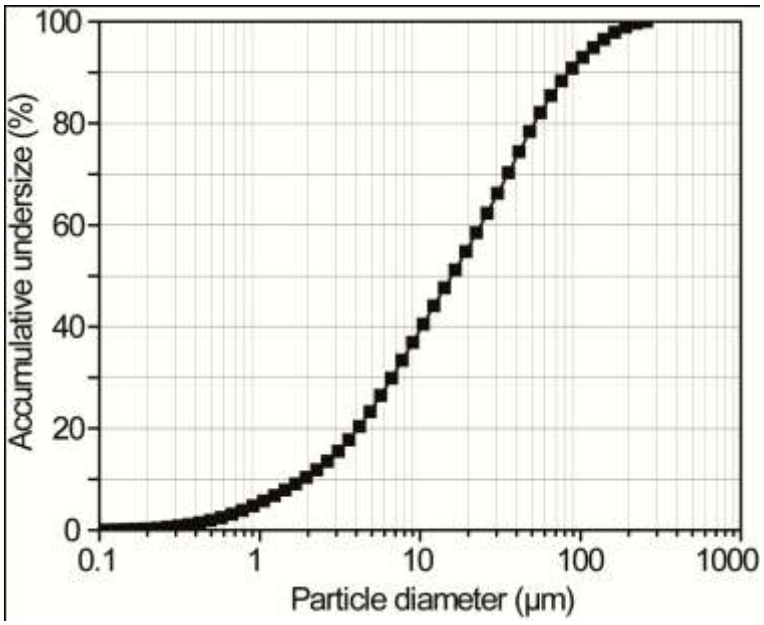

Figure 3. Particle size distribution of MD1

Appendix 4

XRD raw file of La Vi ores

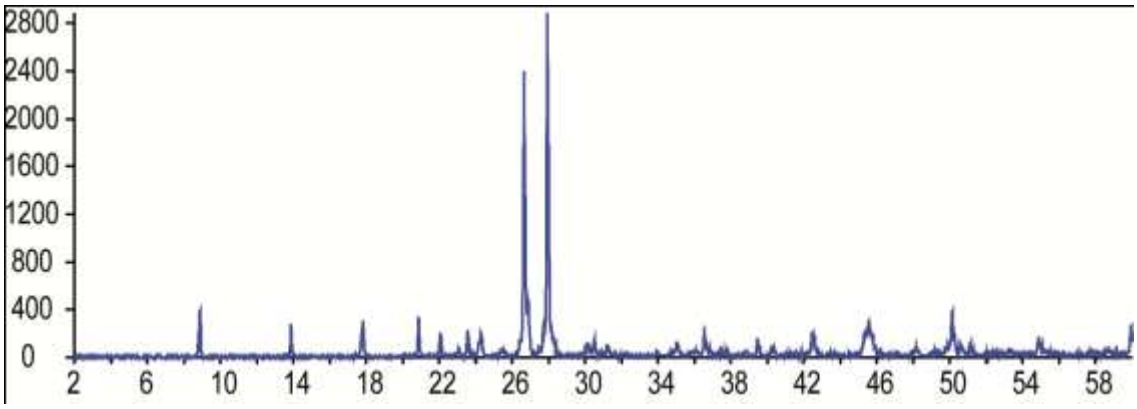

Figure 4. XRD patterns of La Vi ore LAV01.

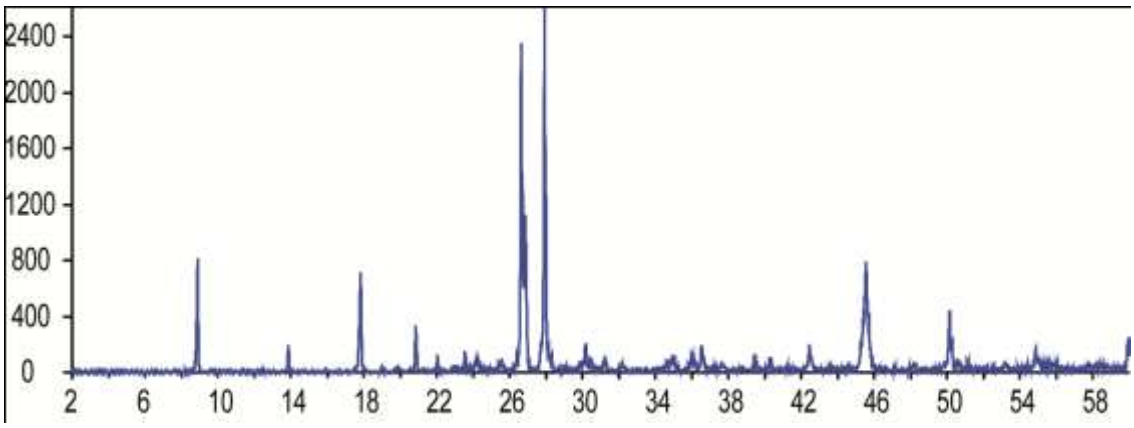

Figure 5. XRD patterns of La Vi ore LAV02.

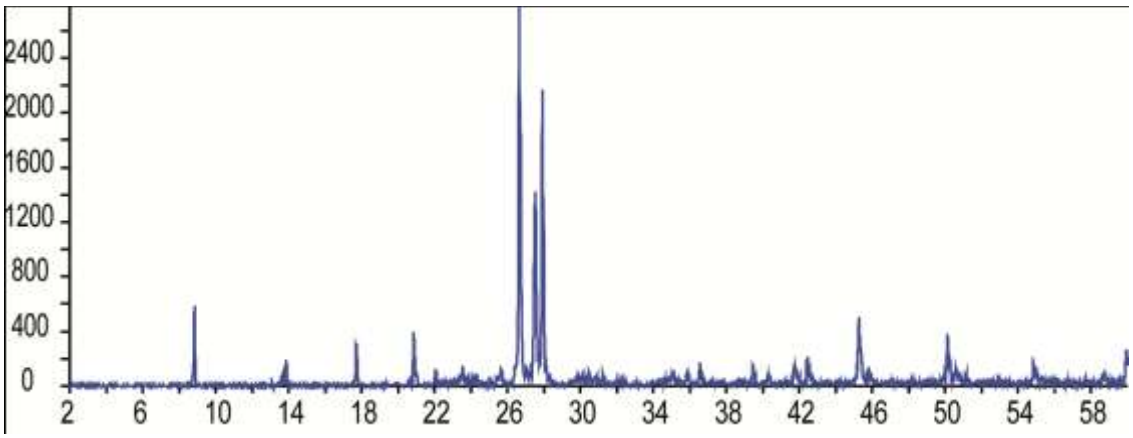

Figure 6. XRD patterns of La Vi ore LAV03.

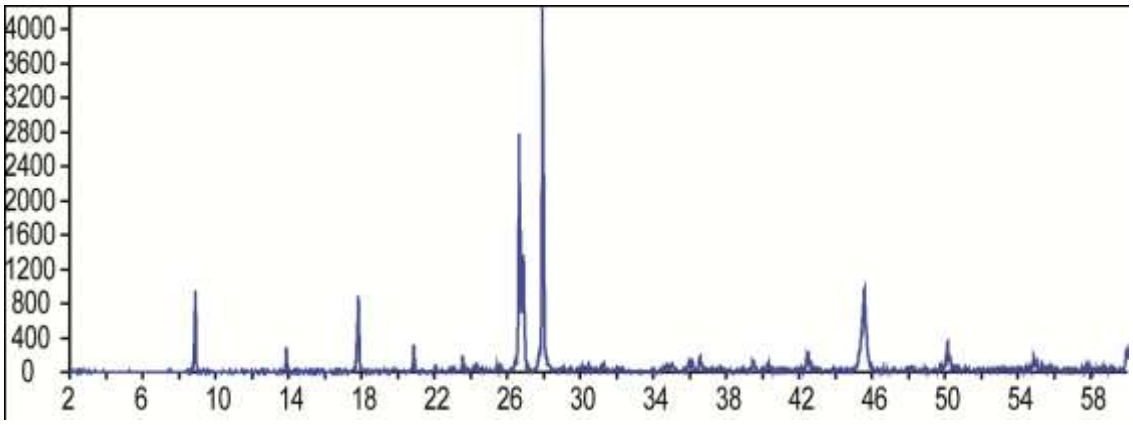

Figure 7. XRD patterns of La Vi ore LAV04.

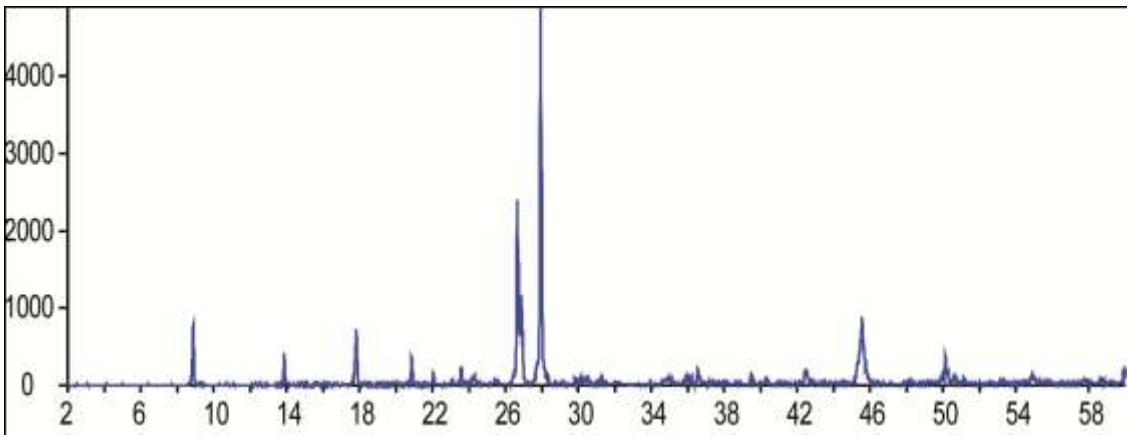

Figure 8. XRD patterns of La Vi ore LAV06.

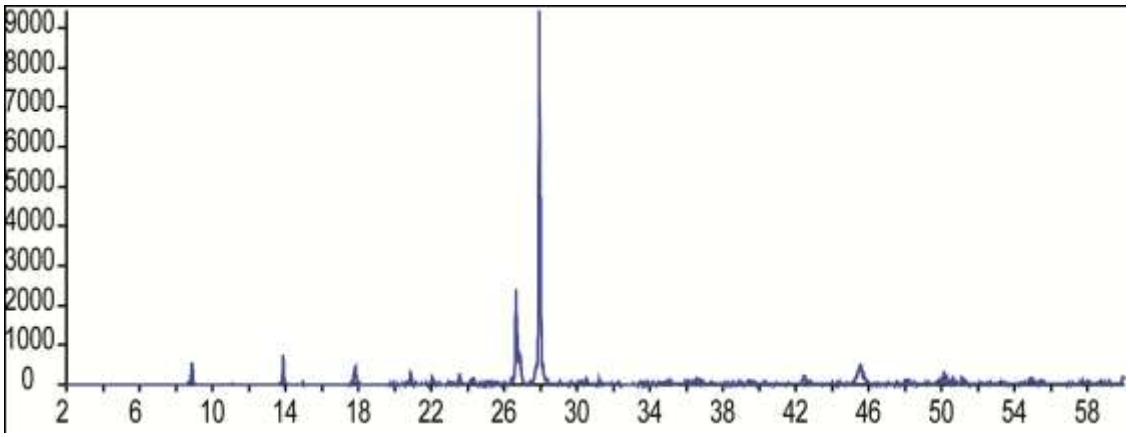

Figure 9. XRD patterns of La Vi ore LAV08.

Appendix 5

Technological experiments data

Table 11. Effect of roasting temperature in closed system on lithium extraction.

Roasting temp., °C	800	850	900	950
Roasting time, h	1.5	1.5	1.5	1.5
S/Li molar ratio	3/1	3/1	3/1	3/1
Ca/F molar ratio	1/1	1/1	1/1	1/1
Leaching temp., °C	85	85	85	85
Leaching time, h	2	2	2	2
H_2O/calcine mass ratio	5/1	5/1	5/1	5/1
Li, ppm	362	960	1065	456
Li extraction, %	17.64	53.01	53.72	22.09

Table 12. Effect of roasting temperature in open system on lithium extraction.

Roasting temp., °C	700		750		800		850	
Roasting time, h	1.5	1.5	1.5	1.5	1.5	1.5	1.5	1.5
S/Li molar ratio	3/1	5/1	3/1	5/1	3/1	5/1	3/1	5/1
Ca/F molar ratio	1/1	1/1	1/1	1/1	1/1	1/1	1/1	1/1
Leaching temp., °C	85	50	85	50	85	50	85	50
Leaching time, h	2	2	2	2	2	2	2	2
H_2O/calcine mass ratio	5/1	10/1	5/1	10/1	5/1	10/1	5/1	10/1
Li, ppm	1370	570	1322	619	1295	569	1142	534
Li extraction, %	69.00	80.44	73.33	87.59	62.43	76.28	57.15	70.9

Table 13. Effect of roasting time on lithium extraction.

Roasting time, h	1		1.5		2		2.5	
Roasting temp., °C	750	750	750	750	750	750	750	750
S/Li molar ratio	3/1	5/1	3/1	5/1	3/1	5/1	3/1	5/1
Ca/F molar ratio	1/1	1/1	1/1	1/1	1/1	1/1	1/1	1/1
Leaching temp., °C	85	50	85	50	85	50	85	50
Leaching time, h	2	2	2	2	2	2	2	2
H_2O/calcine mass ratio	5/1	10/1	5/1	10/1	5/1	10/1	5/1	10/1
Li, ppm	1256	453	1322	619	1202	532	1242	544
Li extraction, %	65.77	61.03	73.33	87.59	69.77	70.52	67.95	73.41

Table 14. Effect of S/Li molar ratio on lithium extraction.

Roasting temp., °C	750	750	750	750	750
Roasting time, h	1.5	1.5	1.5	1.5	1.5
S/Li molar ratio	1/1	1/1	1/1	1/1	1/1
Exp. N^0	1	2	3	4	5
Ca/F molar ratio	1/1	1/1	1/1	1/1	1/1
Leaching temp., °C	85	50	50	50	50
Leaching time, h	2	2	2	2	2
H_2O/calcine mass ratio	5/1	10/1	10/1	10/1	10/1
Li, ppm	939	416	398	334	325
Li extraction, %	36.39	35.72	35.34	29.37	27.27

Table 14. *Continued.*

Roasting temp., °C	750	750	750	750	750
Roasting time, h	1.5	1.5	1.5	1.5	1.5
S/Li molar ratio	2/1	2/1	2/1	2/1	2/1
Exp. N^0	1	2	3	4	5
Ca/F molar ratio	1/1	1/1	1/1	1/1	1/1
Leaching temp., °C	85	50	50	50	50
Leaching time, h	2	2	2	2	2
H_2O/calcine mass ratio	5/1	10/1	10/1	10/1	10/1
Li, ppm	1315	556	587	552	558
Li extraction, %	65.62	57.85	61.21	56.40	56.66

Table 14. *Continued.*

Roasting temp., °C	750	750	750	750	750
Roasting time, h	1.5	1.5	1.5	1.5	1.5
S/Li molar ratio	3/1	3/1	3/1	3/1	3/1
Exp. N^0	1	2	3	4	5
Ca/F molar ratio	1/1	1/1	1/1	1/1	1/1
Leaching temp., °C	85	50	50	50	50
Leaching time, h	2	2	2	2	2
H_2O/calcine mass ratio	5/1	10/1	10/1	10/1	10/1
Li, ppm	1322	570	557	559	573
Li extraction, %	73.33	67.79	66.37	64.33	64.37

Table 14. *Continued.*

Roasting temp., °C	750	750	750	750	750
Roasting time, h	1.5	1.5	1.5	1.5	1.5
S/Li molar ratio	5/1	5/1	5/1	5/1	5/1
Exp. N^0	1	2	3	4	5
Ca/F molar ratio	1/1	1/1	1/1	1/1	1/1
Leaching temp., °C	85	50	50	50	50
Leaching time, h	2	2	2	2	2
H_2O/calcine mass ratio	5/1	10/1	10/1	10/1	10/1
Li, ppm	1198	617	593	585	575
Li extraction, %	75.47	84.13	84.09	82.89	82.02

Table 14. *Continued.*

Roasting temp., °C	750	750	750	750	750
Roasting time, h	1.5	1.5	1.5	1.5	1.5
S/Li molar ratio	7/1	7/1	7/1	7/1	7/1
Exp. N^0	1	2	3	4	5
Ca/F molar ratio	1/1	1/1	1/1	1/1	1/1
Leaching temp., °C	85	50	50	50	50
Leaching time, h	2	2	2	2	2
H_2O/calcine mass ratio	5/1	10/1	10/1	10/1	10/1
Li, ppm	1053	455	459	489	470
Li extraction, %	72.46	74.94	74.55	76.82	74.34

Table 15. Effect of Ca/F molar ratio on lithium extraction.

Roasting temp., °C	750	750	750	750	750
Roasting time, h	1.5	1.5	1.5	1.5	1.5
S/Li molar ratio	5/1	5/1	5/1	5/1	5/1
Ca/F molar ratio	-	1/1	1.5/1	2/1	2.5/1
Leaching temp., °C	50	50	50	50	50
Leaching time, h	2	2	2	2	2
H_2O/calcine mass ratio	10/1	10/1	10/1	10/1	10/1
Li, ppm	645	569	619	485	491
Li extraction, %	81.95	76.09	87.59	72.84	75.06

Table 16. Effect of leaching time on lithium extraction.

Roasting temp., °C	750	750	750	750	750	750	750	750	750	750
Roasting time, h	1.5	1.5	1.5	1.5	1.5	1.5	1.5	1.5	1.5	1.5
S/Li molar ratio	5/1	5/1	5/1	5/1	5/1	5/1	5/1	5/1	5/1	5/1
Ca/F molar ratio	1/1	1/1	1/1	1/1	1/1	1/1	1/1	1/1	1/1	1/1
Leaching temp., °C	85	50	85	50	85	50	85	50	85	50
Leaching time, h	1	1	1.5	1.5	2	2	2.5	2.5	3	3
H_2O/ calcine mass ratio	5/1	10/1	5/1	10/1	5/1	10/1	5/1	10/1	5/1	10/1
Li, ppm	1137	556	1199	555	1198	627	1231	554	1275	548
Li extraction %	72.45	77.01	75.28	76.58	75.47	87.33	74.94	76.22	72.74	75.62

Table 17. Effect of leaching temperature on lithium extraction.

Roasting temp., °C	750	750	750	750	750	750	750	750
Roasting time, h	1.5	1.5	1.5	1.5	1.5	1.5	1.5	1.5
S/Li molar ratio	5/1	5/1	5/1	5/1	5/1	5/1	5/1	5/1
Ca/F molar ratio	1/1	1/1	1/1	1/1	1/1	1/1	1/1	1/1
Leaching temp., °C	room	room	50	50	75	75	85	85
Leaching time, h	2	2	2	2	2	2	2	2
H_2O/ calcine mass ratio	5/1	10/1	5/1	10/1	5/1	10/1	5/1	10/1
Li, ppm	1104	548	1091	627	1088	572	1198	581
Li extraction %	73.63	75.79	77.48	87.33	76.18	77.47	75.47	76.76

Table 18. Effect of water/calcine mass ratio on lithium extraction.

Roasting temp., °C	750	750	750	750	750
Roasting time, h	1.5	1.5	1.5	1.5	1.5
S/Li molar ratio	5/1	5/1	5/1	5/1	5/1
Ca/F molar ratio	1/1	1/1	1/1	1/1	1/1
Leaching temp., °C	50	50	50	50	50
Leaching time, h	2	2	2	2	2
H_2O/calcine mass ratio	1/1	3/1	5/1	10/1	15/1
Li, ppm	4915	1357	1091	619	360
Li extraction, %	59.28	54.27	77.48	87.59	76.85

Table 19. Effect of removal cations temperature by NaOH 0.5 M on lithium extraction. Reaction time: 0.5 h.

Reaction temp., °C	20	30	40	50	60
Li recovery, %	78.69	79.19	83.05	89.82	86.61
Ca removal, %	100	100	100	100	100
Mg removal, %	100	100	100	100	100
Al removal, %	90.44	85.70	60.75	34.20	29.99
Fe removal, %	100	100	100	100	100

Table 20. Effect of removal cations time by NaOH 0.5 M at room temperature on lithium extraction.

Reaction time, h	Li recovery	Ca removal	Mg removal	Al removal	Fe removal
0.5	97.92	100	100	90.44	100
1	96.94	100	100	94.03	100
1.5	77.24	99	100	96.58	99.62
1.5(1)	97.26	100	100	96.58	99.62
1.5(2)	99.81	100	100	96.52	99.61
2	95.77	100	100	95.35	100
2.5	94.30	100	100	96.79	100
3	94.07	100	100	95.73	100

(1); (2). Precipitates were washed.

Table 21. Effect of removal SO_4 by $BaCl_2$ 0.2 M at room temperature on lithium extraction.

Reaction time, h	Li recovery, %	SO_4 removal, %
0.5	97.66	100
1(1)	95.48	100
1(2)	96.34	100
1(3)	95.49	94.95
1(4)	97.80	100
1(5)	93.38	97.17
1(6)	94.09	93.05
1.5	96.48	99.87
2	95.46	99.87

Table 22. Effect of isopropanol leaching time on lithium extraction and LiCl product grade. Isopropanol/salts mass ratio of 10:1.

Leaching time, h	3	5	12	24
Li recovery, %	70.02	70.84	66.34	52.74
LiCl, ppm	924331	918706	864988	876367

Table 23. Effect of isopropanol/salts mass ratio on lithium extraction and LiCl product grade. Isopropanol leaching: 3 h.

isopropanol/salts mass ratio	5/1(1)	5/1(2)	5/1(3)	7/1	10/1
Li recovery, %	87.08	87.66	85.28	85.32	86.60
LiCl, ppm	905763	919274	962981	889596	818196

Appendix 6

Quality of Chemicals used

1. Armac T from AkzoNobel

Armac T is cationic collector was investigated in the mica flotation with other depressor and in the acid environment.

Parameter	Limits
mine number	165 min
Iodine value	32 - 50
Color	0 - 10 Gardner
Moisture	2 % max
Chemical and Physical Data	**Typical Value**
Initial Boiling Point C (@mm Hg)	decomposes at 100C C (@mm Hg)
Solubility in water at 25°C	isopropanol, ethanol, hexane (35C)
HLB value	6.8 Davies Scale 0-40
pH	6-9
Vapour pressure	< 1 mm Hg @20 C
Pour point	65 C
Flash point	150 C
Melting point	55 C
Appearance	Solid at 25°C
Equivalent Mass	324
Specific Gravity	0.845(80)

2. Barium chloride $BaCl_2$ 99.995 suprapur (Merk)

$BaCl_2$ was used to precipitate SO_4^{2-} in the leach liquor after removal cations from second group forward in the periodic table.

Molar mass	208.23 g/mol
Physicochemical information	
Boiling point	1560 °C
Density	3.9 g/cm3 (20 °C)
Melting point	963 °C
pH value	5 – 8 (50g/l, H2O, 20 °C)
Bulk density	1350 kg/m3
Solubility	375 g/l (20 °C)
Toxicological information	
LD 50 oral	LD50 Rat 118 mg/kg

3. Calcium oxide: CaO from Alfa Aesar

CaO is one of an additive mixed with lepidolite concentrate to the purpose reduce HF gas release into the environment.

Molar mass	56.08 g/mol
Physicochemical information	
Boiling point	2850 °C
Density	3.25 – 3.38 g/cm3
Melting point	2572 °C
Refractive index	1.83
Solubility	Soluble in water with generation of heat, and forming $Ca(OH)_2$, in acids, glycerol. Insoluble in alcohol
Sensitivity	Air & Moisture Sensitive

4. Hydrochloride acid (HCl) from Merck

HCl controls the pH of solution after remove all cations and anions in leach liquor

Physicochemical information	
Boiling point	45 °C
Density	1.19 g/cm3 (20 °C)
Melting point	-28 °C
pH value	< -1 (H2O, 20 °C)
Vapor pressure	190 hPa (20 °C)
Solubility	(20 °C) soluble

5. Iron II sulphide FeS tech. from Alfa Aesar

FeS is the main additive for lepidolite concentrate roasting.

Molar mass	87.91 g/mol
Physicochemical information	
Density	4.84 g/cm3 (20 °C)
Melting point	1195 °C
Bulk density	1500 - 2000 kg/m3
Solubility	insoluble (20 °C)

6. Iron sulphate: $FeSO_4$. $7H_2O$ from Merck

$FeSO_4$. $7H_2O$ is the other main additive for lepidolite concentrate roasting.

Molar mass	278.02 g/mol
Physicochemical information	
Density	1.89 g/cm^3 (20 °C)
Melting point	> 60 °C Elimination of water or crystallisation
pH value	3 – 4 (50g/l, H_2O, 20 °C)
Bulk density	600 kg/m^3
Solubility	400 g/l (20 °C)
Toxicological information	
LD 50 oral	LD50 Rat 319 mg/kg

7. Natri silicate: Na_2SiO_3 from Merck

Physicochemical information	
Boiling point	>100 °C (1013 hPa)
Density	1.35 g/cm^3 (20 °C)
pH value	11.0 -11.5 (50 g/l, H_2O, 20 °C)
Solubility	(20 °C) soluble

8. Propanol: C_3H_8O ($CH_3CH(OH)CH_3$) from Merck

Propanol is the solvent to dissolve LiCl in an identify amount.

Molar mass	60.1 g/mol
Physicochemical information	
Boiling point	82.4 °C (1013 hPa)
Density	0.786 g/cm^3 (20 °C)
Evaporation number	11
Explosion limit	1 – 13.4 % (V)
Flash point	12 °C
Ignition temperature	425 °C
Melting point	- 89.5 °C
pH value	(H_2O, 20 °C) neutral
Vapor pressure	43 hPa (20 °C)
Refractive index	1.378
Solubility	(20 °C) soluble
Toxicological information	
LD 50 oral	LD50 Rat 5045 mg/kg
LD 50 dermal	LD50 Rabbit 12800 mg/kg

9. Sodium hydroxide: NaOH from Merck

NaOH is the reagent to precipitate the cations in leach liquor except the cations in the first group in the periodic table.

Molar mass	40.0 g/mol
Physicochemical information	
Density	2.13 g/cm^3 (20 °C)
Melting point	323 °C
pH value	14 (50g/l, H_2O, 20 °C)
Vapor pressure	(20 °C)
Solubility	1090 g/l (20 °C)

10. Sulfuric acid from Merck

H_2SO_4 is environment reagent in the flotation step

Molar mass	98.08 g/mol
Physicochemical information	
Boiling point	335 °C
Density	1.84 g/cm^3 (20 °C)
Melting point	-20 °C
pH value	0.3 (49g/l, H_2O, 25 °C)
Vapor pressure	0.0001 hPa (20 °C)
Solubility	(20 °C) soluble, (caution! Development of heat)

11. Sulfur: S from Merck

S is one kind of additive for roasting procedure

Molar mass	32.06 g/mol
Physicochemical information	
Boiling point	444 °C (1013 hPa)
Density	1.96 – 2.07 g/cm^3 (20 °C)
Flash point	160 °C
Ignition temperature	235 °C Dust
Melting point	113 - 119 °C
Vapor pressure	< -0.01 hPa (20 °C)
Bulk density	400 – 500 kg/m^3
Solubility	(20 °C) practically insoluble
Toxicological information	
LD 50 oral	LD50 Rat > 5000 mg/kg
LD 50 dermal	LD50 Rabbit > 2000 mg/kg

Appendix 7

Laboratory Equipment

1. Centrifugeuse Biofuge Primo Heraeus

This machine separates particles in a suspension from a liquid by centrifugation.

Rotor designation	Swinging bucket rotor, 4 x 100 ml
Maximum permissible load (g)	4 x 200
Maximum speed nmax (min-1)	4000
Maximum RCF value at nmax	2522
Maximum radius (cm)	14.1
Minimum radius (cm)	5.0
Angle (°)	90
Acceleration time (s)	25
Braking time (s)	20
Permissible temperature range autoclavable (number of cycles)	121 °C, unlimited

Function/ parameter	Value
Environmental conditions	Indoor use Max elevation 2000m above sea level Max. relative humidity 80% up to 31 °C, linearly decreasing down to 51 °C relative humidity at 40 °C
Permissible temperature of the environment	2 °C to 40 °C
Run time	1 min – 9h 59 min, hold = permanent operation
Maximum speed nmax	15000 min-1
Maximum kinetic energy	< 100 kNm
Noise at maximum speed	< 62dB (A)
Maximum sample temperature after 30 min permanent operation	Room temperature + 15 K
Dimension (H x W x D), mm	380 x 475

2. Filters 2.5 µm from Whatnam

This filter was used for both roasting and leaching procedure.

Material	Circles
Limit	0.4 psi wet burst, 1870 sec/ 100 mL
Diameter	240 mm
Thickness	200 µm
Ash	≤ 0.007 %
Pore size	2.5 µm (particle retention)
Basis weight	$100 m^2$

3. Tube furnace R120/1000/12-Nabertherm with controller B180

Tube furnace was used for roasting procedure

Outer dimension (W x D x H), mm	1300 x 420 x 730
Heated tube length, mm	1000
Length constant temp. ΔT 10k, mm	330
Power rating, kV	6
Weight, kg	170
Power supply, V	400
T max, °C	1200
Material of working tube	C530 (sillimantine)
Outer diameter, mm	120
Inner diameter, mm	100
Length, mm	1400
Max. heat-up ramp., k/h	200